Universidad Autónoma de San Luis Potosí
Facultad de Ingeniería
Centro de Investigación y Estudios de Posgrado

Diseño de Herramientas de Control PI para un Convertidor CD-CD de Alta Ganancia sin Transformador

T E S I S

Que para obtener el grado de:

Maestro en Ingeniería Eléctrica, opción Electrónica de Potencia para Fuentes Alternas de Energía

Presenta:
IMT. Erick Moreno Negrete

Asesor:
Dr. César Fernando Francisco Méndez Barrios

Co-Asesor:
Dr. Diego Langarica Córdoba

San Luis Potosí, S. L. P. Octubre de 2021

UASLP
Universidad Autónoma de San Luis Potosí

FACULTAD DE INGENIERÍA

20 de mayo de 2021

ING. ERICK MORENO NEGRETE
P R E S E N T E.

En atención a su solicitud de Temario, presentada por los **Dres. César Fernando Francisco Méndez Barrios y Diego Langarica Córdova**, Asesor y Coasesor de la Tesis que desarrollará Usted con el objeto de obtener el Grado de **Maestro en Ingeniería Eléctrica**, me es grato comunicarle que en la sesión del H. Consejo Técnico Consultivo celebrada el día 20 de mayo del presente, fue aprobado el Temario propuesto:

TEMARIO:

"Diseño de Herramientas de Control PI para un Convertidor CD-CD de Alta Ganancia sin Transformador"

1. Introducción.
2. Modelo Matemático del Convertidor CD-CD.
3. Diseño del Controlador: Enfoque Lineal.
4. Diseño del Controlador: Enfoque No Lineal.
5. Validación Numérica.
6. Observaciones Finales y Trabajos a Futuro.

Apéndice.
Referencias.

"MODOS ET CUNCTARUM RERUM MENSURAS AUDEBO"

A T E N T A M E N T E

UNIVERSIDAD AUTONOMA DE SAN LUIS POTOSI
FACULTAD DE INGENIERIA
DIRECCION

DR. EMILIO JORGE GONZÁLEZ GALVÁN
DIRECTOR.

www.uaslp.mx

Av. Manuel Nava 8
Zona Universitaria • CP 78290
San Luis Potosí, S.L.P.
tel. (444) 826 2330 al39
fax (444) 826 2336

Copia. Archivo.
*etn.

Índice general

PI CONTROL TOOLS DESIGN FOR A HIGH GAIN TRANSFORMERLESS DC-DC CONVERTER

E. MORENO-NEGRETE
C. F. MENDEZ-BARRIOS
D. LANGARICA-CORDOBA

Center for Research and Graduate Studies
Faculty of Engineering
Universidad Autonoma de San Luis Potosi

To *Melissa Itzel*, who preserves the stability of my days despite life's nonlinearities, exogenous disturbances, and uncertainties. Thanks for being the equilibria of my dynamic system.

To my mother *Emi* with love. Through your support and actions inspired me to pursue the knowledge more than anything else. Love is the one thing we're capable of perceiving that transcends dimensions of time and space.

To *J.A.* who was with me for a long period of time, maybe things didn't happen as we wished and we both got hurt but I want you to know that I esteem and miss you, even with nostalgia, old friend...

"If I have seen further it is by standing on the shoulders of Giants"
–Issac Newton

Dedicated to the memory of those we lost during the COVID-19 Pandemic. *Sé que ya no están con nostros, pero me niego a creerlo. Que los fuertes sean más justos y que los justos sean más fuertes. Un poco más fuertes cada día...*

ACKNOWLEDGEMENTS

For God so loved the world that he gave his one and only Son, that whoever believes in him shall not perish but have eternal life. John 3:16

In the name of the Great Architect of the Universe, the All Compassionate, the All Merciful. Thank You for not blinking at my hopes and dreams in difficult times and for teaching me that brave hearts never fail.

To my Parents, Emi and Enrique, my brothers, Liz, Luis and Enrique, and my nephews, Elian, Luis Gerardo, Andre and Aime. You are my Columns and my strength.

My special thanks to Professor Víctor Esteban Espinoza López, without his advices and brutal honesty, my journey for this degree couldn't be accomplished.

I want to especially thank Lic. Olivia Sigler who kindly received me on Teacher's Day in 2019, listened my moment of weakness and introduced me to Dr. Morales to finally convince me to select CIEP as my first option to Graduate School.

I dedicate this sincere work to the people who were with me from distance and always listened my disturbances, my cycling friends: Luis García, Wero García, Javier Torres and Isaias Alvarado. And to my friends who always sent me their strength no matter the conditions: Jorge Felix, Alba Olvera, Guillermo Almazán, Osbaldo Álvarez, Raúl Tapia, Erick Moreno and Zaira Ugalde.

I would like to pass my gratitude and heartily (as I did in my Bachelor Thesis) to my friends Dr. Tito Serna and MPA. Gabriel De Leon for the motivational talks, meetings and good advices.

For my coach and friend Rene Ortiz, who helps me on a daily basis to cope with demons and turn discomfort into second options by leaving everything in the 400m oval in order to pursue my 42.195km dream, he introduced me to the Pegasso family and gave me support while I was studying in San Luis Potosí to continue training under the tutelage of José Luis García.

This work can't be possible without the support of my colleagues that made my days at the CIEP a beautiful experience, Juan Diego, Julián Alejandro, Eduardo, Liz and Frank. Especially to Iñaki, a true friend who was with me in every step of the way, you are part of this success. *Gracias por ayudarme en los camiones cuando me perdía, por no rendirte en nuestra amistad en el momento mas oscuro y por siempre estar ahí, incluso en aquellas madrugadas en el Edificio P*.

In this journey I met a lot of people that inspire me, one of them is José Enrique Hernández Díez who share with me his knowledge and patience, he taught me upgrade my writing skill, and I appreciate the Meet Talks of another topics, art, music and poetry. *Merci Pote*.

My truly and deeply thanks to Professor Raúl Balderas-Navarro, who seed in me the passion to see inexplicable things with a lot of ways to reach solutions. And more important, he taught me see with another eyes a kind society and world's hope, *Gracias por los cafés, las películas y las pláticas sinceras*.

I want to extend my special thanks to all my Professors that make CIEP one of the greatest research institutions in México, speacially to Drs. Víctor Manuel Cárdenas Galindo, Mario Arturo González García and Homero Miranda Vidales who with their advices and kindnesses, I master this beautiful area of knowledge.

Para el Pueblo de México y Mi Rioverde, por confiar en mi y fondear mis estudios que con su noble esfuerzo y trabajo hacen que instituciones públicas como el Conacyt y la UASLP puedan becar y ofrecer las condiciones adecuadas para investigar, mi deuda es con ustedes, no les voy a fallar.

Last but not least, I want to express my gratefulness to my Advisor, Professor César Fernando for gave me the opportunity to work with him, for the special talks of life nonlinearities, sports, family, math and kind. Aswell as my Co-advisor, Professor Diego who was with me in all power electronics doubts, simulations and life experiences enriched my mind and made me mature my results and my speeches. *Gracias totales*.

RESUMEN

El desarrollo del presente trabajo de tesis se motiva principalmente a las microrredes eléctricas como una solución a los problemas de desigualdad energética en sectores conurbados y rurales que han sido afectados por los diseños centralizados a las ciudades. Basado principalmente en el control de convertidores de corriente directa a corriente directa (CD-CD), se selecciona una topología adecuada por su alta razón de conversión, bajo peso y sin utilizar transformador, en donde se desarrolla sus modelos en larga y pequeña señal para su posterior utilidad.

Esta tesis estudia las bases y guías de la topología ASL-SU2C que tiene una celda multiplicadora de inductores y capacitores, incluyendo el modelado en un enfoque clásico utilizando las leyes de Kirchhoff y Ohm, además de su representación en energía usando flujos y cargas por medio de la teoría de puertos-Hamiltonianos.

El estudio del control se divide esencialmente en dos partes, el control lineal y el no lineal. En la primera se emplean dos esquemas de control para un lazo simple y un lazo doble (comúnmente llamado control en cascada). Se lleva a cabo el desarrollo y análisis de estabilidad denominado σ-estabilidad, metodología en la que se busca generar un espacio paramétrico que marque gráficamente los límites de estabilidad y cierre en regiones de estabilidad a través de un desplazamiento en el eje imaginario del plano complejo, entonces, se logra el máximo decaimiento exponencial como consecuencia.

La segunda parte de la tesis es basada principalmente en la teoría de puertos Hamiltonianos y bajo el espíritu de Lyapunov para asegurar estabilidad global asintótica (EGA). Adicionalmente se realiza el estudio de un estimador de incertidumbres basado en la teoría de Inmersión e Invariancia (I&I) para otorgarle capacidades adaptables al control cuando el convertidor sufre variaciones paramétricas.

Con el objetivo de analizar las propuestas de control se utiliza el software MATLAB/SIMULINK bajo operaciones nominales, y con cambios de carga en donde comparamos los controladores propuestos para después discutir los resultados. Finalmente las conclusiones y el trabajo a futuro terminan nuestra contribución.

ABSTRACT

The development of this thesis work is mainly motivated by electrical microgrids (MG) as a solution to the problems of energy inequality in urban and rural sectors that have been affected by centralized designs in cities. Based mainly on the control of direct current to direct current (DC-DC) converters, a suitable topology is selected for its high conversion ratio, low weight, and without using a transformer, where its models are developed in large and small-signal for its later usefulness.

This thesis studies the bases and guides of the ASL-SU2C topology that has a multiplier cell of inductors and capacitors, including modeling in a classical approach using Kirchhoff and Ohm's laws, in addition to its representation in energy using fluxes and charges through the port-Hamiltonian (pH) theory.

The control study is essentially divided into two parts, linear and non-linear control. The first one employs two control schemes for a single-loop and a double-loop (commonly called cascade control). The development and stability analysis called σ-stability is carried out, a methodology in which it is sought to generate a parametric space that graphically marks the stability boundaries and closing regions of stability through a shift in the imaginary axis of the complex plane, then, maximum exponential decay is achieved as a consequence.

The second part of the thesis is based mainly on the theory of Hamiltonian ports and in the spirit of Lyapunov to ensure global asymptotic stability (GAS). Additionally, the study of an estimator of uncertainties based on the theory of Immersion and Invariance (I&I) is carried out to give it capabilities adaptable to the control when the converter undergoes parametric variations.

In order to analyze the control proposals, the MATLAB/SIMULINK software is used under nominal operations, and with load changes where we compare the proposed controllers and then discuss the results. Finally, the conclusions and future work finish our contribution.

CONTENTS

LIST OF FIGURES

LIST OF TABLES

ACRONYMS

A-PI Adaptive-Propotional-Integral Control

ASL Active Switched-Inductor

AVG Average Value

AC Alternating Current

CENACE National Energy Control Center

CRE Energy Regulatory Commission

CFE Federal Electricity Commission

CBC Classic Boost Converter

DG Distributed Generation

DES Distributed Energy Sources

DC Direct Current

GAS Global Asymptotic Stability

IEEE Institute of Electrical and Electronics Engineers

II Immersion and Invariance

MG Microgrid

PSC Passive Switched-Capacitor

PI Proportional-Integral Control

pH Port-Hamiltonian

PBC Passivity-Based Control

PQ Power Quality

SB Stability Boundaries

$v(t)$	Voltage
V	Average Voltage
$i(t)$	Current
I	Average Current
$u(t)$	Control Law
δ	Duty Cycle
x	State Vector
$x^\star$	Reference Vector
y	Output Vector
λ	Constant group of Parameters
s	Complex Variable
$\tilde{(\cdot)}$	Small, Incremental Signal
f	Frequency
S_n	Switching State
$G(s)$	Transfer Function
$adj(\cdot)$	Adjugate Matrix
$det(\cdot)$	Determinant of a Matrix
$\mathcal{T}$	Parameters Space Path
$H(x)$	Hamiltonian Function
$\mathbb{R}$	Set of Real Numbers
$\mathbb{R}^{n\times m}$	Set of $n \times m$ Real Matrices
$diag[A_{(1,1)},\ldots,A_{(n,n)}]$	Diagonal Matrix
$\rightarrow$	Morphism
$\Rightarrow$	Functional Predicate
$\Re\{z\},\Im\{z\}$	Real part; Imaginary part of a number z
j	$\sqrt{-1}$
$\emptyset$	Empty Set
$\cup,\cap$	Union, Intersection
$\subseteq,\subset$	Is a Subset of, is a Proper Subset of

1 INTRODUCTION

In the last few years, we have witnessed phenomena never seen before in the field of electric energy. Mexican public institutions such as CENACE, CRE, CFE, among others, have made a series of efforts for the creation of public policies that support specific problems that affect directly and indirectly the National Electric System (see Figure 1.1). However, beyond the problems that some methodologies can solve, the risk of synchronization, control, and power quality is a consequence of backbone networks designed in one-way processes.

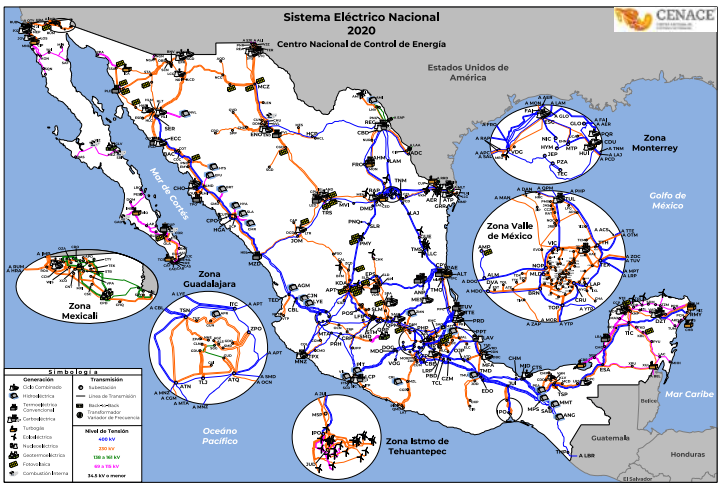

Figure 1.1: National Electric System. Backbone Transmission Network in Mexico [1].

Working on direct options that do not damage the power grid, respecting national and international regulations is currently a research sector in the country. Furthermore, various sources (see [2], see also [3]) assure a high economic-social impact in the use of alternative devices to grid consumption, which grants a series of facilities, rights, and obligations to the end-user.

An intermittent solution to the problems of conventional generation is the use of distributed generation (DG) that has been in use at the National Electric System but increasing over the years. Moreover, the data depicted in Figure 1.2 shows the total capacity in small and medium scale contracts, where it is worth noting that in the case of solar energy, small scale contracts are more considerable than medium-scale capacity. In addition, the Figure 1.3 represents the case of the potential of photovoltaic energy in Mexico, and more specifically in the case of San Luis Potosi, where the *Altiplano*, *Centro* and part of

the *Media* regions have a high potential of approximately 5 to 5.4 kWh (taking into account that these are data from 1999-2018).

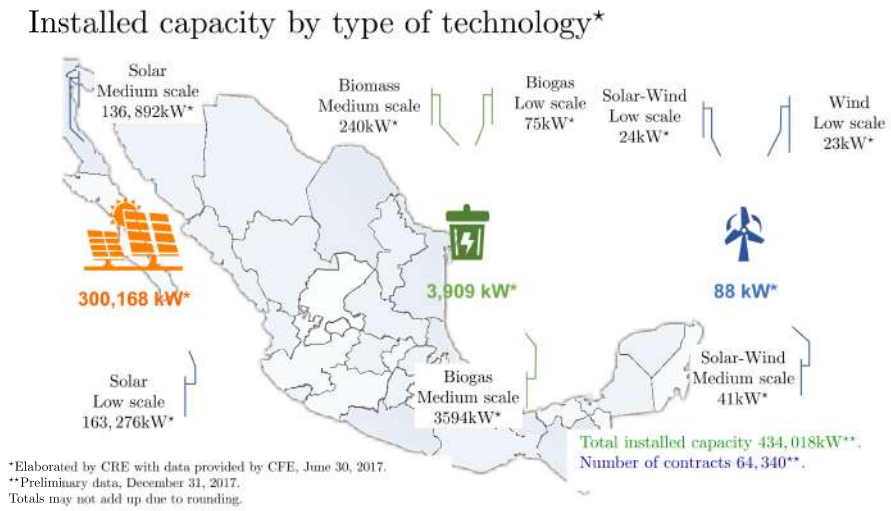

Figure 1.2: Small and medium scale interconnection contracts in Mexico [4].

Figure 1.3: Photovoltaic power potential in Mexico [5].

This chapter reviews some technical concepts that mark technological trends through distributed generation systems, where some of the most critical aspects are presented. With the introduction of these technologies, several questions arise that lead us directly to using the microgrid approach as a solution to DG's problems. Furthermore, the motivation of this thesis work is developed in the controllers of

individual power electronics systems, whose application can be of support within the structure of a microgrid architecture. Lastly, the technological surveillance, the achievements, and how this research is composed end the chapter.

1.1 DISTRIBUTED GENERATION

The concept of distributed generation, as mentioned above, is born based on the idea of redesign conventional generation systems. In addition, interconnecting small and medium scale systems in the conventional networks cause great benefits such as assisting in the generation by preventing overloads and relieving the inertia of the generators in power plants. An example of this is given in Figure 1.4, revealing that a classic grid that only provides potential from producers to consumers can be seriously affected if the demand becomes higher than what can be produced. On the other hand, a distributed generation scheme allows the integration of massive generation of energy from other types of sources and the aggregation of low-scale systems that also contribute to the flow of energy.

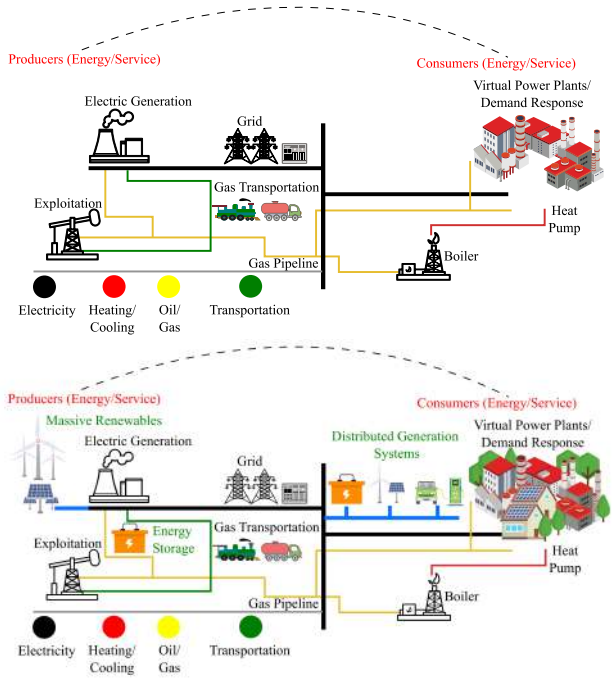

Figure 1.4: Comparison between conventional and distributed generation.

Accordingly to [6], the purpose of DG is to provide a source of active electric power and, it is not necessary to be able to provide reactive power. As a new approach in the electricity industry, multiple definitions can be described DG; the guidelines of DG was introduced in the IEEE 929-2000, a standard primarily based on photovoltaic sys-

tems, being replaced by the IEEE 1547 [7], which provides a good definition of DG and deals with all types of generation. The use of DG allows for a regulated and harmonious environment on the part of consumers, which in the case of a post-modernist grid, all agents act in separate consumption-generation flows and allows for the possibility of integrating new and better technologies.

1.1.1 *Value of Distributed Generation*

The value of DG rises thanks to its high advantages, in general to cost-effectiveness analyses, the profits it leaves to those who apply these designs, communication, among others. In general, the use of DG provides:

- Avoid the expensive and inefficient long-distance transmission of power.
- Support local economies and communities.
- A better life quality for those in which they are decentralized to the power grid.
- Resilient designs in case of natural disasters.

1.2 DG TECHNOLOGIES

Distributed generation technologies are mainly classified according to the type of contract that each country imposes for its interconnected systems depending in their grid code, for example in the case of Mexico, in Table 1.1 we can see an extract of the technical requirements for interconnection of power plants in the grid code [8]; this is how we can define if the contract is small, medium, large or massive-scale.

Table 1.1: Classification of a Power Station according to its capacity.

Synchronous area	Power Station Type A	Power Station Type B	Power Station Type C	Power Station Type D
National Interconnected System	$P < 500kW$	$500kW \leqslant P < 10MW$	$10MW \leqslant P < 30MW$	$P \geqslant 30MW$

DG has a large variety of technologies in terms of performance and role in the power network. It is essential to have a concise understanding of why these resources are necessary, their physical modeling, and their advantages. In this regard, we present some of the most critical technologies of DG.

1.2.1 *Fuel-Based Technologies*

There is a large number of fuel-based technologies, the combination of highly used materials such as fossil fuels, hydrogen as well as other types of fluids that have the property of combustion, including biomass and biogas generators, are part of this category and present us with the best of some resources in conjunction with power electronics. In this category, we find renewable fuels, as we can see in Figure 1.5, which have significant applications that nowadays present great advances in transportation.

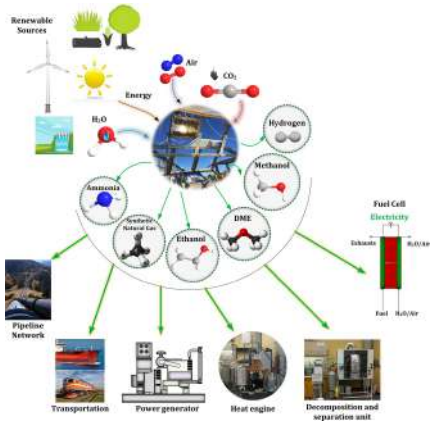

Figure 1.5: Clean fuel production from renewable fuels and some applications [9].

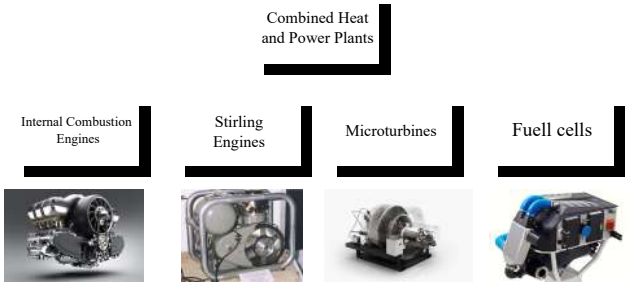

Figure 1.6: Micro-cogeneration systems classification.

Another type of fuel-based technology is micro-cogeneration, which is usually found in different uses such as in the home, in the countryside, in some commercial centers, and as a backup power source in small buildings that are needed when there is an electrical problem. In Figure 1.6 we can see the four most significant categories of this type of energy source. It should be noted that the use of micro-cogeneration allows flexibility in the power to be applied to their loads; a vital assertion is that the transportation of electricity is undoubtedly more expensive than the fuel and commissioning of micro-cogeneration systems.

1.2.2 *Renewable Energy-Based Technologies*

Renewable energies are perhaps the most famous technologies used for distributed generation systems: wind turbines, small hydro plants, and solar cells. When a system of this type of technology is composed of several types of it, it is known as a farm, as we can see in Figure 1.7. One of the significant advantages of this technology is that they are becoming easier to acquire. In the case of solar panels, they are manufactured individually and, as a result, a DES technology that can be used in a wide range of applications such as large to massive-scale systems as well as individual to low-scale systems, e. g., Figure 1.8. However, due to the construction processes, is difficult to have high efficiency in solar panels, besides a high cost of aerogenerators, including in both a technical continuous improvement.

Figure 1.7: Wind farm *Dominica* in San Luis Potosi [10].

Figure 1.8: Solar farm *Munisol* in Sonora [11].

1.2.3 *Energy Storage-Based Technologies*

Technologies based on energy storage are the most important and have the highest availability. There are multiple classifications of this type of technology, as we can see in Figure 1.9. In general, energy storage has played three leading roles and enhancing levels of power and frequency.
Energy storage systems are divided according to the class of tech-

nology used, such as mechanical, electrochemical, chemical, electrical, and thermal. In such approaches, the electric battery is the traditional method to store energy, which includes excellent availability and a large market where almost every electronic device includes or relies on it as its primary source. For example, large-scale storage based on electrochemical systems (see Figure 1.10) have been able to withstand severe changes in electrical systems, and their use in catastrophic events has ensured that specific sensitive loads are never disconnected. However, the high cost of this technology is still an essential factor in design considerations.

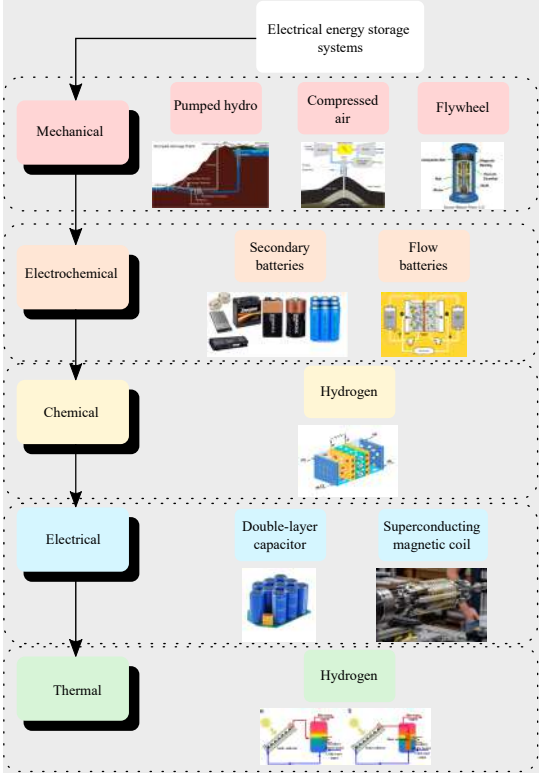

Figure 1.9: Class of energy storage Systems.

Figure 1.10: *Tesla* [12] massive energy-based system *Megapack*.

1.3 THE MICROGRID APPROACH

One of the biggest problems in distributed generation systems is synchronizing all its units and establishing an efficient control for the flow of energy. A promising solution to this problem is the microgrid (MG) approach, which is the interconnection of a group of distributed generation units, and due to the low-scale of its systems, it is possible to facilitate the integration of all systems with individual controls.
A MG is an interconnection of distributed energy sources (DES), such as microturbines, wind turbines, fuel cells, and photovoltaics integrated with storage devices, such as batteries, flywheels, and power capacitors on low voltage distribution systems (as a reference, see [13]). Even more, in [14] support the idea that a MG assumes a cluster of loads of *microsources* (DES systems at low-scale), which provides power and heat to some applications with multiple ports, as we can see in Figure 1.11 a standard structure with three different voltage buses, breakers for each one and a controller energy management.

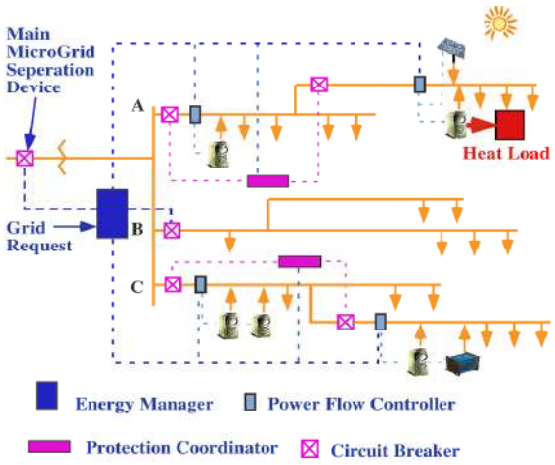

Figure 1.11: Microgrid Architecture.

The MG architecture (see Figure 1.12) is normally divided into two, for a DC-bus and AC-bus, which depends on the type of voltage bus to operate, where we can find almost all types of power electronic converters. Furthermore, a third category is designed using some coupled magnetics for interconnection in the grid.

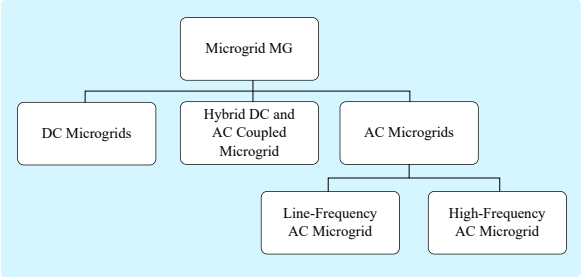

Figure 1.12: Classification of microgrids based on power type [15].

In particular, direct current microgrids (see Figure 1.13) operate DC-DC converters, injecting power to the DC bus and, by means of a decentralized converter, can inject its potential into the utility grid. DC microgrids have great advantages thanks to the high modularity and broad applications of their individual systems, and on a DC-bus, they can be able to satisfy basic needs such as washing machines and lighting systems as can be seen in Figure 1.14 to more specific applications. However, the commissioning of a microgrid is not a simple task as a number of responsibilities have to be fulfilled in order not to overexpose the power supplies of the microgrid.
Some possible criteria for the MG to fulfill the responsibility are as follows:

1. Ensure that the necessary electrical loads and heat are fulfilled by the microsources;
2. Ensure that the MG satisfies operational contracts with the utility;
3. Minimize emissions and/or system losses; and
4. Maximize the operational efficiency of the microsources.

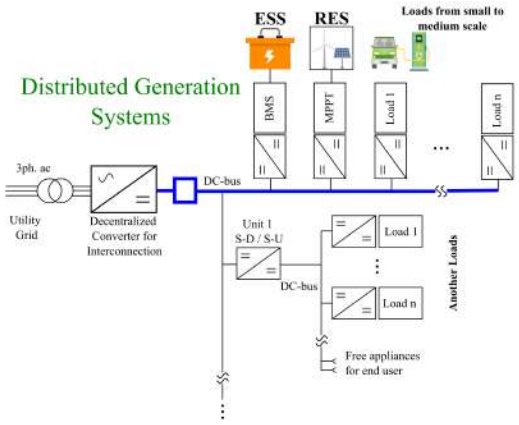

Figure 1.13: Generic example of a DC-MG.

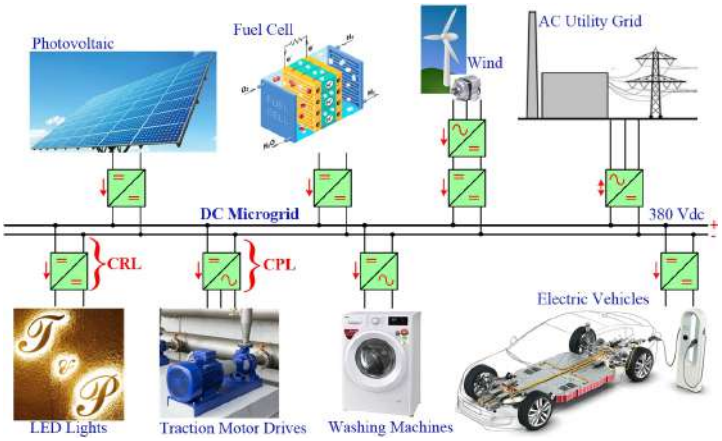

Figure 1.14: Future direct current (DC) microgrids [16].

Notwithstanding, the problem of the design object is based mainly on power electronics, so on many occasions, we can find new devices whose properties are sophisticated, but at the same time are high-gain, low-stress in the components to ensure an amount of useful life and above all that the weight of the converters is less and less. Therefore, the motivation for this work comes directly from the needs that can be exemplified in a converter for later use and to ensure the correct control of this class of devices. Then, the overall control objectives of a MG are to ensure:

1. proper working of preloaded operations that change from one equilibrium point to another point (without causing operational hazards) but satisfying the tolerance limits loaded by the designer.

2. necessary power distribution levels (active and reactive) in the microgrid and in its source or distribution channel.

3. perfectly integrated disconnection and connection.

4. optimization of the power electronics systems in case of overload and their observation and mitigation of failures when they exceed their critical load value.

1.4 MOTIVATION

At this point, we have generally talked about DG systems, MG, their advantages, and some of the disadvantages of different types of DES technologies. The interconnection of each distributed generation technology with the DC-bus is achieved using power electronics converters, which are responsible for injecting certain power levels and updating the energy management between the microgrid, the operator, the manifesting loads, and the distributed generation sources.
The control objective of energy management is voltage regulation and

stabilization; controls are classified as centralized, decentralized, and local. All three have different attributes, but the local control, which is the most basic category, performs the stabilization of the individual power electronic devices, which allows us to concentrate on the needs that these have when they are connected with sources of distributed generation. Therefore, we are motivated to develop individual control schemes that can face these responsibilities to be applied in a MG for low-scale systems. In addition, the IEEE [17] defines a control problem as *"a design problem concerned with constructing a device called the controller whose goal is to force the controlled variable of the plant or process to behave in a desired manner. The elements of the control problem are control objective, a model of the process to be controlled, admissible controllers, and a means of evaluating the performance of a control strategy."*
As mentioned above, the use of MG can contribute to the problems of distributed generation technologies to monitor, regulate and control the flow of energy. Additionally, MG can help for the interconnection of specific schemes in the electrical network and work independently (also known as island mode) for certain types of applications. In particular, a topic of interest is the electrification of the communities where the electrical power line is difficult to access, such as the case of Figure 1.15 where we can see challenging access for its population, and that, due to their geographical location, they lack benefits in consequence of not having electricity in their homes (see as supplementary information [18]). Undoubtedly, this type of scheme will change how electrical energy is distributed and consumed for all types of sectors [19]; however, there are still intermittent questions about the capacity that a microgrid may have to be carried out in a particular community. Beyond knowing whether or not an operator of the energy mechanisms is needed, certain operating expenses and continuous improvement must also be considered.

Figure 1.15: Community of *El Resumidero*, Rioverde, San Luis Potosi, Mexico.

However, with a motivation for an ambitious project such as evaluating the microgrid in island mode for a community without electricity, specific objectives have to be addressed first; ensuring the proper functionality of these stand-alone systems using local control, even more to having sufficient power capacity for their use, is an important

issue. Consequently, the approach of using control engineering to develop tools for the proper operation of power electronics converters in addition to face several targets such as regulation, reliability and performance, this research work is justified.

1.5 LITERATURE REVIEW

Power electronics converters, in a nutshell, are responsible for bringing a level of current and voltage as input to another level of output while ideally respecting its power. The efficiency is linked to this last concept because being devices switched by high-frequency levels, the parasitic elements of their passive devices usually take a certain percentage, thus affecting the system's efficiency. Notably, direct current to direct current (DC-DC) converters that mostly use distributed generation technologies to inject into a DC-bus are the step-up topologies. Step-up converters have a wide range of applications, as we can see in Figure 1.16, and depending on this, specific categories can be selected for use.

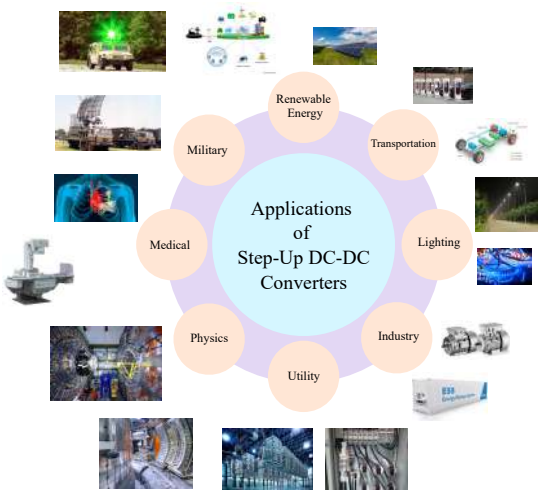

Figure 1.16: Applications of DC-DC converters.

The technological surveillance begins mainly motivated by [20], in which we can see a novel for step-up DC-DC converters. On the other hand, in terms of control, we have to satisfy that our approaches:

- Ensure asymptomatic stability and
- Be an alternative to heuristic tunings methods.

There is currently a broad interest in power electronic converters with a high conversion ratio due to the emergence of new needs in many applications for step-up converters. Consequently, the literature reports a large number of configurations available for voltage boost, as we can see in Figure 1.17.

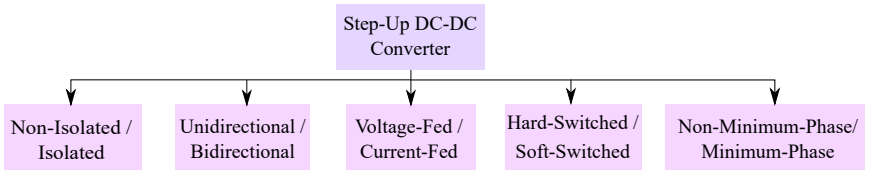

Figure 1.17: Categories for step-up converters.

Among the most common categories are the type converters: isolated or non-isolated, unidirectional and bidirectional, with minimum and non-minimum phase, powered by voltage or by current (see Figure 1.18). Furthermore, different voltage elevation techniques have been reported, among these: switched capacitor, switched inductor, switched capacitor and inductor, voltage multiplier, magnetic coupling, and multiple stages.

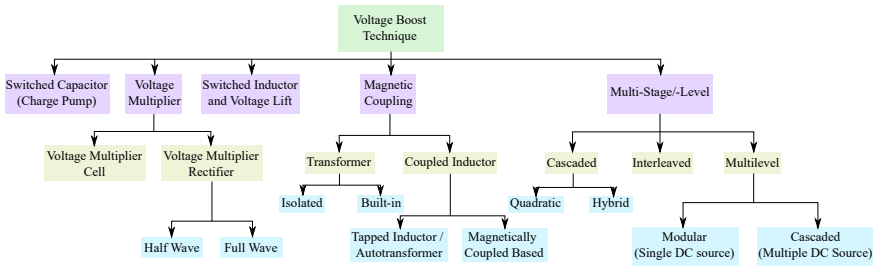

Figure 1.18: Voltage booster technologies.

In this sense, this research work proposes to use a non-isolated unidirectional configuration powered by voltage, with the purpose of processing energy by a renewable source and be able to be part of a MG in order to follow the ideas introduced above.
On the other hand, concerning the dynamic modeling of power converters, there are two approaches: traditional modeling using Kirchhoff's laws and modeling based on the converter's energy. Both methodologies have been widely used for the synthesis of controllers [21].

In this work, we revised five step-up topologies whose technical aspects in terms of efficiency were similar (see Table 1.2); their electrical features are depicted in Table 1.3. We can notice that all these converters are high-gain; however, one of the essential factors in the selection of these candidates was their ability to switch from continuous conduction mode (CCM) and discontinuous conduction mode (DCM) employing the factor K_{crit} including the duty cycle δ, and the capacity of R_{crit}.

The value of R_{crit} is critical in the control design since it is an indicator for robustness tests to consider that allows several data to the system can be taken only knowing the switching frequency in which the converter operates, R_{crit} depends mainly on the K_{crit} factor that arises from the equivalent inductance L_{eq} and these two give us the information of the operation boundaries since it is desirable only to operate in CCM.
Beyond that the efficiencies are in similar values, it is worth highlighting the value of R_{crit} in the converter considered is the one that has the most excellent flexibility to support load steps, in addition to the fact that in technical matters it is the one with the least number of devices uses what makes it also the most profitable in terms of cost-benefit. Also, we can see in Figs. 1.19–1.20 the boundaries between CCM and DCM as well as the voltage gain as functions of the duty cycle, again the considered topology (ASL-SU2C) have outstanding performance when the conversation ratio (duty cycle) tends to the unity.

Table 1.2: Technical aspects of the DC-DC topologies.

Converter	K_{crit}	L_{eq}	R_{crit}	Peak efficiency (reported)
Considered	$\frac{\delta(1-\delta)^2}{2(1+3\delta)}$	$\frac{2L_oL}{2L+L_o}$	$0.05194f_{sw}$	96.84%
In [22]	$\frac{\delta(1-\delta)}{12\delta+6}$	$\left[\frac{1}{L_1}+\frac{1}{L_2}+\frac{1}{L_3}\right]^{-1}$	$0.00664f_{sw}$	97.8%
In [23]	$\frac{\delta(1-\delta)^2}{8(\delta+2)}$	$\left[\frac{1}{L_1}+\frac{1}{L_2}+\frac{1}{L_3}\right]^{-1}$	$0.04645f_{sw}$	96.5%
In [24]	$\frac{\delta(1-\delta)^2}{2(1+\delta)}$	L	$0.00746f_{sw}$	92.2%
CBC [25]	$\delta(1-\delta)^2$	L	$0.00426f_{sw}$	65%

Table 1.3: Electrical features of the considered and other transformerless hybrid DC-DC topologies.

Converter	Gain	Number of semiconductor devices	Number of inductors & capacitors	Constant input current
Considered	$\frac{1+3\delta}{1-\delta}$	2 Switches 2 Diodes	3 Inductors 3 Capacitors	No
In [22]	$\frac{1+2\delta}{1-\delta}$	1 Switches 3 Diodes	3 Inductors 5 Capacitors	Yes
In [23]	$\frac{2+2\delta}{1-\delta}$	1 Switches 5 Diodes	3 Inductors 7 Capacitors	Yes
In [24]	$\frac{1+\delta}{1-\delta}$	2 Switches 1 Diodes	1 Inductors 2 Capacitors	No
CBC [25]	$\frac{1}{1-\delta}$	1 Switches 1 Diodes	1 Inductors 1 Capacitors	Yes

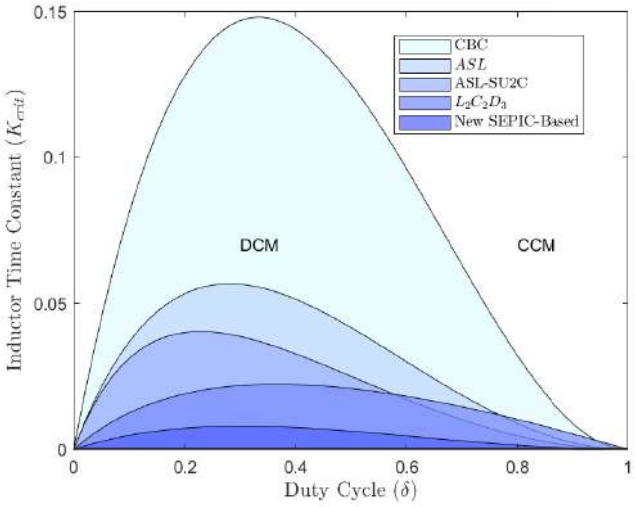

Figure 1.19: CCM and DCM as a function of the duty cycle δ.

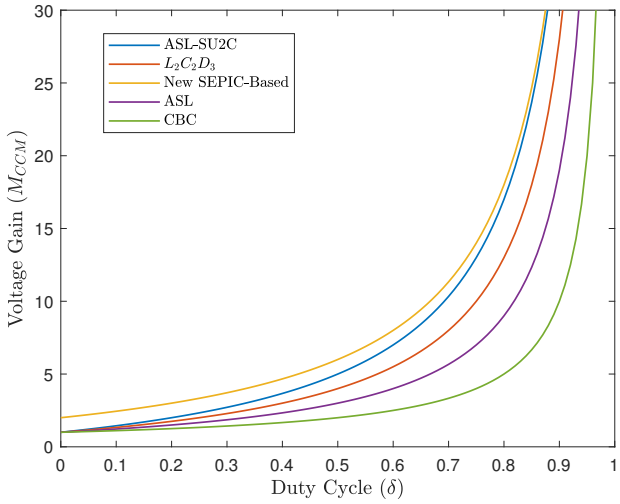

Figure 1.20: Voltage gain as a function of the duty cycle δ.

1.6 RESEARCH OBJECTIVES

Once the converter used in this work has been selected and returned to the motivations, beyond carrying out local control for this system with all the design guidelines, modeling in dynamic equations and control have not been reported. Under this premise, the research scopes are based only on the control design; however, the sequential challenge to this research is the interconnection of more schemes of this type in a microgrid. Therefore the research objectives based locally on the control are the following

Main Objective

Design a control scheme to achieve the correct operation of a step-up DC-DC converter with a high conversion ratio with parametric uncertainty and changes in load.

Specific Objectives

- To select a step-up topology.
- To derive the dynamical model of the power electronic converter.
- To synthesize a control law that ensures asymptotic stability of the closed-loop under parametric uncertainty and external disturbances.
- To perform numerical validation of the control law.

1.7 SCOPE AND CONTRIBUTIONS

In this thesis, two control techniques are mainly reviewed. In the linear approach, the developments are made through the crossing roots theory, thus designing a geometric approximation of the stability boundary using cascade control. In the nonlinear approach, using the widely developed ideas in passivity theory, passive PI control is designed with the characteristic of adaptability using the immersion and invariance observer to estimate the changes in load.

This research work was carried out for the most part in the Center for Research and Graduate Studies (CIEP) at the Faculty of Engineering of the University of San Luis Potosi. Thanks to the experiences developed during the thesis process, it was possible to submit the following conference papers:

- E. Moreno-Negrete, J.E. Hernández-Díez, C.F. Méndez-Barrios, D. Langarica-Córdoba, H. Miranda-Vidales, L. Félix, *PI Control Scheme Design of High Gain Transformerless DC-DC Converter* at the 23rd European Conference on Power Electronics and Applications EPE-ECCE 2021.
- E. Moreno-Negrete, C.F. Méndez-Barrios, D. Langarica-Córdoba, *On the PI-PBC Controllers for a High-Gain Transformerless DC-DC Converter* at Latin American Congress on Automation and Robotics LACAR 2021.

1.8 THESIS OVERVIEW

This thesis work is structured as follows:

Chapter 2 presents a series of mathematical preliminaries, including the modeling of the considered converter, stability via $\mathcal{D}$-decomposition theory, and concepts of port-Hamiltonian for switched power converters used throughout the thesis work.

In chapter 3, the linear analysis is presented under the considerations of a system designed in a single control loop in comparison with a cascade control, developing the methodology called σ-stability for its stability analysis in the vein of previous works motivated for $\mathcal{D}$-decomposition theory and robust control.

In Chapter 4, the modeling of the system under the Hamiltonian formulation is discussed; in addition to reviving the concepts of passive PI converters under the incremental model, also the immersion and invariance observer is designed.

Chapter 5 presents the results of the numerical simulation of the closed-loop system in the MATLAB environment. Linear and nonlinear control schemes are used, a load system is considered under ideal conditions, and the load changes in which the observer is included to face the parametric uncertainties; in addition, the limitations of using σ-stability are added through some examples based on the transient-response specifications for each controller.

Finally, in chapter 6, the conclusions of the work carried out are derived, and it is discussed in some lines about possible future work in the spirit of the motivation of this thesis.

Part I

PRELIMINARIES

"A dynamical system consists of three elements, a setting (called the state space); a mathematical rule or dynamic; and initial condition or state".

— Haddad & Chellaboina

2

MATHEMATICAL MODEL OF THE DC-DC CONVERTER

It is well known that switched capacitor and inductor structures in DC-DC converters have the advantages of low cost, small size, high power density and fast dynamic response (see, e.g., [20]). This is also discussed in [26], where the general ideas of step-down and step-up structures are presented for its implementation in high gain hybrid transformerless DC-DC converters. Among these, the most common network topologies are passive switched-capacitor (PSC or SU2C), active switched-inductor (ASL) and hybrid ASL (see generally, [27]; see also, [28]). Actually, the above-mentioned topologies are commonly used in a variety of applications, such as: transportation, telecommunications, renewable energy, to mention a few. As stated in [29], these are applications in which DC-bus voltage regulation under the presence of parametric, input and load variations is required.
This chapter is organized as follows. Firstly, the next section is dedicated to the dynamic model of the considered topology ASL-SU2C DC-DC converter under the same considerations and values established in [30]. To this end, we derive switched and averaged models, where such a linear model is only valid around a particular operating point. Secondly, the linear model of the system is designed using the small-signal approach, and the desired transfer functions for the control loops are obtained. The following section develops the ideas behind the $\sigma-$stability analysis used afterward to carry out the controller's design.
On the other hand, a set of theorems and definitions most commonly used in passivity theory are presented, particularly port-Hamiltonian and their proper structure for switched power converters. Additionally, the study of immersion and invariance theory as a class of first-order observers is presented to add adaptive properties to the closed-loop in the moments of parametric variation.

2.1 STEP-UP DC-DC CONVERTER MODELLING

Consider the ASL-SU2C electrical circuit and its composing elements depicted in Figure 2.1 with its corresponding parameters in Table 4.1, the general advantages of the ASL-SU2C are:

1. lower count of switches devices,
2. lower voltage stress,
3. two power switches during on and off modes,

4. experimental peak efficiency [30] of 96.84%,
5. load resistance $R_{crit} \approx 259\Omega$.

The full operation of this converter consists in two different switching states $S_1 = S_2 = 1$ and $S_1 = S_2 = 0$ (ON and OFF states, respectively), noticing that a property in the switched inductor and capacitor structures the ASL network $L = L_1 = L_2$ as well as in the SU2C $C = C_1 = C_2$. These are described through its correspondent equivalent circuits by Kirchhoff's voltage and current laws. Thus, first, we derive the so-called switched model by combining both analyses in a state-space representation. Second, we apply the before mentioned small-signal analysis to derive an averaging differential model in terms of the state variable $x = [i_L, v_C, i_{Lo}, v_{Co}]^T$ and the control input $u = \delta$. Here, δ represents the duty cycle for a pulse width modulation considering the above-mentioned switching states. It is important to mention that no matter how detailed a model is, it can never make an accurate representation of a real physical system. For this modeling, it was decided not to include parasitics of the passive elements and other extensions of uncertainty that can be modeled using a specific input source. However, it is desirable to perform the physical prototype and compare whether adding the errors caused by these small dynamic changes is worthwhile (if so, we recommend reading [31] where a guide for models with uncertainty is presented).

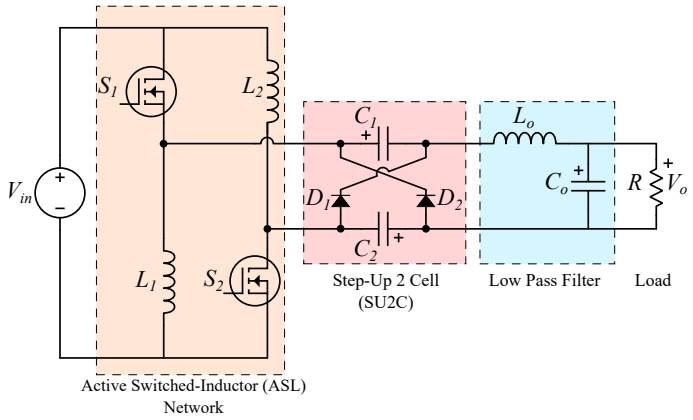

Figure 2.1: ASL-SU2C electrical circuit.

Table 2.1: Parameters and nominal conditions

L	C, C_o	L_o	R	δ	V_{in}	V_o	f_{sw}	P_o
223µH	1µF	2.34mH	338Ω	0.75	20V	260V	50kHz	200W

One starts by noting that the full operation of the circuit can be described by constant (DC signal) and dynamical (transient) behaviors.

More precisely, $x = X + \tilde{x}$ and $u = D + \tilde{u}$, where, $X = [I_L, V_C, I_{Lo}, V_{Co}]^T$ denote a constant operating point computed by means of nominal conditions

$$\begin{aligned} V_C &= V_{in}\left(\frac{1+D}{1-D}\right), \\ V_{Co} &= V_{in} + V_C(1+D), \\ I_{Lo} &= \frac{V_{Co}}{R}, \\ I_L &= I_{Lo}\left(\frac{1+D}{1-D}\right), \end{aligned} \tag{2.1}$$

the filter cut-off frequency is defined by

$$f_c = \frac{1}{2\pi\sqrt{L_o C_o}} = 3290.12\text{Hz}. \tag{2.2}$$

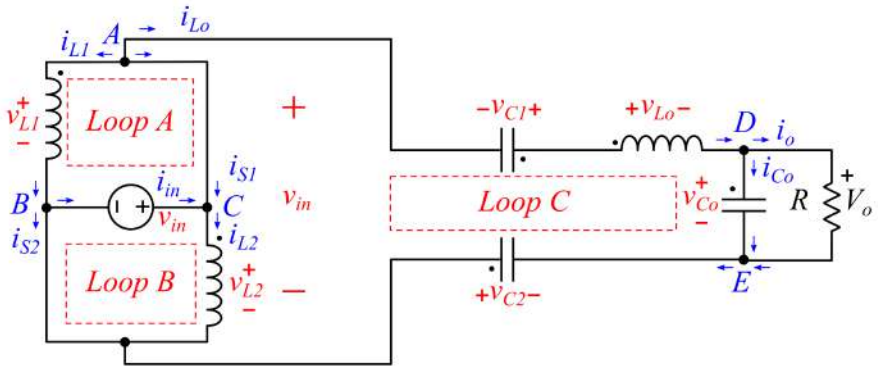

Figure 2.2: Mode ON, $S_1 = S_2 = 1$.

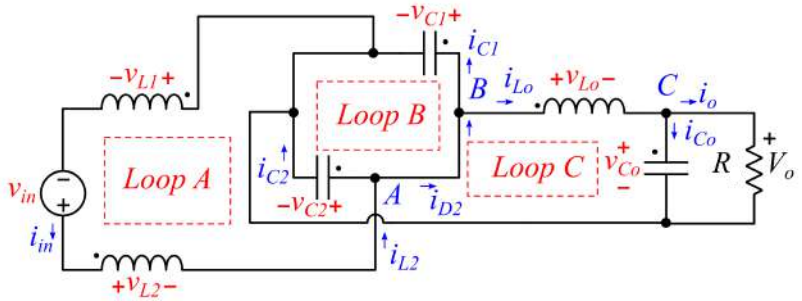

Figure 2.3: Mode OFF, $S_1 = S_2 = 0$.

Performing ON and OFF modes depicted in Figs. 2.2–2.3, and combining state equations into a single averaged state-space model using

$$\dot{\mathbf{x}} = [\mathbf{A}_{on}\delta + \mathbf{A}_{off}(1-\delta)]\,\mathbf{x} + [\mathbf{B}_{on}\delta + \mathbf{B}_{off}(1-\delta)]\,v_{in}, \tag{2.3}$$

we have

$$\begin{bmatrix} \dot{i}_L \\ \dot{v}_C \\ \dot{i}_{Lo} \\ \dot{v}_{Co} \end{bmatrix} = \begin{bmatrix} 0 & -\frac{1-\delta}{2L} & 0 & 0 \\ \frac{1-\delta}{2C} & 0 & -\frac{1+\delta}{2C} & 0 \\ 0 & \frac{1+\delta}{Lo} & 0 & -\frac{1}{Lo} \\ 0 & 0 & \frac{1}{Co} & -\frac{1}{RCo} \end{bmatrix} \begin{bmatrix} i_L \\ v_C \\ i_{Lo} \\ v_{Co} \end{bmatrix} + \begin{bmatrix} \frac{1+\delta}{2L} \\ 0 \\ \frac{\delta}{Lo} \\ 0 \end{bmatrix} V_{in}. \tag{2.4}$$

Simulating the system under nominal conditions, we obtain the waveforms shown in Figure 2.4 matching our modeling with the values reported under the same conditions where the input inductor current ripple is 25% with 5.383A average current, the output inductor current ripple is 33% with 0.769A average current and the output capacitor voltage ripple is 8% with 260V average voltage.

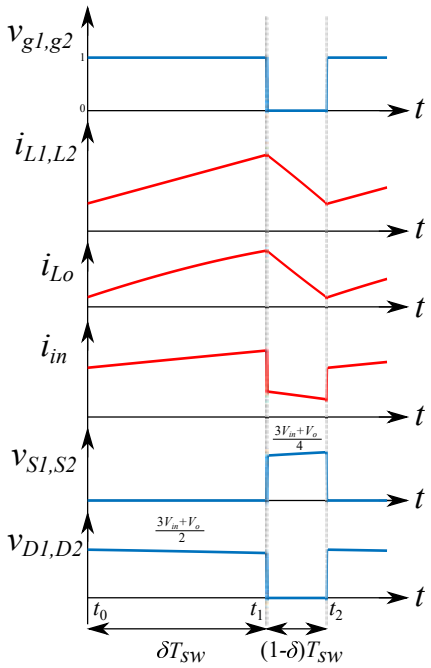

Figure 2.4: Key waveforms of the considered converter in CCM operation.

2.2 SMALL SIGNAL APPROACH

The nonlinear system in (2.4) is commonly called large-signal due to the sum of the constant and transient behaviors that compose the dynamics of the converter. Furthermore, separating the DC signal of

the nonlinear system, we can compute the transient behavior as small state signals

$$\tilde{x} = \left[\tilde{i}_L, \tilde{v}_C, \tilde{i}_{Lo}, \tilde{v}_{Co}\right]^T, \tag{2.5}$$

with $\tilde{u}$ governed by the averaged model; thus, the small-signal model is computed as

$$\dot{\tilde{\mathbf{x}}}(t) = \underbrace{\begin{bmatrix} 0 & -\frac{1-U}{2L} & 0 & 0 \\ \frac{1-U}{2C} & 0 & -\frac{1+U}{2C} & 0 \\ 0 & \frac{1+U}{Lo} & 0 & -\frac{1}{Lo} \\ 0 & 0 & \frac{1}{Co} & -\frac{1}{RCo} \end{bmatrix}}_{\mathbf{A}} \tilde{\mathbf{x}}(t) + \underbrace{\begin{bmatrix} \frac{V_C+V_{in}}{2L} \\ -\frac{I_L+I_{Lo}}{2C} \\ \frac{V_C+V_{in}}{Lo} \\ 0 \end{bmatrix}}_{\mathbf{F}} \tilde{u}(t). \tag{2.6}$$

Equation (2.6) describes the dynamic part in this approach. Thus, in the spotlight of Laplace transform (see, [32]-[33], for further details), the transfer functions depending on the state are defined by the equation

$$\frac{\tilde{\mathbf{X}}(s)}{\tilde{U}(s)} := [s\mathbf{I} - \mathbf{A}]^{-1}\,\mathbf{F} \equiv \frac{\mathrm{adj}\,[s\mathbf{I} - \mathbf{A}]\,\mathbf{F}}{\det\,[s\mathbf{I} - \mathbf{A}]}, \tag{2.7}$$

and considering the particular electric circuit parameters depicted in Table 4.1, one computes the corresponding numerical transfer functions

$$\begin{aligned} G_1(s) &:= \frac{\tilde{V}_{Co}(s)}{\tilde{U}(s)} = \frac{6.838 \times 10^{10} s^2 - 2.301 \times 10^{15} s + 3.833 \times 10^{19}}{s^4 + 2959 s^3 + 1.152 \times 10^9 s^2 + 2.143 \times 10^{12} s + 2.994 \times 10^{16}}, \\ G_2(s) &:= \frac{\tilde{I}_L(s)}{\tilde{U}(s)} = \frac{3.587 \times 10^5 s^3 + 2.786 \times 10^9 s^2 + 4.267 \times 10^{14} s + 1.531 \times 10^{18}}{s^4 + 2959 s^3 + 1.152 \times 10^9 s^2 + 2.143 \times 10^{12} s + 2.994 \times 10^{16}}. \end{aligned} \tag{2.8}$$

These provide a frequency-based interpretation of the dynamical behavior of the ASL-SU2C electrical circuit used for the control scheme design in Chapter 3. Note that $G_1(s)$ is of non-minimum phase due to the change of sign in the numerator and that $G_2(s)$ is of minimum phase.

2.3 STABILITY VIA THE BOUNDARY CROSSING THEOREM

In the last sections, the converter was mathematically modeled through a conventional approach where the system is divided into two parts,

its representation in the state-space and the small-signal (linear) model; however, these are only the dynamic description of the system. In this section, and under the premise of developing the linear control method designed in this thesis, we review some mathematical theories for stabilization used in robust control.

One classical problem determining the stability of a system via transfer function is the study of its coefficients in the characteristic equation of the closed-loop system. The approach of The Boundary Crossing Theorem reported in [34] and also in [35] presents the preliminary idea of a *stability boundary*.

THEOREM 2.3.1

Let us consider the complex plane $\mathcal{C}$, and let $\mathcal{S}$ be any given open set. We know that $\mathcal{S}$, which is its boundary $\partial\mathcal{S}$ together with the interior $\mathcal{U}^0$ of the closed set $\mathcal{U} = \mathcal{C} - \mathcal{S}$, form a partition of the complex plane, that is

$$\begin{aligned} \mathcal{S} \cup \partial\mathcal{S} \cup \mathcal{U}^0 &= \mathcal{C}, \\ \mathcal{S} \cap \mathcal{U}^0 = \mathcal{S} \cap \partial\mathcal{S} &= \partial\mathcal{S} \cap \mathcal{U}^0 = \emptyset. \end{aligned} \tag{2.9}$$

With the restriction that all the sets are non-empty. Considering $P(\lambda, s)$ a family of polynomials of fixed degree n, which is continuous concerning the parameter λ on a fixed interval.

THEOREM 2.3.2

Boundary Crossing Theorem

Suppose that $P(\lambda_1, s)$ has all its roots in $\mathcal{S}$, where $P(\lambda_2, s)$ has at least one root in $\mathcal{U}$. Then, there exists at least one root ρ in $(\lambda_1, \lambda_2]$ such that

1. $P(\rho, s)$ has all its roots in $\mathcal{S} \cap \partial\mathcal{S}$.
2. $P(\rho, s)$ has at least one root in $\partial\mathcal{S}$.

The proofs of this pair of theorems are carried out in the spotlight of *Rouché's Theorem* granting the possibility to find at least one root in the interior $\mathcal{U}$ that lies directly in (2.9).

Example 1. Consider the polynomial

$$p(s) = \lambda_1 s + \lambda_2,$$

with the parameters region $\mathcal{P} := [\lambda_1, \lambda_2]$, and suppose that $p(s)$ is a Hurwitz polynomial for some point in $\mathcal{P}$. Now let the parameters travel along the paths $\mathcal{T}_1, \mathcal{T}_2$ referring to Figs. 2.5–2.6, from $(\lambda_{1_o}, \lambda_{2_o})$ to $(\lambda_{1_f}, \lambda_{2_f})$. The trajectory $\mathcal{T}_1$ respects the continuous property, there

is no loss of degree along even if a parametric variation occurs, so, the root motion for $s_i(\lambda_1, \lambda_2)$ is continuous too, with $i \in \{1, \ldots, n\}$ and has $s = 0$ as a root at $\lambda_1 = 0$ and thus boundary crossing does occur. On the other hand, when the parameters travel along the path $\mathcal{T}_2$ and reach discontinuous points has a $j\omega$ root for finite ω including a loss of degree, therefore, boundary crossing does not occur.

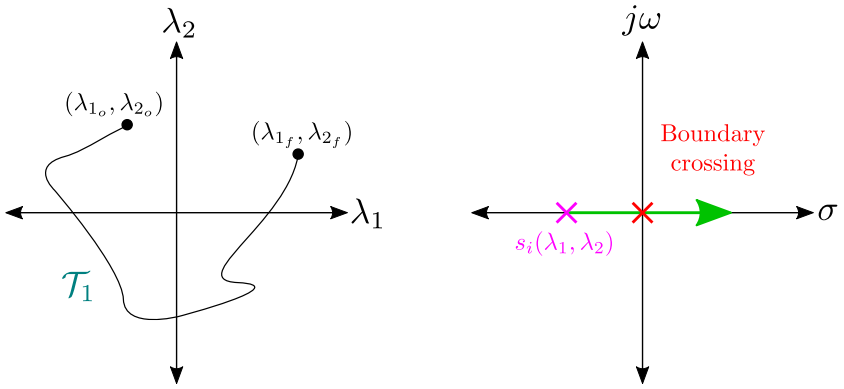

Figure 2.5: Parameters space and root locus for $\mathcal{T}_1$.

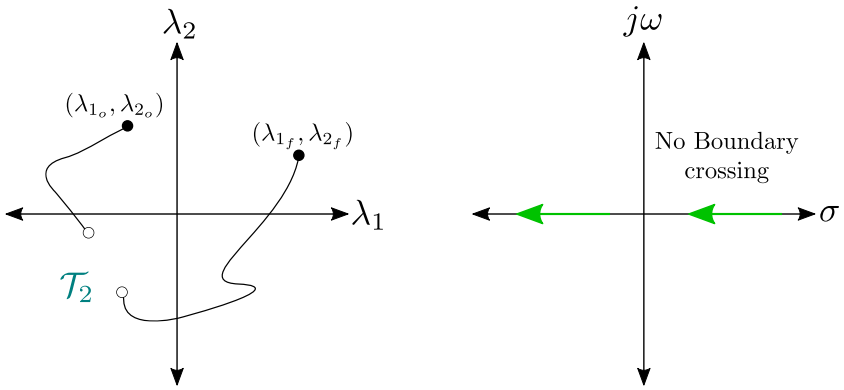

Figure 2.6: Parameters space and root locus for $\mathcal{T}_2$.

The above results guarantee in an abstract way how to obtain the stability boundary as an alternative to the classical approaches and stability tests given any polynomial. As a purely mathematical tool, it has to be adapted to the case of study; therefore, under the right conditions (linear approach), it can be strongly associated with a graphical representation and singularly by algebraic curves (see [36] as a reference), a peculiarity of *Hilbert's 16th Problem*.

2.4 $\mathcal{D}$-DECOMPOSITION THEORY

The above results allow us to demonstrate the existence of the boundary crossing for trajectories that respect the continuity properties, but

the remaining question would be what would happen if the trajectory ends at the same point where it began e. g., Figure 2.7.

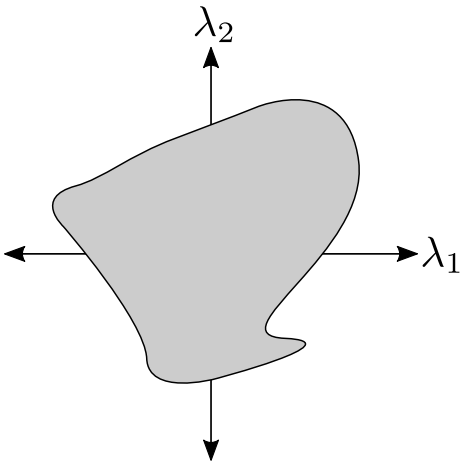

Figure 2.7: Closed path.

In order to solve the characterization of the interior of the parametric plane created by a closed path, a couple of motivations in the work of the theory of $\mathcal{D}-$decomposition presented in [37] and [38] by the same author to share some results in the spotlight of [39] the first approach of stability domain for the third order polynomial with two uncertain parameters. Some important data are listed below

- The technique was first introduced by Vysnegradski [39] in 1877 in a study of the stability domains of governors and was rediscovered in the USSR.
- Neimark [40] popularized the $\mathcal{D}$-decomposition developing a method for the stability domain analysis in 1947.
- *Robust control: the parameter space approach* and *Nonlinear systems: the parameter analysis and design* by Ackermann, J. [41], and Siljak D. [42] were the first Western literature that addressed the method.
- "Its use for the design of low-order controllers for linear systems is very efficient", *Analytical Design for PID controllers* by Diaz-Rodriguez, Ivan D. *et. al.* [43].

This work, in conjunction with the boundary crossing theorem, determined the characteristics of stability domains and made an advance in robust control under a parametric approach.
To describe the $\mathcal{D}-$decomposition, we use some particular definition presented in [44] wherein a technical manner treats the first approaches using the *Index Property* to graph some stability domains.

DEFINITION 2.4.1

$\mathcal{D}$—decomposition

Consider a linear system whose characteristic equation is

$$\sum_{i=1}^{n} \lambda_i G(s) = 0, \tag{2.10}$$

where s is the Laplace transform complex variable ($s = \sigma + j\omega$), the G_i are rational functions and the λ are real valued parameters.
Now, the n dimensional vector space Λ, of which the λ coordinates, can be decomposed into sets denoted by $D(k, N-k)$, which corresponds to

$$\sum_{i=1}^{n} \lambda_i G(s) = 0,$$

having k zeros in the left half s plane (LHP) and $N-k$ zeros in the right half s plane (RHP), where N is the total number of zeros of the characteristic equation.
The system is stable for those values of the λ_i which lie inside the set $D(N, 0)$. Such decomposition of the parameter space Λ into sets $D(k, N-k)$ is called $\mathcal{D}$-decomposition.

2.4.1 *$\mathcal{D}$-decomposition method*

In this part, we review some exciting results of the works mentioned above to make some remarks for using this theory for one and two parameters. Finally, the question that will be the result and used in the linear approach of this work is added and other compelling results.

One real parameter

Consider the one-parameter family of polynomials

$$P(s, \lambda) = \{a(s) + \lambda b(s), \lambda \in \mathbb{R}\}, \tag{2.11}$$

where $a(s)$ and $b(s)$ are given mth- and nth-degree polynomials with real coefficients, respectively ($n \geqslant m$).

THEOREM 2.4.1

Let $a(s)$ and $b(s)$ be the nth-degree polynomials with real coefficients. Then the polynomial $P(s, \lambda) = a(s) + \lambda b(s)$, has no more $(n+1)$ seg-

ments of $\mathcal{D}$-decomposition by λ and not more than $\lceil \frac{n}{2} \rceil$ stability segments.

The values of λ for which roots pass from one half-plane to another are

$$\lambda(\omega) = -\frac{a(j\omega)}{b(j\omega)}, \quad \Im(\lambda) = 0, \quad \omega \in (-\infty; \infty), \quad a_n + \lambda b_n = 0.$$

Example 2. The polynomial $P(z, \lambda) = z^n + \lambda z^{n-1} + \epsilon z^{n-2} + \alpha$, where $1 < \epsilon < 1 + \frac{2}{(n-2)^2}$ and $\alpha = 1 - \epsilon - \frac{1}{n^2}$, has $\lceil \frac{n}{2} \rceil$ stability segments. Using the formulas for λ provided in Theorem 1, the segments of $\mathcal{D}$-decomposition are $(n-1)$ for the case.

Using the formulas for λ provided in Theorem 1, the segments of $\mathcal{D}$-decomposition are $(n-1)$ for $n = 8$ has $\lceil \frac{n}{2} \rceil$, thus there are 9 segments of $\mathcal{D}$-decomposition and 4 stability domains as shown in Figure 2.8.

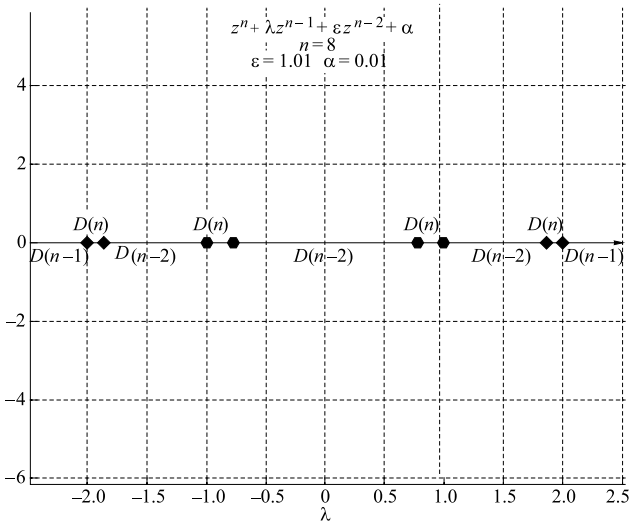

Figure 2.8: Stability domains in Example 2 [37].

The equation for the parameter λ is as follows, noting that $z = e^{j\omega}$

$$\lambda(\omega) := \left(-z^n - \epsilon z^{n-2} - \alpha\right) z^{-n+1},$$
$$\lambda(\omega) := -e^{j\omega} - \epsilon e^{-j\omega} - \alpha e^{-(n-1)j\omega}.$$

If $\Im(\lambda) = 0$, and using $\sin(\omega) = \Im\left(e^{j\omega}\right)$

$$\Im(\lambda) = \Im(e^{j\omega}) - \epsilon\Im(e^{-j\omega}) - \alpha\Im(e^{-(n-1)j\omega}) = 0,$$
$$\Im(\lambda) = (\epsilon - 1)\sin(\omega) + \alpha\sin(n-1)\omega = 0,$$

has n solutions on the interval $[0, \pi]$, because $|\alpha| > |\epsilon - 1|$.

One complex parameter

Let us consider the one-parameter family of polynomials

$$P(s,\lambda) = \{a(s) + \lambda b(s),\ \lambda \in C\}, \tag{2.12}$$

where $a(s) = a_n s^n + \ldots + a_1 s + a_0$ and $b(s) = b_n s^n + \ldots + b_1 s + b_0$ are the nth-degree polynomials with real coefficients. The equation

$$\lambda(\omega) = -\frac{a_0 + a_1 j\omega + \ldots a_n (j\omega)^n}{b_0 + b_1 j\omega + \ldots b_n (j\omega)^n}, \quad \omega \in (-\infty, \infty),$$

defines the curve of $\mathcal{D}$-decomposition of the complex plane of λ

THEOREM 2.4.2

Let $a(s)$ and $b(s)$ be the nth-degree polynomials with real coefficients. Then the polynomial $P(s,\lambda) = a(s) + \lambda b(s)$, $\lambda \in C$, has no more than $(n-1)^2 + 2$ domains of $\mathcal{D}$-decomposition by λ.

Example 3. The $\mathcal{D}$-decomposition by the complex parameter λ of the polynomial $P(z) = z^n + \lambda z^{n-1} + \alpha$, $\lambda \in C$, $\alpha > 1$, consists of $(n-1)^2 + 1$ domains.

$$\lambda(\omega) = -e^{j\omega} + \alpha e^{(-n+1)j\omega},$$

if $n = 6 \wedge \alpha = 1.5$

$$\Re\{\lambda(\omega)\} := -\cos(\omega) + 1.5\cos(\omega),$$
$$\Im\{\lambda(\omega)\} := -\sin(\omega) + 1.5\sin(\omega).$$

The result of computing the real and imaginary parts of the parameter is depicted in Figure 2.9

Two parameters

THEOREM 2.4.3

Let $a(s)$, $b(s)$ and $c(s)$ be the nth-degree polynomials with real coefficients. Then the polynomial $P(s,\lambda_1,\lambda_2) = a(s) + \lambda_1 b(s) + \lambda_2 c(s)$, $\lambda_1, \lambda_2 \in \mathbb{R}$, has no more than $(2n(n-1)+3)$ domains of $\mathcal{D}$-decomposition of the parameter plane (λ_1, λ_2).

Example 4. Consider a cubic polynomial reduced to Vyshnegradsky's form (that is with $a_3 = 1$, $a_0 = 1$):

$$P(s,\lambda_1,\lambda_2) = s^3 + \lambda_2 s + \lambda_1 s + 1. \tag{2.13}$$

Solving the system and decomposing the polynomial in real and imaginary parts, we find:

$$\lambda_1(\omega) := \omega^2, \quad \lambda_2(\omega) := \frac{1}{\omega},$$

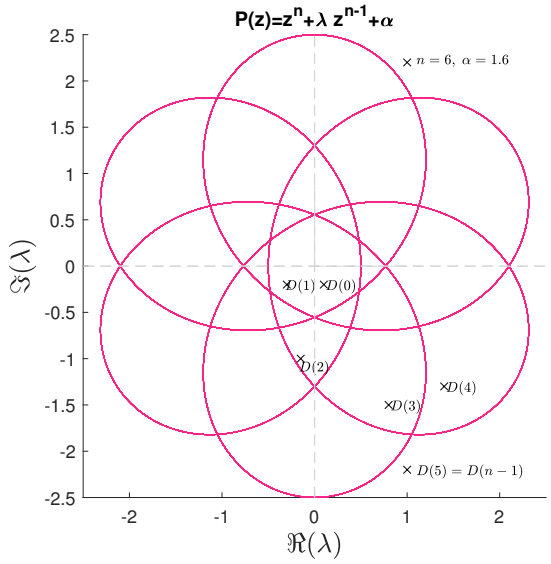

Figure 2.9: Decomposition for Example 3.

has no more than one stability domain and 15 domains of $\mathcal{D}$-decomposition, and the sketch in the parametric plane is in Figure 2.10.

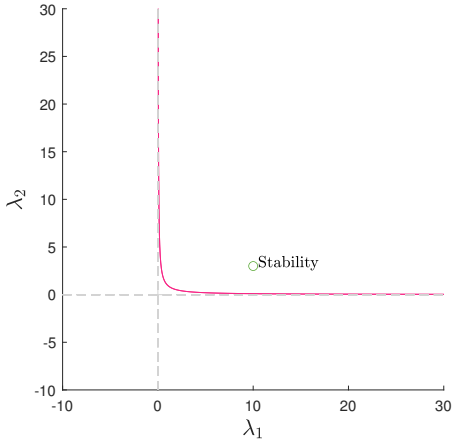

Figure 2.10: $\mathcal{D}$-decomposition for Example 4.

As a final result of the previous examples, the following remarks allude in a technical way to the procedure that needs to be carried out to obtain the parametric planes of $\mathcal{D}-$decomposition.

REMARK 2.4.1

For constructing the $\mathcal{D}$-decomposition of one parameter

- Find the $D(k, N-k)$ index for one segment of the real axis of the parameter space either by counting encirclements about an arbitrary point in the parameter segment or from another considerations.

- Complete the indexing of the other segments using the index property.
- The system is stable for values of the parameter in $D(N, 0)$.

REMARK 2.4.2

For constructing the $\mathcal{D}$-decomposition of two parameters

- Find the intersections in the parameter space, set $s = 0$ and/or $\pm\infty$. This will result in a linear relationship for the parameters (usually horizontal or vertical lines in the (λ_1, λ_2) plane).
- Let $s = j\omega$ in the polynomial, then equating real and imaginary parts to zero to find each relationship for parameters.
- Determine the $D(k, N-k)$ index for one region in the (λ_1, λ_2) plane and use the index rule to find the indexes of the remaining regions.

D-decomposition for Aperiodicity

One interesting result listed in [38] is that the same technique can be used to build the regions with certain number of real roots. Indeed the number of real roots can change when a multiple real root arises, that is for some $s \in \mathbb{R}$

$$\begin{aligned} P(s, \lambda) &= 0, \\ P'(s, \lambda) &= 0. \end{aligned} \tag{2.14}$$

Similar equations can define the domain of aperiodic stability, that is, the set of parameters that guarantee that all roots are *stable and real*.

DEFINITION 2.4.2

The decomposition of the parameter space k into the regions

$$A_l = \{k : a(s, k) \text{ has } l \text{ real simple negative roots}\},$$

with $l = 0, 1, \ldots, n$ is called $\mathcal{A}$-decomposition.

Specifically, for the cubic polynomial in Vishnegradsky the boundary is defined by

$$(j\omega)^3 + \lambda_2(j\omega)^2 + \lambda_1(j\omega) + 1 = 0,$$

applying the derivative

$$3(j\omega)^3 + 2\lambda_2(j\omega) + \lambda_1 = 0,$$

finally solving the system of two equations for λ_1 and λ_2 we have

$$\lambda_1(\omega) := \omega^2 - \frac{2}{\omega}, \quad \lambda_2(\omega) := \frac{1}{\omega} - 2\omega.$$

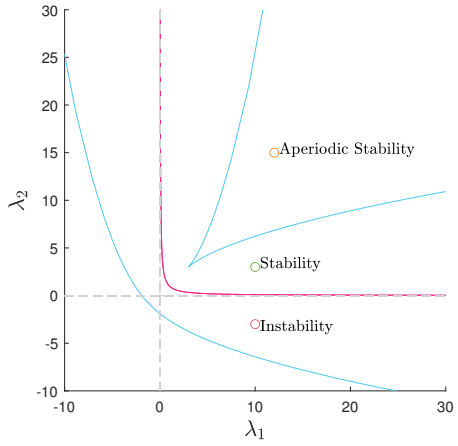

Figure 2.11: Stability and aperiodicity regions for Example 4.

In Equation 2.11 we can see the different stability domains given their partitions, where the $\mathcal{A}-$decomposition is a result enclosed in the stability region.

Given these mathematical tools, the following question for control theory arises: if there is a shift in the σ axis that causes a movement in the roots, will it be associated with the maximum exponential decay? To give an example graphically, see Figure 2.12, considering a second-order step response and let us move the poles to the right or the left, their movement have the same frequency over the range of variation in σ. As the poles move to the left, the response damps out more rapidly, making a faster convergence to the desired value, noticing that the peak time is the same for the waveforms because the imaginary part keeps constant. We could think how to associate this analogy with **Example 4**. Since the roots of the Vishnegradsky polynomial maintain their location in the complex plane, a pole motion will enclose all possible shifting regions before reaching the aperiodic stability, as we can see in Figure 2.13.

Finally, this result is known as $\sigma-$stability, a methodology presented in [45], where we can see the use of delayed controllers in their use for some mechanical systems. In the light of this approach, in Chapter 3 we develop a substitute method for stability analysis in power electronic devices.

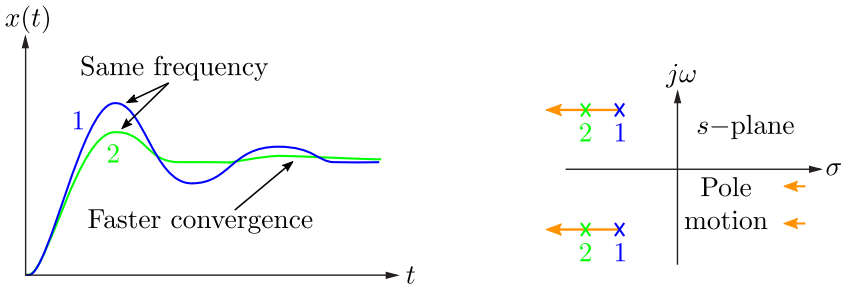

Figure 2.12: Step responses with σ-axis shift for a second-order system.

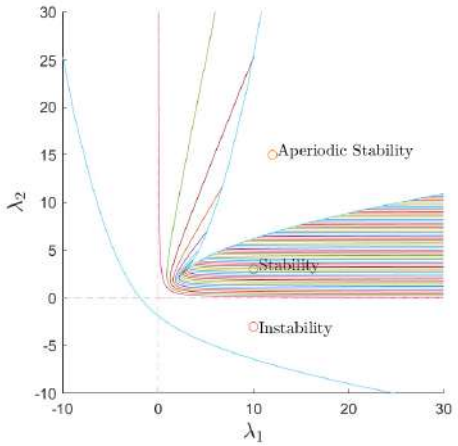

Figure 2.13: Stability and aperiodicity regions for Example 4.

2.5 PORT-HAMILTONIAN SYSTEMS

Linear control systems cover many applications, are intuitive, easy to design, and relatively simple. In the last section, the bases for developing a tool based on the small-signal model were generated; however, some precision requirements, rejection of exogenous disturbances, and full-range stability considered in this work justify using a nonlinear tool approach.

A relatively new perspective in control systems is energy-based control, which is widely used in mechanical systems [46], and developed and studied from energy considerations instead of the cause and effect approach. In the vast majority of cases, the energy-based control is described by the Euler-Lagrange equations of energy and motion [47], which emerges from a solid mathematical background based on passivity theory [48–50].

Port-Hamiltonian (pH) system models enclosed a large class of nonlinear systems and arise from an interconnection network point of view [51]. The recent progress in the perspective of pH has been achieved thanks to the direct way of obtaining its representation, in addition, that it respects the principle of conservation of energy; there-

fore, to robustify this type of control, we should emphasize the losses of the system that its parasitic elements can affect in the model.

Passive systems are a class of dynamic systems in which the exchange of energy with its environment plays a vital role. In passive systems, no more energy can be stored than is supplied from the outside; being this difference, the energy dissipated. In other words, these systems comply with the following,

$$\text{Stored Energy} + \text{Dissipated Energy} = \text{Energy Supplied}$$

The fundamental concept of power electronics devices (PED) is energy conversion. Moreover, an energy-based viewpoint could benefit from the evolution of the control of power electronic converters because the nature of elements such as capacitors and inductors during the switched-mode granted this concept.

In general, a port-Hamiltonian system has the form

$$\begin{aligned} \dot{x} &= (J(x) - R(x))\,\nabla H(x) + g(x)u, \\ y &= g^{\top}(x)\nabla H(x), \end{aligned} \tag{2.15}$$

where

- $x \in \mathbb{R}^n$ is the vector state;
- $u, y \in \mathbb{R}^m$ are the port variables;
- $H(x) : \mathbb{R}^n \to \mathbb{R}$ is the Hamiltonian function;
- $J(x) \in \mathbb{R}^{n\times n}$ is the interconnection matrix (which is *skew-symmetric*). Represents the elements system and define its structure;
- $R(x) \in \mathbb{R}^{n\times n}$ is the dissipation matrix (which, is symmetric and semi-positive definite). Represents the losses of the system;
- $g(x) \in \mathbb{R}^{n\times m}$ is an interconnection matrix describing, the port connection of the system outside the world. It yields the flow of energy to/from the system through the port variables u and y.

REMARK 2.5.1

1 A Hamiltonian function $H(x)$ bounded from below $H(x) > c$ with a minimum at $x^{\star}$.

2 An skew-symmetric interconnection matrix $J(x) = -J^{\top}(x)$.

3 A semi-positive definite dissipation matrix $R(x) = R^{\top}(x) \geqslant 0$.

Then the system, in closed-loop (i. e.for $u = 0$), is asymptotically stable.

Developing a pH model for a suitable converter was a challenge because of the high nonlinear nature of power electronics. Consequently, the most famous controllers were not long in coming. In particular, the PID control technique is a work that nowadays is still a topic of research.
In this section, a note on stabilization PI for pH is presented. To summarize the fundamental ideas of modeling, the formulation is described through the nonlinear incremental model. Next, a couple of prepositions are presented to describe the energy-based problem, which is solved using a suitable Lyapunov function. Finally, an immersion and invariance technique is studied to estimate some changes in the system.

2.6 PORT-HAMILTONIAN FOR SWITCHED POWER CONVERTERS

In this section, in the vein of the works presented in [52], [53] and [54], the rules for pH systems are depicted; nevertheless, some equations abuse notation in order to get good practice for the considered class of switching converters.

The pH form considering switched power converters (2.15) is rewritten as

$$\dot{x} = \left(J_0 + \sum_{i=1}^{m} J_i u_i - R \right) \nabla H(x) + E, \tag{2.16}$$

then, the total energy stored in inductors and capacitors is

$$H(x) = \frac{1}{2} x^\top Q x, \quad Q = Q^\top > 0, \tag{2.17}$$

knowing that the vector $E \in \mathbb{R}^n$ contain the (fixed) external voltage and current sources.

Given any class of nonlinear system of the form

$$\begin{aligned} \dot{x} &= f(x) + g(x)u, \\ y &= h(x), \end{aligned} \tag{2.18}$$

where x, u, y are functions of time, $x(t) \in \mathbb{R}^n$, $u(t), y(t) \in \mathbb{R}^m$, with $m \leqslant n$, the functions f, h are locally Lipschitz and the matrix $g(x)$ has full rank. Then, an assignable equilibrium state $x^\star \in \mathbb{R}^n$, is formed

from matching its derivatives to zero, or in the use of pH formulation (see [55] for further details) as

$$x^\star \in \mathcal{E} := \left\{ x^\star \in \mathbb{R}^n \mid g(x)^\perp f(x^\star) = 0 \right\}, \tag{2.19}$$

where $g(x)^\perp \in \mathbb{R}^{(n-m)\times n}$ is called a full-rank left-annihilator of $g(x)$, i. e., $g(x)^\perp g(x) = 0$ and $\operatorname{rank}\{g(x)^\perp\} = n - m$, and define the constant input and output vectors associated to $x^\star$ as

$$\begin{aligned} u^\star &:= \left(g^\top(x^\star)g(x^\star)\right)^{-1} g^\top(x^\star)f(x^\star), \\ y^\star &:= h(x^\star). \end{aligned} \tag{2.20}$$

DEFINITION 2.6.1 — **Nonlinear Incremental Model**

$$\begin{aligned} \dot{\tilde{x}} &= f(x) + gu^\star + g\tilde{u}, \\ \tilde{y} &= h(x) - h(x^\star), \end{aligned} \tag{2.21}$$

where $\tilde{(\cdot)} := (\cdot) - (\cdot)^\star$ are the incremental variables.

In a similar fashion, the pH form considered in (2.16) can be modeled for a class of converters, including switching external sources, and it is described by

$$\dot{x} = \left(J_0 + \sum_{i=1}^{m} J_i u_i - R\right) \nabla H(x) + \left(G_0 + \sum_{i=1}^{m} G_i u_i\right) E, \tag{2.22}$$

where G_i, $i \in \bar{m}$, are $n \times n$ matrices. Comparing (2.16) and (2.22) one can notice that, besides the fixed sources $G_0 E$, the model contains switching sources $\sum_{i=1}^{m} G_i u_i E$. Notwithstanding, in system (2.18) one can observe the following

REMARK 2.6.1 — If the system (2.18) is a port controlled Hamiltonian system, then

$$f(x) := (J_0 - R)\nabla H(x) + G_0 E, \tag{2.23}$$

and

$$g(x) := \sum_{i=1}^{m} (J_i Q x + G_i E). \tag{2.24}$$

2.6.1 *Passivity of the Nonlinear Incremental Model*

Proposition 2.1. *[56] Consider a large class of power converters described by (2.21). The admissible equilibria depicted in (2.18), i.e., $x^\star$ satisfies*

$$0 = \left(J_0 + \sum_{i=1}^{m} J_i u_i^\star - R \right) \nabla H(x^\star) + \left(G_0 + \sum_{i=1}^{m} G_i u_i^\star \right) E, \tag{2.25}$$

for some $u^\star \in \mathbb{R}^m$. The nonlinear incremental model of the system for the output $\tilde{y} := \mathcal{C}(x^\star)\tilde{x}$. The map $\mathcal{C} : \mathbb{R}^n \to \mathbb{R}^{m\times n}$ is defined as

$$\mathcal{C}(x^\star) := \begin{bmatrix} E^\top G_1^\top Q - (x^\star)^\top Q J_1 Q \\ \vdots \\ E^\top G_m^\top Q - (x^\star)^\top Q J_m Q \end{bmatrix} \in \mathbb{R}^{m\times n}, \tag{2.26}$$

is passive. More precisely, the system verifies the dissipation inequality

$$\dot{V} \leqslant \tilde{y}^\top \tilde{u},$$

where $\tilde{x} := x - x^\star$, $y^\star = \mathcal{C}x^\star$, and in an abuse of notation, the (positive definite) storage function $V : \mathbb{R}^n \to \mathbb{R}_+$ is given by

$$H(\tilde{x}) \equiv V(x) = \frac{1}{2}\tilde{x}^\top Q \tilde{x}. \tag{2.27}$$

The system defines a passive mapping $\tilde{u} \to \tilde{y}$ with a convex twice continuously differentiable storage (positive definite) function $V(x) : \mathbb{R}^n \to \mathbb{R}_+$, then, the time derivative of the storage function along the trajectories is:

$$\begin{aligned} \dot{V}(x) &= \tilde{x}^\top Q \dot{\tilde{x}} \\ &= \tilde{x}^\top Q \left[\left(J_0 + \sum_{i=1}^{m} J_i u_i^\star - R \right) \nabla V(x) + g(x)\tilde{u} \right] \\ &= -\tilde{x}^\top Q R Q \tilde{x} + \tilde{x}^\top Q g(x) \tilde{u}, \end{aligned}$$

since the output is defined as $y := g^\top(x)\nabla H(x) = g^\top(x)Qx$, one can notice that this result can be supportive if incremental output is defined as $\tilde{y}^\top = \tilde{x}^\top Q^\top g(x)$, the proof is completed replacing into the storage function and using the non-negativity of R to get

$$\begin{aligned} \dot{V}(x) &= -\tilde{x}^\top Q R Q \tilde{x} + \tilde{y}^\top \tilde{u} \\ &\leqslant \tilde{y}^\top \tilde{u}. \end{aligned}$$

REMARK 2.6.2

In general, the control objective of pH systems is to shape the storage function of the system into a desired function assigning to the closed-loop the dynamics $\dot{x} = (J - R)\nabla\mathcal{H}(x) + g\mathcal{V}$, where $\mathcal{H}(x)$ is the desired storage function and $\mathcal{V}$ is a free external signal. **Fixing** $\mathcal{V} = \tilde{u}$, the objective will be achieved with $\mathcal{H}(x) = H(x)$; and by definition of an admissible equilibrium point 2.24, the matching equation

$$-g(x^\star)u^\star = (J - R)\nabla H(x^\star), \tag{2.28}$$

always has a solution.

2.7 IMMERSION AND INVARIANCE APPROACH

The concept of invariance has been widely used in control theory. Slow and fast invariant manifolds have been used to stabilize and analyze the slow adaptation class of systems.
In passivity-based control (PBC), stabilization is achieved by finding an output such that the system is passive (with some suitable storage function that preserves the dissipation energy) [57].

As we see in [53], it is assumed that the load resistance and other parasitic elements appear on the dissipation matrix R, i. e.

$$R(x) = R_0(x) + \theta e_k e_k^\top, \tag{2.29}$$

where $R_0(x) \in \mathbb{R}^{n\times n}$ is the dissipation matrix of known elements of the converter, e_k is the kth vector of the standard n-dimensional Euclidean basis. Taking into account (2.22), the converter can be written in terms of known elements and the values to estimate as

$$\dot{x} := \mathcal{M}(x, u) - \theta\mathcal{K}e_k, \tag{2.30}$$

where $\mathcal{M} : \mathbb{R}^n \times \mathbb{R}^m \to \mathbb{R}^n$ is the known function

$$\mathcal{M}(x, u) := \left(J_0 + \sum_{i=1}^{m} J_i u_i - R_0\right) Qx + \left(G_0 + \sum_{i=1}^{m} G_i u_i\right) E, \tag{2.31}$$

and the estimate equation

$$\mathcal{K} := e_k^\top Qx. \tag{2.32}$$

Proposition 2.2. *Consider a large class of a switched power electronic converter described by (2.22), with dissipation matrix of the form (2.29) and the definitions (2.31) and (2.32). The I& I estimator*

$$\begin{aligned}\dot{\zeta} &= \frac{\mu}{\gamma}\mathcal{K}\left\{e_k^\top Q\mathcal{M}(x,u) - \left(\gamma\zeta - \frac{\mu}{2}\mathcal{K}^2\right)Q_{kk}\mathcal{K}\right\},\\ \hat{\theta} &= \gamma\zeta - \frac{\mu}{2}\mathcal{K}^2,\end{aligned} \tag{2.33}$$

ensures parameter convergence if and only if, $\mathcal{K}(t)$ is bounded away from zero

A quick example of the results using the I&I uncertainty estimator is presented in the logic in Figure 2.14, divided into three parts, its input power source, the converter, and the control. Adding the extra dynamics in the control law allows immersion into the untimely changes that appear concerning time in the dissipation matrix. Once the complements of $R(x)$ are generated as seen in Equation 2.29 at the designer's convenience, the estimator is started and must be even faster than the control in order to be able to follow either faster or slower (see Figs. 2.15–2.16) depending on the selection of the parameters μ, γ values which are usually small.

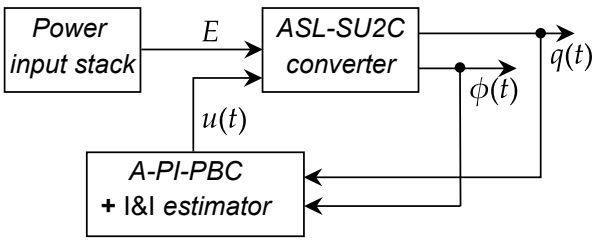

Figure 2.14: Control scheme for adaptive PI-PBC.

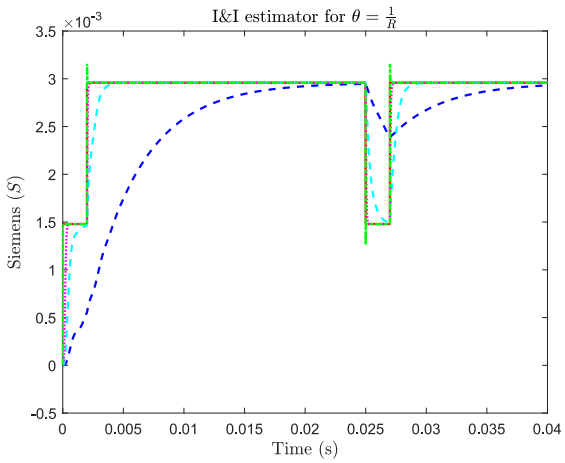

Figure 2.15: I&I estimation for θ.

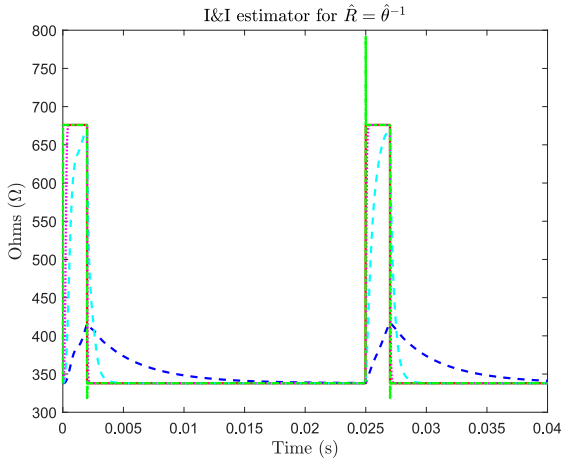

Figure 2.16: I&I estimation for R.

2.8 CHAPTER CONCLUSION

In this chapter, we reviewed the methodologies necessary for the control proposals in the following chapters. In the first instance, the models in the state-space of the considered converter neglecting uncertainties in the converter and parasitic elements are derived using the small-signal approach to obtain the transfer functions as a linear control method. In addition, the stability analysis was introduced employing the boundary crossing theorem, and together with the $\mathcal{D}$-decomposition theory, parametric spaces can be created from the parameters of a polynomial, and the $\mathcal{A}$-decomposition is mentioned as an interesting study where all the roots become real regardless of their nature. In the second instance, energy-based models are studied, explicitly using the representation in port-Hamiltonian, where some definitions and propositions within the passivity theory are reviewed. Finally, the generalized study of first-order I&I estimators was added as a proposal to add adaptive properties to passivity-based control.

Part II

LINEAR APPROACH

"Linear systems have an important modular virtue: You can take them apart, and put them together again - the pieces add up".

—James Gleick

3

CONTROLLER DESIGN: LINEAR APPROACH

In this chapter, we study regulation problems through the use of the well-known Proportional-Integral (PI) controllers, widely used in industrial applications due to their simplicity, effectiveness, and low cost [58]. These controllers are famously recognized for improving tracking error and coping with the presence of load variations. There are different tuning methods for PI controllers design (see, for instance, [59], and, [60]). However, some of these methods come from a heuristic methodology, and others are quite difficult to be applied in high-order systems. Hence, it is required to develop tuning methodologies that allow a simple analytical design (regardless of the system order), which enables considering some characteristic performances. Then, our study is based on a PI-control scheme and, by exploiting the continuous root property of polynomials, we propose a simple tuning rule that allows establishing the controller gains that guarantee the converging-exponential bound of the system response.
In the scope of this chapter, two cases of design of controllers for single-loop and double-loop are presented. Using the mathematical tools displayed in the preliminaries of this work, we develop a methodology that allows the correct operation of the controls through an analytical study. The double-loop scheme is one of the most used for power electronic converters; the intermittent question is how the loops should evolve to have no problem in the regulation and or tracking of the states.

3.1 SINGLE AND DOUBLE-LOOP CONTROLLERS

This section studies in detail the ASL-SU2C control scheme design for output voltage control. Two different approaches are proposed: i) single-loop and ii) double-loop. The latter, better known as cascade control, uses an inner current-loop and an outer voltage-loop. The design process is carried out by using the well-known crossing roots stability theory (see, for instance, [45]). In this regard, the controller parameters tuning is developed employing the σ-stability analysis criteria. This analysis provides valuable information regarding the location of the characteristic root in order to assure asymptotic stability and a desirable exponential decay on the closed-loop system response. To this end, our main proposition describes the location of these roots in terms of the PI controller's parameters.
The single-loop control scheme, depicted in Figure 3.1 is a straightforward classical feedback controller $C_{PI}(s)$ and open-loop plant $G_1(s)$.

The goal of the control is to regulate the voltage across the load resistance around a constant desired value.

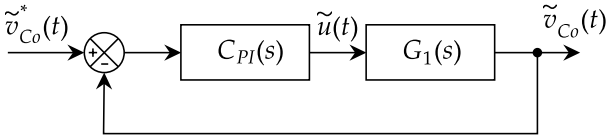

Figure 3.1: Single-loop control scheme.

The double-loop control scheme (cascade control) can be understood as two nested loops, which includes an inner current-loop with controller $C_c(s)$ and open-loop plant $G_2(s)$, and an outer voltage-loop with controller $C_v(s)$ and plant $G_3(s)$.

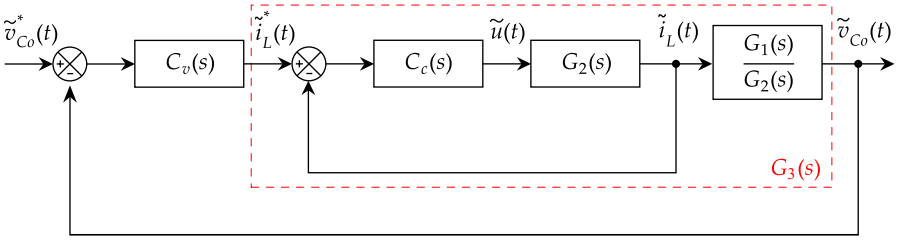

Figure 3.2: Double-loop control scheme.

Where $G_3(s)$ is the transfer function containing the inner current-loop in series with the block $G_1(s)/G_2(s)$, that is

$$G_3(s) := \left[\frac{C_c(s)G_2(s)}{C_c(s)G_2(s)+1}\right]\left[\frac{G_1(s)}{G_2(s)}\right], \tag{3.1}$$

such relation is depicted in Figure 3.2. Furthermore, the design of the three PI controllers $C_{PI}(s)$, $C_c(s)$ and $C_v(s)$ must be treated separately. Let us denote $C_m(s) := k_p^{(m)} + k_i^{(m)}\frac{1}{s}$, where, $m \in \{PI, c, v\}$. The control objective in this second scheme is to perform voltage regulation as in the first scheme; however, in addition to the dynamics of the inner current-loop, it allows a fast convergence to the desired values as long as the dynamic of the inner current loop evolves faster than the outer voltage-loop.

3.2 σ−STABILITY ANALYSIS

Motivated by the fact that we have a plant in a closed-loop with a PI-controller in all the above control schemes, our study is based on the system's characteristic equation. Then, in the following result, we

analyze the stability of the open-loop stable systems class. Let G be a strictly proper transfer function, given by

$$G(s) = \frac{N(s)}{D(s)},$$
$$\text{with } \begin{cases} N(s) := b_m s^m + b_{m-1} s^{m-1} + \cdots + b_1 s + b_0, \\ D(s) := a_n s^n + a_{n-1} s^{n-1} + \cdots + a_1 s + a_0. \end{cases} \tag{3.2}$$

Using this notation and with the knowledge that a PI controller is defined as $C(s) = k_p + k_i/s$, the characteristic equation of a closed-loop employing $G(s)$ as the plant is given by

$$\Delta(s; k_p, k_i) := s\, D(s) + N(s)\,(k_p\, s + k_i)\,. \tag{3.3}$$

The stability analysis begins with the fact that for a proper class of power electronic converters, wherein their transfer functions must be stable in open-loop. In other words, the analysis can be pursued if and only if $D(s)$ is a Hurwitz polynomial; otherwise, the system will remain unstable independently of the control action. In addition, the controller parameters (k_p, k_i) determine the transient response of the analysis, and the choice of these parameters implies that all the characteristic roots are located on the left-half plane (LHP) in the complex plane. The stability analysis is described by three different system-controller pairs $G(s), C(s)$. First, a voltage single-loop $G_1(s), C_{PI}(s)$, and second, a double-loop in two steps: current inner-loop $G_2(s), C_c(s)$ and voltage outer-loop $G_3(s), C_v(s)$, correspondingly to the above PI control schemes. The fundamental ideas used in the present analysis are the well-known crossing roots stability theory (see, for instance, [35]). Such an approach is strongly based on the fact that the characteristic roots vary continuously concerning continuous variations of their parameters as root continuity property [61]. Taking into account these observations, let us consider the following definitions

DEFINITION 3.2.1 — **Frequency crossing set**

The frequency set $\Omega \subset \mathbb{R}$ is the set of all $\omega \in \mathbb{R}$ such that, there exists at least a pair (k_p, k_i) for which

$$\begin{aligned} \Delta(j\omega; k_p, k_i) &= (j\omega)\, D(j\omega) + N(j\omega)\,(j\omega\, k_p + k_i) \\ &= 0. \end{aligned} \tag{3.4}$$

REMARK 3.2.1

It is clear that if we take the complex conjugate of (3.4), the following equality holds:

$$\begin{aligned}(-j\omega)D(-j\omega)+N(-j\omega)\left((-j\omega)k_p+k_i\right)\\ =\overline{(j\omega)D(j\omega)+N(j\omega)\left((j\omega)k_p+k_i\right)}.\end{aligned} \tag{3.5}$$

Without doubt, only non-negative frequencies are considered, i. e., $\Omega \subset \mathbb{R}_+ \cup \{0\}$.

DEFINITION 3.2.2

Stability crossing boundaries

The stability crossing boundaries $\mathcal{T}$ is the set of all parameters

$$\mathcal{T} := \left\{(k_p, k_i) \in \mathbb{R}^2 \mid \exists \omega^\star \in \Omega \Rightarrow \Delta(j\omega; k_p, k_i) = 0\right\}.$$

In this regard, we study the behavior of the rightmost characteristic roots ($\sigma-$stability analysis) by deriving controller parameters conditions such that the characteristic equation has at least one root on a vertical $\sigma-$axis in the complex plane. This is straightforwardly Proposition 3.1.

Proposition 3.1. *Let an open-loop system for a proper class of power electronic converters described by a transfer function $G(s)$ with $D(s)$ as a Hurwitz polynomial and the parameter $b_0 > 0$. Consider a fixed value $\sigma \in \mathbb{R} \mid \{\sigma < 0\}$, and let $s^\star := \sigma + j\omega$. Then, there is at least two characteristic roots at $\Re\{s\} = \sigma$, if and only if, the parameters k_p and k_i are given by*

$$k_p(\omega) := -\frac{\sigma}{\omega}\Im\left\{\frac{1}{G(s^\star)}\right\} - \Re\left\{\frac{1}{G(s^\star)}\right\}, \tag{3.6}$$

$$k_i(\omega) := \left(\omega + \frac{\sigma^2}{\omega}\right)\Im\left\{\frac{1}{G(s^\star)}\right\}, \tag{3.7}$$

where $\omega \in \mathbb{R}_+$ such that $G(s^\star) \neq 0$. Furthermore, there is at least one characteristic root at $s = \sigma$ (real crossing), if and only if

$$k_i(\sigma) := -\sigma\, k_p - \sigma\, G^{-1}(\sigma). \tag{3.8}$$

Proof. Using Definition 3.2 we get

$$\begin{aligned}\Delta(j\omega, k_p, k_i) &= 0,\\ j\omega\, D(j\omega) + (j\omega\, k_p + k_i)N(j\omega) &= 0,\\ j\omega\, k_p + k_i &= -j\omega\frac{D(j\omega)}{N(j\omega)},\end{aligned}$$

as a set of equations that uses the concept of $\mathcal{D}-$decomposition during the two parameters k_p, k_i and identifying the existence of the shift in σ-axis, now the characteristic equation employing $s^\star = \sigma + j\omega$ is

$$j\{\omega\ k_p\} + \{\sigma\ k_p + k_i\} = -(\sigma + j\omega)\,\frac{1}{G(s^\star)},$$

then, applying some algebraic manipulations and concepts of complex variable, we can easily separate equations for k_p, k_i such that

$$\begin{aligned} j\{\omega\ k_p\} + \{\sigma\ k_p + k_i\} &= -(\sigma + j\omega)\left[j\Im\left\{\frac{1}{G(s^\star)}\right\} + \Re\left\{\frac{1}{G(s^\star)}\right\}\right], \\ &= j\left[-\omega\Re\left\{\frac{1}{G(s^\star)}\right\} - \sigma\Im\left\{\frac{1}{G(s^\star)}\right\}\right] + \\ &\left[\omega\Im\left\{\frac{1}{G(s^\star)}\right\} - \sigma\Re\left\{\frac{1}{G(s^\star)}\right\}\right], \end{aligned}$$

the proof is complete only using the algebraic fact of $jb + a$ and lies finally on the set (3.6) and (3.7). Equation (3.8) is derived by fixing $j\omega = 0$ to get a set of straight lines with a slope. □

Hence, by considering $\sigma < 0$, we can also derive the set of all parameters (k_p, k_i); and for a particular case when $\sigma = 0$ in the previous preposition, by sweeping ω over the interval $[0, \infty)$ allows us to build all the complete stability crossing boundaries. Notice that inside any parameters-space region delimited by these curves, no root crossing is achievable, and consequently, the number of unstable characteristic roots (stability index) is fixed. In general, these curves partition the parameters-space in regions with a well-defined stability property (stable or unstable). This is why they are also called *stability boundaries (SB)*. The same arguments are posed for any other σ value, noting that these new curves highlight regions in which all roots are not only at the LHP in the complex plane but the left side of a σ vertical axis.

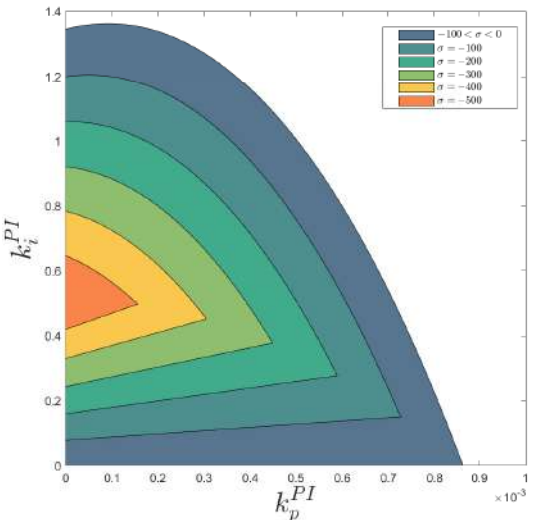

Figure 3.3: Single-loop SB.

Finally, the solutions of our result are presented in Figs. 3.3–3.5, where it should be noted that not to redo the non-minimum phase in closed-loop, only positive gains are considered. For a single control loop, we can choose within the parametric plane, however in the cascade control the pair of gains that are selected for the inner current-loop, the designer must make the result now for the outer voltage-loop as it is attached to default values, in this case, $(k_p^c, k_i^c) = (0.056, 5.4 \times 10^3)$.

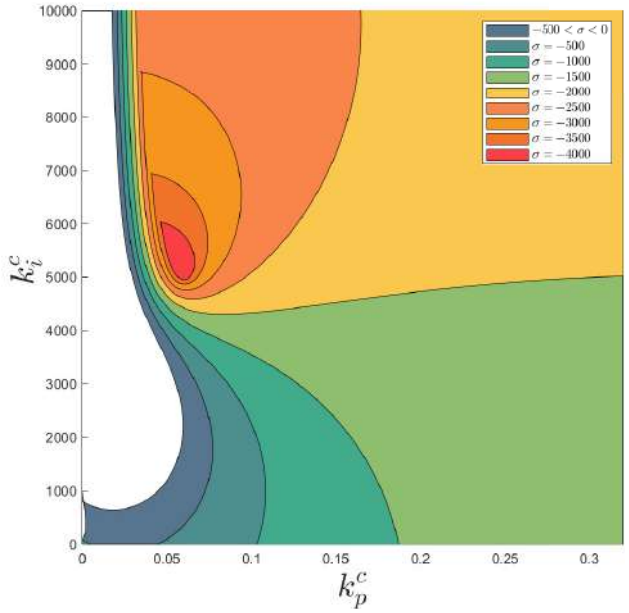

Figure 3.4: Inner current-loop SB.

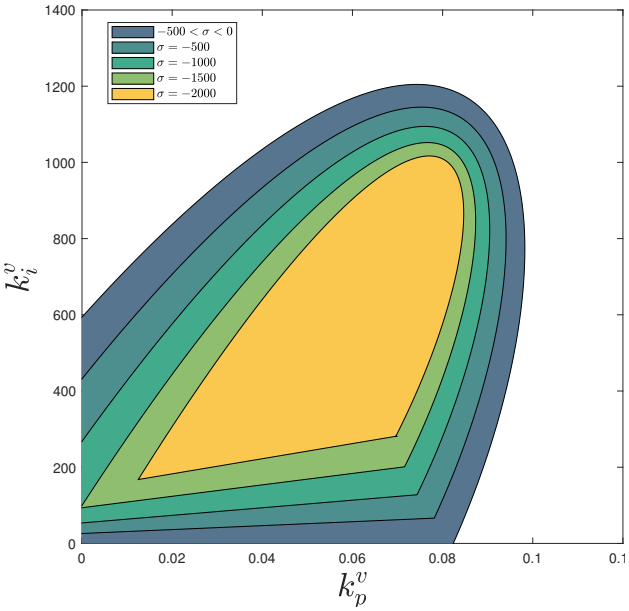

Figure 3.5: Outer voltage-loop SB.

As an example of profit selection in the regions of the parameter space, note a particular case in the inner current-loop. Since different gains are selected within the ranges of σ where their step responses are depicted in Figure 3.6 and also in Figure 3.7 its bode diagram, it is worth noting the case in $\sigma = -500$ where it fails to settle and remains oscillating. In the bode diagram we can see a resonant frequency peak where it matches the frequency of oscillation in its response to the step. Therefore, although the analysis of stability regions is entirely numerical in combination with tuning methodologies such as Ziegler-Nichols and Cohen-Coon, it can robustly support the results.

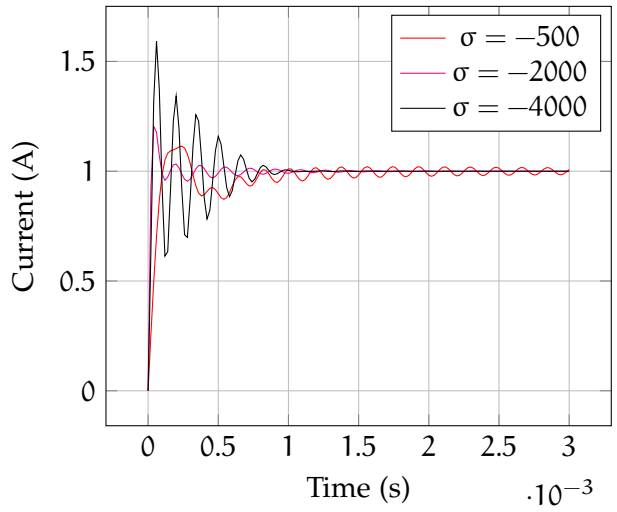

Figure 3.6: Step plot response for inner current-loop.

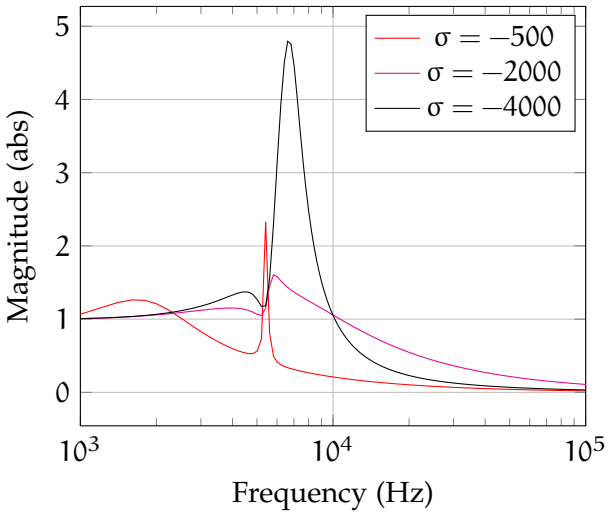

Figure 3.7: Bodeplot response for inner current-loop.

3.3 CHAPTER CONCLUSION

In this chapter, the linear control proposal was developed employing two different scenarios for control purposes. The study called σ-stability is explored utilizing two control schemes regarding single-loop for an output voltage regulator and double-loop employing output voltage regulation with a nested current regulation to obtain the stability boundaries graphically and thus analyze the stability of the ASL-SU2C converter by the numerical limits of the pair of gains (k_p, k_i). This stability analysis is essential since it clarifies the selection of PI gains values. Using their parameters regions employing the maximum exponential decay (this occurs when moving the σ axis), i. e., employing this study, it is possible to guarantee exponential stability. Finally, a small study is added on its response to the step and frequency and how to associate an oscillatory response by selecting stability regions.

Part III

NONLINEAR APPROACH

"...Even if these games could be described through linear equations, small changes in conditions would alter the outcome. Even in the most optimistic world view, these methods are not going to do well".

—Koleman Strumpf

4

CONTROLLER DESIGN: NONLINEAR APPROACH

This chapter describes the nonlinear tool for the control of the ASL-SU2C converter mentioned above. The approach is divided into two parts, stabilization of the state vector by means of the PI-PBC methodology and the development of a first-order uncertainty estimator, giving adaptive abilities to the control when facing uncertainties due to changes in the converter load. The modeling of the system is given by its representation in flows and charges (instead of currents and voltages) in order to obtain its port-Hamiltonian formalism in a more straightforward way. Finally, a series of simulations are considered to evaluate the performance of the closed-loop system via phase portrait plots and evaluate the load estimation.

4.1 PI-PBC STABILIZATION

Proposition 4.1. *[62] Consider a switched power converter described by (2.22). Let $x^\star$ be an equilibrium point with the corresponding constant input $u^\star$ and output $y^\star$. Assume*

4.1.a The storage function of passive elements are continuously differentiable and strictly convex such that

$$u^\top y \leqslant \dot{H} = \frac{\partial H}{\partial x} f(x,u), \quad \forall (x,u) \in \mathbb{R}^n \times \mathbb{R}_+. \tag{4.1}$$

4.1.b The switched power converter in closed loop with the PI controller

$$\begin{aligned} \dot{\xi} &= -\tilde{y}, \\ \tilde{u} &= K_i \xi - K_p \tilde{y}, \end{aligned} \tag{4.2}$$

with $\tilde{y} = C\tilde{x}$ and C given by (2.26) (see Figure 4.1), and $K_i = K_i^\top, K_p = K_p^\top$, ensures all state trajectories $(x(t), \xi(t))$ are bounded and

$$\lim_{t\to\infty} \| \tilde{y}(t) \| = 0,$$

if, in addition, the closed-loop satisfies the detectability assumption.

4.1.c ***detectability condition***

$$\tilde{y} \equiv 0 \Rightarrow \lim_{t\to\infty} \| \tilde{x}(t) \| = 0,$$

where $\xi^\star = K_i^{-1} u^\star$. Then, $\lim_{t\to\infty} x(t) = x^\star$.

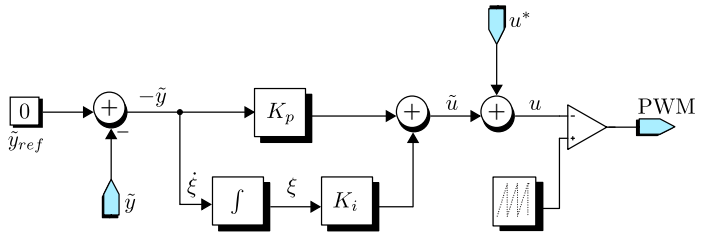

Figure 4.1: Common control scheme process using PI-PBC.

4.2 CASE OF STUDY

The ASL-SU2C converter shown in Figure 4.2 whose averaged model is given by the equations

$$\begin{aligned}
2\dot{\phi}_{L_n} &= E(1+u) - \frac{q_{C_n}}{C_n}(1-u),\\
2\dot{q}_{C_n} &= \frac{\phi_{L_n}}{L_n}(1-u) - \frac{\phi_{L_o}}{L_o}(1+u),\\
\dot{\phi}_{L_o} &= \frac{q_{C_n}}{C_n}(1+u) + Eu - \frac{q_{C_o}}{C_o},\\
\dot{q}_{C_o} &= \frac{\phi_{L_o}}{L_o} - \frac{q_{C_o}}{C_o r_L},
\end{aligned} \tag{4.3}$$

where $\phi = Li$ and $q = Cv$ are the fluxes and charges respectively. $L_n = L_1 = L_2, L_o$, are the value of inductances, $C_n = C_1 = C_2, C_o$ are the value of capacitances, r_L is the load, E the input voltage, with u is the continuous control equal to the slew rate of PWM. The converter parameters values are shown below in Table 4.1.

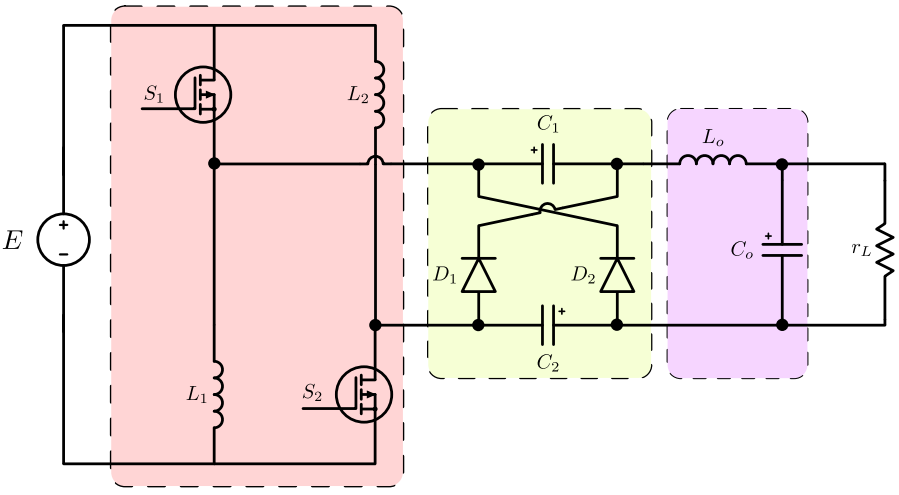

Figure 4.2: Schematic of the considered converter.

Considering (2.22), the system can be expressed in pH form with the definitions

$$
\begin{aligned}
x &= \begin{bmatrix} \phi_{L_n} & q_{C_n} & \phi_{L_o} & q_{C_o} \end{bmatrix}^\top, \\
Q &= \begin{bmatrix} 1/L_n & 0 & 0 & 0 \\ 0 & 1/C_n & 0 & 0 \\ 0 & 0 & 1/L_o & 0 \\ 0 & 0 & 0 & 1/C_o \end{bmatrix}, \\
R &= \begin{bmatrix} 0 & 0 & 0 & 0 \\ 0 & 0 & 0 & 0 \\ 0 & 0 & 0 & 0 \\ 0 & 0 & 0 & 1/r_L \end{bmatrix}, \\
D &= \begin{bmatrix} 1/2 & 0 & 0 & 0 \\ 0 & 1/2 & 0 & 0 \\ 0 & 0 & 1 & 0 \\ 0 & 0 & 0 & 1 \end{bmatrix}, \\
G_0 E &= \begin{bmatrix} E & 0 & 0 & 0 \end{bmatrix}^\top, \\
G_1 E &= \begin{bmatrix} E & 0 & E & 0 \end{bmatrix}^\top, \\
J_0 &= \begin{bmatrix} 0 & -1 & 0 & 0 \\ 1 & 0 & -1 & 0 \\ 0 & 1 & 0 & -1 \\ 0 & 0 & 1 & 0 \end{bmatrix}, \\
J_1 &= \begin{bmatrix} 0 & 1 & 0 & 0 \\ -1 & 0 & -1 & 0 \\ 0 & 1 & 0 & 0 \\ 0 & 0 & 0 & 0 \end{bmatrix}.
\end{aligned}
$$

Then, the pH system is defined as

$$
D^{-1}\dot{x} = (J_0 + J_1 u - R)\,\nabla H(x) + (G_0 + G_1 u)\,E, \tag{4.4}
$$

$$
D^{-1}\dot{x} = \begin{bmatrix} 0 & -(1-u) & 0 & 0 \\ 1-u & 0 & -(1+u) & 0 \\ 0 & 1+u & 0 & -1 \\ 0 & 0 & 1 & -1/r_L \end{bmatrix} \cdot \begin{bmatrix} \phi_{L_n}/L_n \\ q_{C_n}/C_n \\ \phi_{L_o}/L_o \\ q_{C_o}/C_o \end{bmatrix} + \begin{bmatrix} E \\ 0 \\ 0 \\ 0 \end{bmatrix} + \begin{bmatrix} E \\ 0 \\ E \\ 0 \end{bmatrix} u,
$$

the admissible equilibria of the system can be parametrized by the reference v_d, which is equivalent to regulation of the capacitor charge q_{C_o} to the constant value $q^\star_{C_o} = C_o v_d$, therefore

$$x^\star = \begin{bmatrix} \frac{1}{r_L}\frac{u_p^\star}{u_n^\star} L_n v_d \\ \frac{C_n v_d (v_d - E u^\star)}{v_d u_p^\star} \\ \frac{1}{r_L} L_o v_d \\ C_o v_d \end{bmatrix} \approx \begin{bmatrix} 0.0012 \\ 0.00014 \\ 0.0018 \\ 0.00026 \end{bmatrix}. \tag{4.5}$$

Table 4.1: Parameters of the switching converter

L_n	C_n, C_o	L_o	rL	$u^\star$	E	v_d	f_{sw}	P_o
223µH	1µF	2.34mH	338Ω	0.75	20V	260V	50kHz	200W

Performing a transformation with the variable z such that

$$z := D^{-1} x, \quad \Rightarrow \quad \dot{z} = D^{-1}\dot{x}, \tag{4.6}$$

the total stored energy in the system now taking into account the transformation is

$$\mathcal{H}(z) = \frac{1}{2} z^\top \hat{Q} z, \quad \hat{Q} = DQ. \tag{4.7}$$

Then, the incremental passivity model using z is defined as

$$\dot{\tilde{z}} + \dot{z}^\star = (J_0 + J_1 u - R)\,\hat{Q}\,(\tilde{z} + z^\star) + G_0 E + G_1 E\,(\tilde{u} + u^\star), \tag{4.8}$$

with its admissible equilibria given by

$$0 = (J_0 + J_1 u^\star - R)\,\hat{Q} z^\star + G_0 E + G_1 E u^\star. \tag{4.9}$$

Subtracting equations (4.8) and (4.9) allow deducing the following equation

$$\dot{\tilde{z}} = (J_0 + J_1 u - R)\,\hat{Q}\tilde{z} + J_1 \hat{Q} z^\star + G_1 E \tilde{u}. \tag{4.10}$$

This makes it easy to evaluate the passivity theorem [63] and to fulfill the dissipation inequality [64] such that

$$\begin{aligned} \dot{\mathcal{H}}(\tilde{z}) &= \tilde{z}^\top \hat{Q} \dot{\tilde{z}}, \\ &= \tilde{z}^\top \hat{Q} \left[(J_0 + J_1 u - R)\,\hat{Q}\tilde{z} + J_1 \hat{Q} z^\star + G_1 E \tilde{u}\right], \\ &= \tilde{z}^\top \hat{Q} R \hat{Q} \tilde{z} + \tilde{z}^\top \hat{Q} \left(J_1 \hat{Q} z^\star + G_1 E\right) \tilde{u}, \\ &\leqslant \tilde{z}^\top \hat{Q} \left(J_1 \hat{Q} z^\star + G_1 E\right) \tilde{u} = \tilde{y}\tilde{u}^\top, \end{aligned} \tag{4.11}$$

and without doubt, the mapping $\tilde{u} \to \tilde{y}$ derives

$$\tilde{y} = \left[E^\top G_1^\top - (z^\star)^\top \hat{Q} J_1 \right] \hat{Q} \tilde{z}, \tag{4.12}$$

applying algebra to return to the original state variable we have

$$\tilde{y} = \left[E^\top G_1^\top - (x^\star)^\top Q J_1 \right] Q \tilde{x}. \tag{4.13}$$

Finally, the incremental output of the converter is defined as follows

$$\begin{aligned} \tilde{y} &= \left[E^\top G_1^\top Q - (x^\star)^\top Q J_1 Q \right] \cdot \tilde{x} \\ &= \frac{C_n E + q^\star_{C_n}}{C_n L_n} \tilde{\phi}_{L_n} - \frac{L_o \phi^\star_{L_n} + L_n \phi^\star_{L_o}}{C_n L_n L_o} \tilde{q}_{C_n} + \frac{C_n E + q^\star_{C_n}}{C_n L_o} \tilde{\phi}_{L_o}. \end{aligned} \tag{4.14}$$

Performing (4.14) global stability is ensured with the control law

$$u = K_i \xi - K_p \tilde{y} + u^\star, \quad \dot{\xi} = -\tilde{y}, \quad u^\star = 0.75, \tag{4.15}$$

and satisfactorily complies the detectability condition such that

$$\lim_{t \to \infty} \| \tilde{y}(t) \| = 0, \quad \lim_{t \to 0} \| \tilde{y}(t) \| \approx -123, \quad \therefore \quad \lim_{t \to \infty} x(t) = x^\star.$$

Two simulation cases were performed to analyze the passivity-based control; the proportional or integral gain is fixed for the first and second cases, respectively (see Table 4.2). The phase portrait representation for the inductor current i_{L_n} in the ASL network and the capacitor output voltage v_{C_o} was used to observe how the controlled trajectory reaches its equilibrium points. Their trajectories can be observed in Figs. 4.3–4.4 where we can highlight that the integral action does not affect the growth of the current; on the other hand, the changes in the proportional action will suffer from overshoot in the current; therefore, through these experiments, we arrived at the following assertions for the tuning of gains in the ASL-SU2C converter

1. PI-PBC guarantees global stability at any gain (satisfies the proof of the passivity theorem) as long as $K_p, K_i \in \mathbb{R}^+$.

2. The control performs excellent results for both voltage and current when the inequality $K_p < K_i$ is satisfied.

Table 4.2: Simulation Samples.

Case 1	K_p	K_i	Case 2	K_p	K_i
Open-loop	0.0	0.0	Open-loop	0.0	0.0
Sample 1	4×10^{-4}	0.1	Sample 6	2×10^{-4}	1.0
Sample 2	4×10^{-4}	0.5	Sample 7	4×10^{-4}	1.0
Sample 3	4×10^{-4}	1.0	Sample 8	6×10^{-4}	1.0
Sample 4	4×10^{-4}	1.5	Sample 9	8×10^{-4}	1.0
Sample 5	4×10^{-4}	2.0	Sample 10	1.0×10^{-3}	1.0

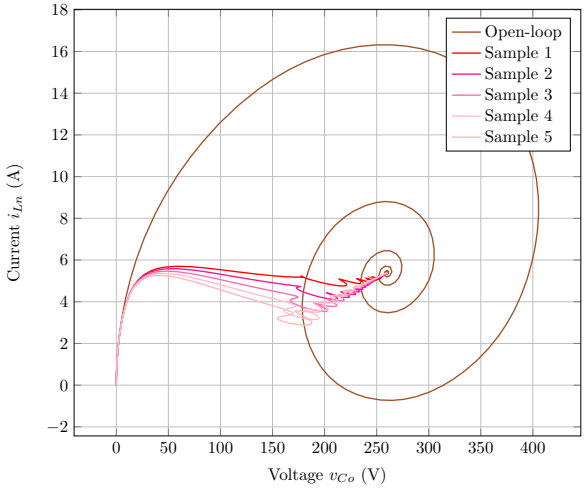

Figure 4.3: Phase Portrait for Case 1.

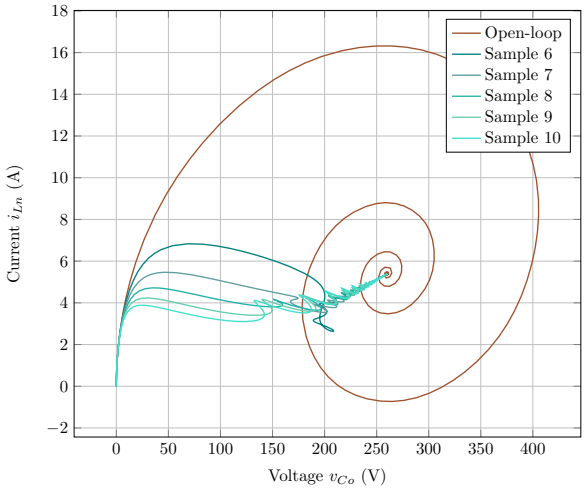

Figure 4.4: Phase Portrait for Case 2.

4.3 A-PI-PBC STABILIZATION

In adaptive control, a natural candidate for the target dynamics is the closed-loop with the known-parameters. It is interesting to note that, even though the target dynamics are not known (since they depend on the unknown parameters), I&I is still applicable [65]. Besides, in power electronic converters, these target dynamics are represented by the parasitic elements in passive components, switching components, and load changes. Due to this, we recall (2.31) and using as main motivation the first-order estimator presented in [53], we ensure the parameter convergence of $r_L = 1/\theta$ similarly as the incremental output due to $\tilde{\theta} = \hat{\theta} - \theta$,

$$\lim_{t\to\infty} \| \tilde{\theta}(t) \| = 0, \tag{4.16}$$

$$e_{\mathcal{K}} = \begin{bmatrix} 0 & 0 & 0 & 1 \end{bmatrix}, \tag{4.17}$$

$$\mathcal{K} = \frac{q_{C_o}}{C_o}, \tag{4.18}$$

$$Q_{kk} = \frac{1}{C_o}. \tag{4.19}$$

Therefore, the first-order estimator for ASL-SU2C system considering changes in $r_L(t)$ is given by

$$\begin{aligned} \dot{\zeta} =& \frac{\mu q_{C_o}}{\gamma C_o} \left\{ \frac{\phi_{L_o}}{C_o L_o} + \left(\frac{\mu q_{C_o}^2}{2C_o^2} - \gamma\zeta \right) \frac{q_{C_o}}{C_o^2} \right\}, \\ \hat{\theta} =& \gamma\zeta - \frac{\mu}{2C_o^2} q_{C_o}^2, \end{aligned} \tag{4.20}$$

finally, based on the chosen pair of gains, the adaptive control is carried out having a resistance change from 338Ω to 295Ω with the resulting estimation $\hat{r_L}$ depicted in Figure 4.5

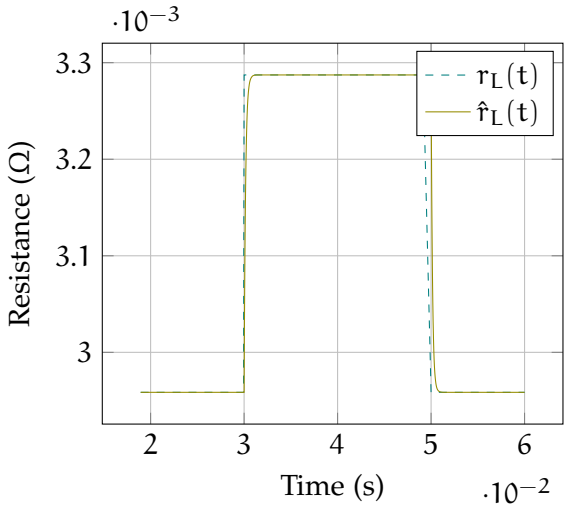

Figure 4.5: Load resistance estimation, with $\gamma = 10$ and $\mu = 5 \times 10^{-5}$.

4.4 CHAPTER CONCLUSION

The nonlinear dynamics of the ASL-SU2C converter are explored in this chapter. Knowing that the objective of control based on passivity is stabilization, our study is essentially based on reproducing PI-PBC. On the verge of preliminary mathematical tools, the average model of the converter is developed through its representation in flows and charges. As part of the stabilization, two cases were taken into account for use in a phase portrait where a gain pair was chosen, looking for a path that would not put the current i_{L_n} of inductors at risk. Finally, the A-PI-PBC stabilization is carried out by adding the dynamics of a first-order I&I estimator during a momentary change in load, thus validating the control proposal.

Part IV

NUMERICAL VALIDATION

5 NUMERICAL VALIDATION

This chapter presents simulations using MATLAB for the control proposals designed for a linear and nonlinear approach. The open-loop response is presented to observe the equilibrium points and transients of the states to be evaluated. The numerical evaluation of the linear control is carried out by selecting values within the stability regions, and a case where the σ-stability study presents oscillatory response is also shown. On the other hand, the evaluation of the nonlinear control is performed by selecting a pair of gains within the trajectories previously studied for its phase portrait. Finally, three robustness tests are executed, two of them changing the load values and the last one taking the load to its critical value R_{crit} to observe how the control reacts to the change from CCM to DCM and to be able to arrive at a discussion for the developed tools.

5.1 OPEN-LOOP RESPONSE

For the numerical validation, we start with this section where the proposed steady-state system is tested, as the responses are shown in Figs. 5.1–5.4 match the values already reported for their voltage and current values, in this scenario, we do not take into account the inductor and capacitor ripples for control purposes as well as parametric variations and parasites of passive elements.

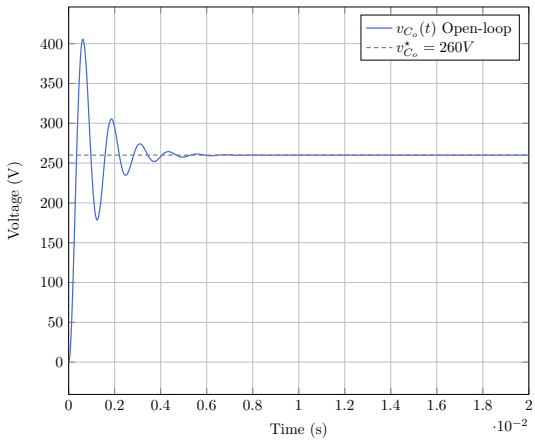

Figure 5.1: Open-loop response for voltage output.

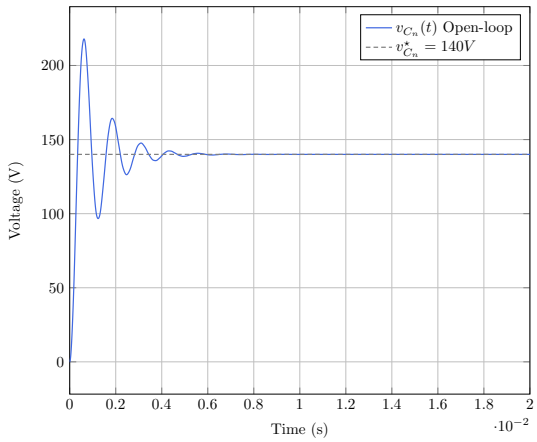

Figure 5.2: Open-loop response for voltage in PSC (SU2C) network.

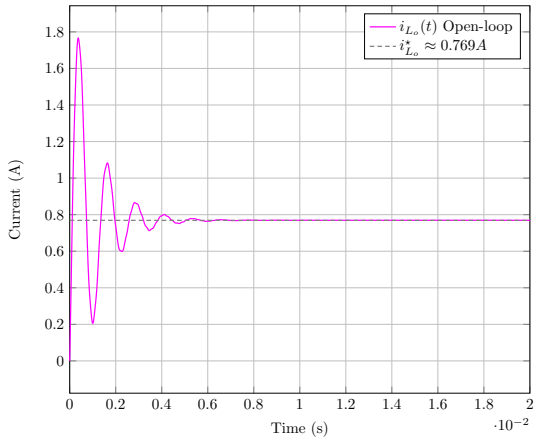

Figure 5.3: Open-loop response for current output.

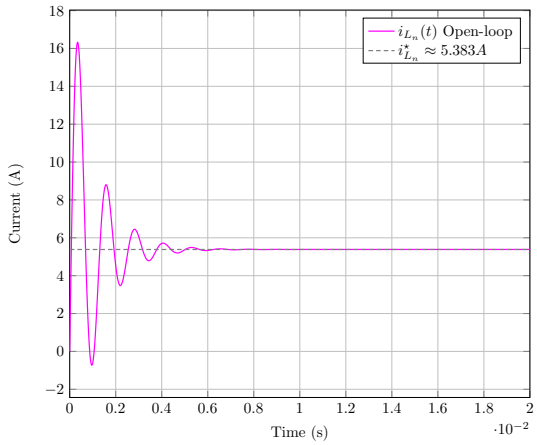

Figure 5.4: Open-loop response for current in ASL network.

5.2 LINEAR CONTROL

All numerical computations and simulations shown in this section were developed using the Matlab software (Simulink/SimPowerSystems). We study two cases for single-loop and double-loop PI control schemes. The resulting parameters-space for σ-stability analysis are shown above in Figure 3.3 and Figs. 3.4–3.5, respectively. The first result for a single-loop is obtained by a direct application of Proposition 3.1, and the pair of gains is chosen as $(k_p^{PI}, k_i^{PI}) = (0.1 \times 10^{-3}, 0.5)$ from the region $\sigma \geqslant 500$. Similarly, in double-loop, we study the inner current-loop shown in Figure 3.4. Using this figure, we choose $(k_p^c, k_i^c) = (0.056, 5.4 \times 10^3)$ from the region $\sigma < -4000$. Subsequently, we choose $(k_p^v, k_i^v) = (0.081, 95.5)$ from the region $-500 < \sigma < 0$ in order to fulfill a pole placement at least ten times farther than that of the inner current-loop. Thus, stability is ensured, and the inner current-loop exponential decay is designed faster than the voltage outer-loop. The performance of the control schemes is presented in Figs. 5.5–5.8 and Figs. 5.10–5.13 for the single and double loops by applying a soft start technique and the control action later at $t = 0.01s$ as we can see in the control laws depicted in Figure 5.9 and Figure 5.14.

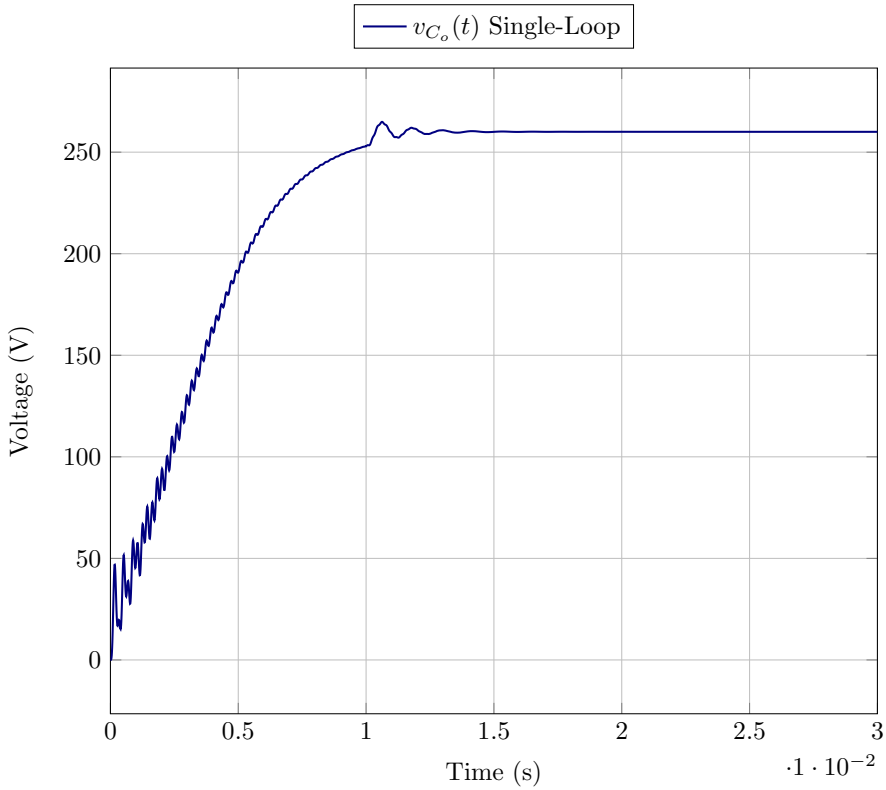

Figure 5.5: Voltage $v_{C_o}(t)$ in single-loop at nominal operation.

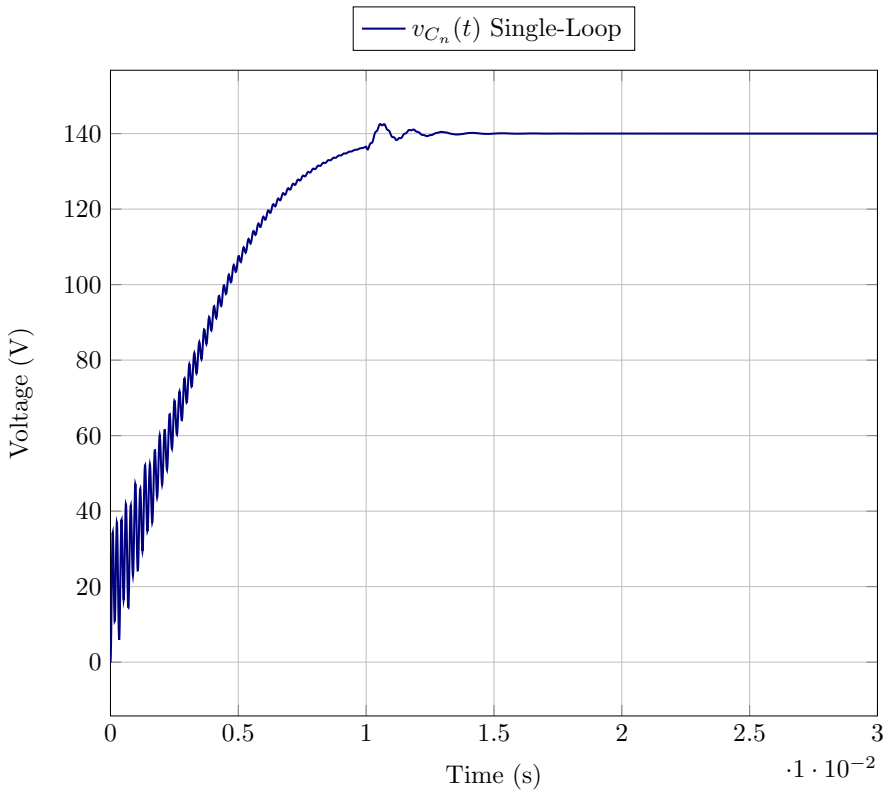

Figure 5.6: Voltage $v_{C_n}(t)$ in single-loop at nominal operation.

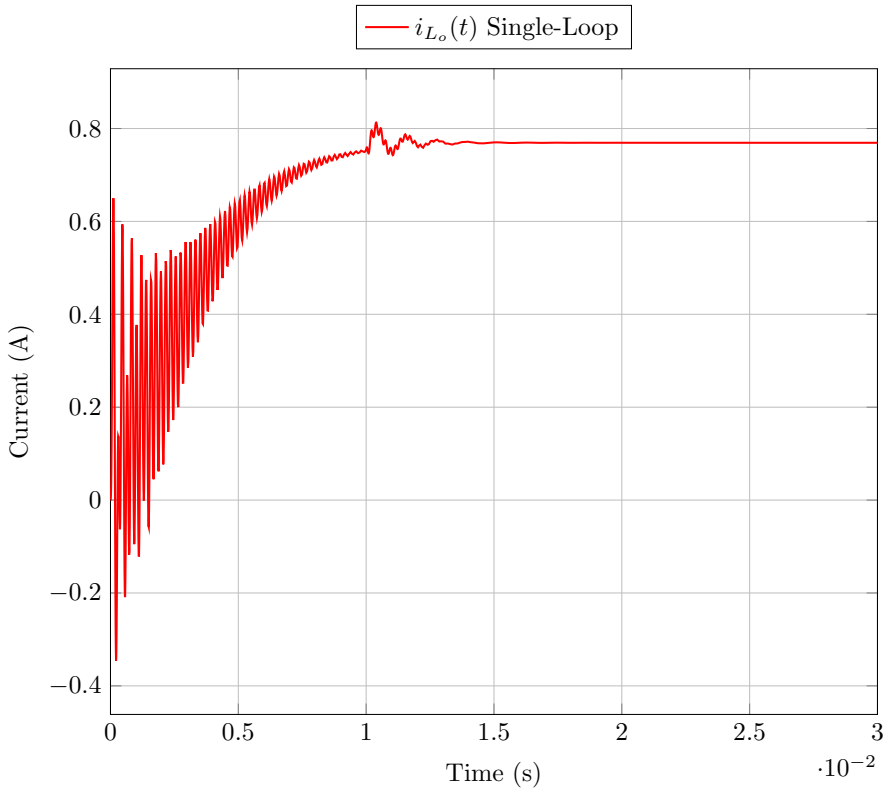

Figure 5.7: Current $i_{L_o}(t)$ in single-loop at nominal operation.

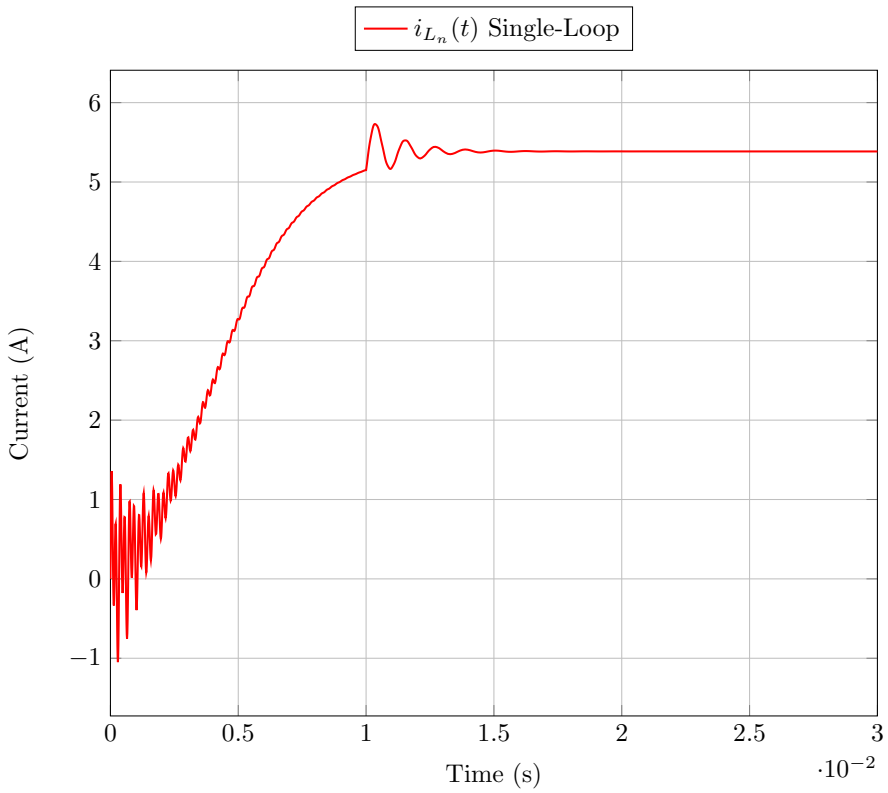

Figure 5.8: Current $i_{L_n}(t)$ in single-loop at nominal operation.

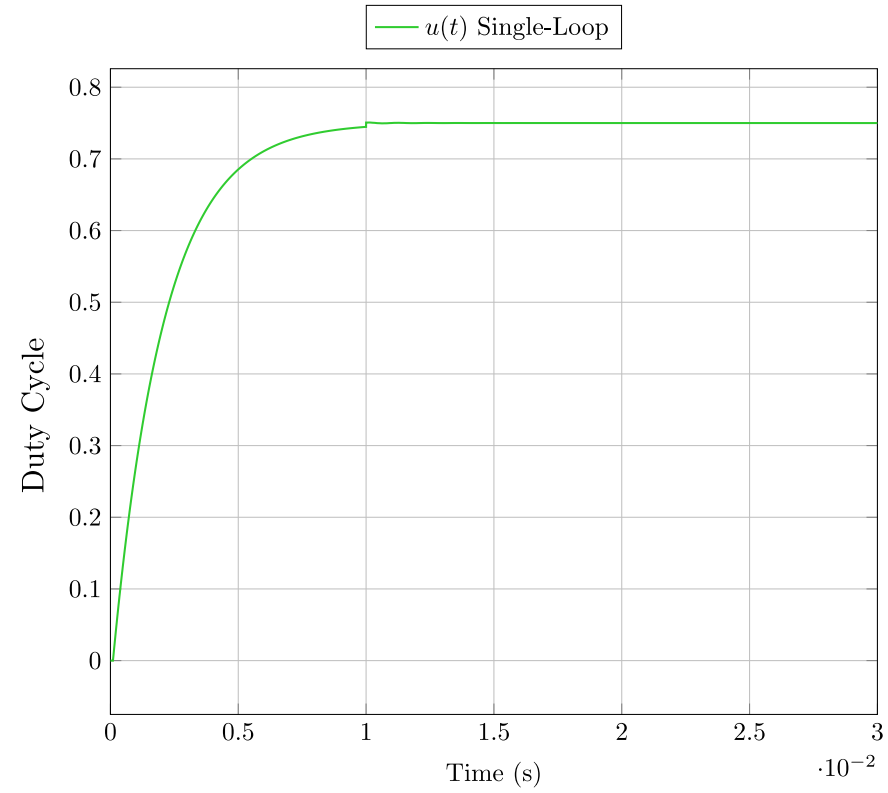

Figure 5.9: Control law $u(t)$ in single-loop at nominal operation.

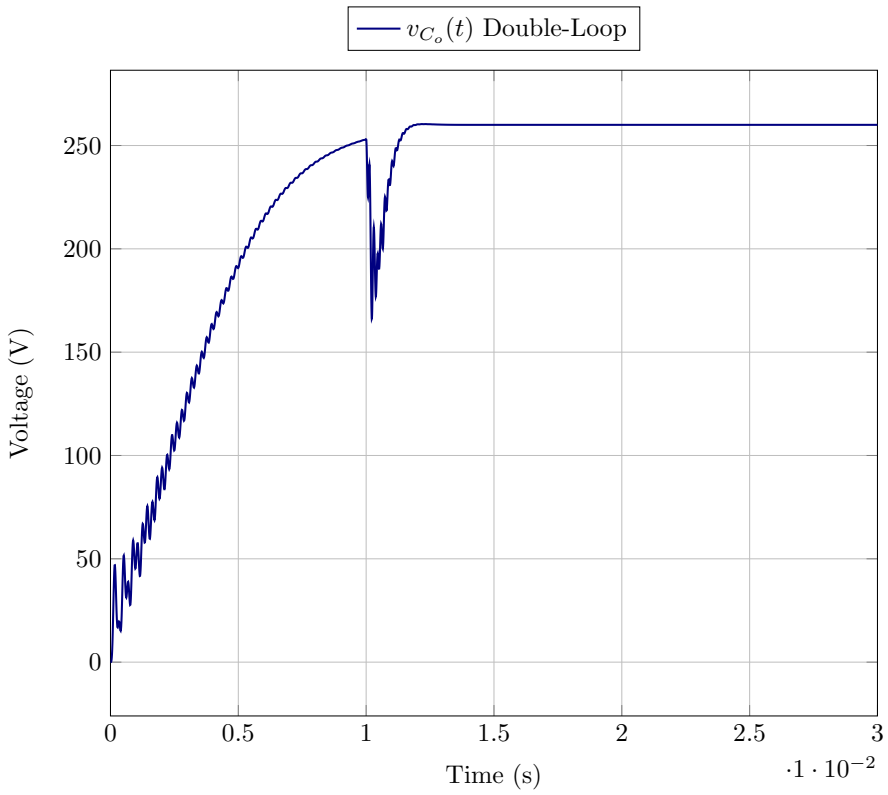

Figure 5.10: Voltage $v_{C_o}(t)$ in double-loop at nominal operation.

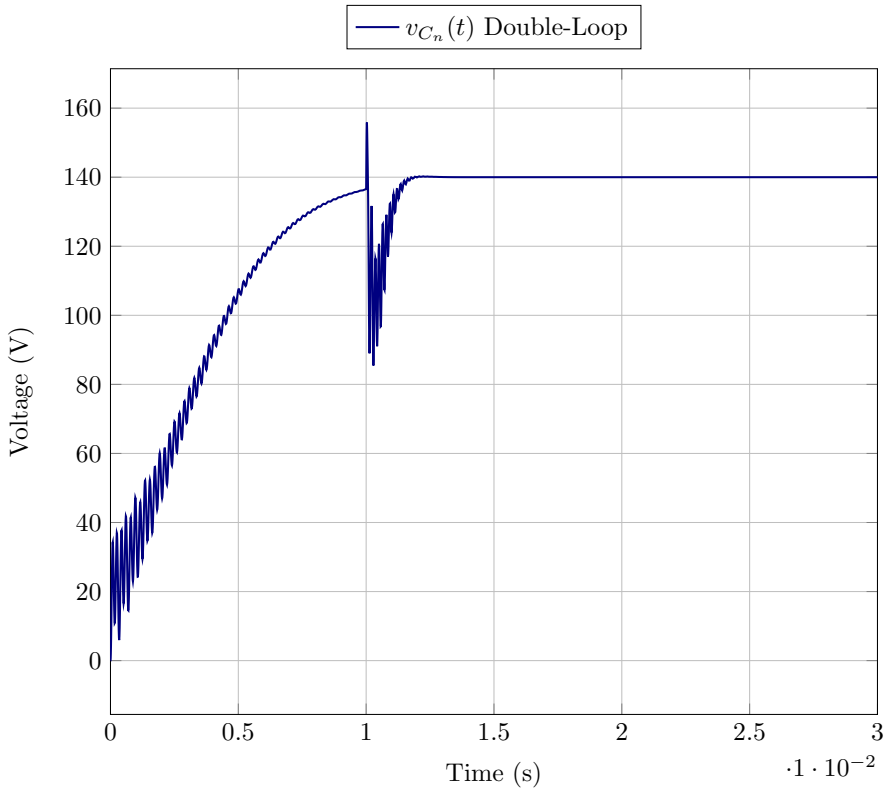

Figure 5.11: Voltage $v_{C_n}(t)$ in double-loop at nominal operation.

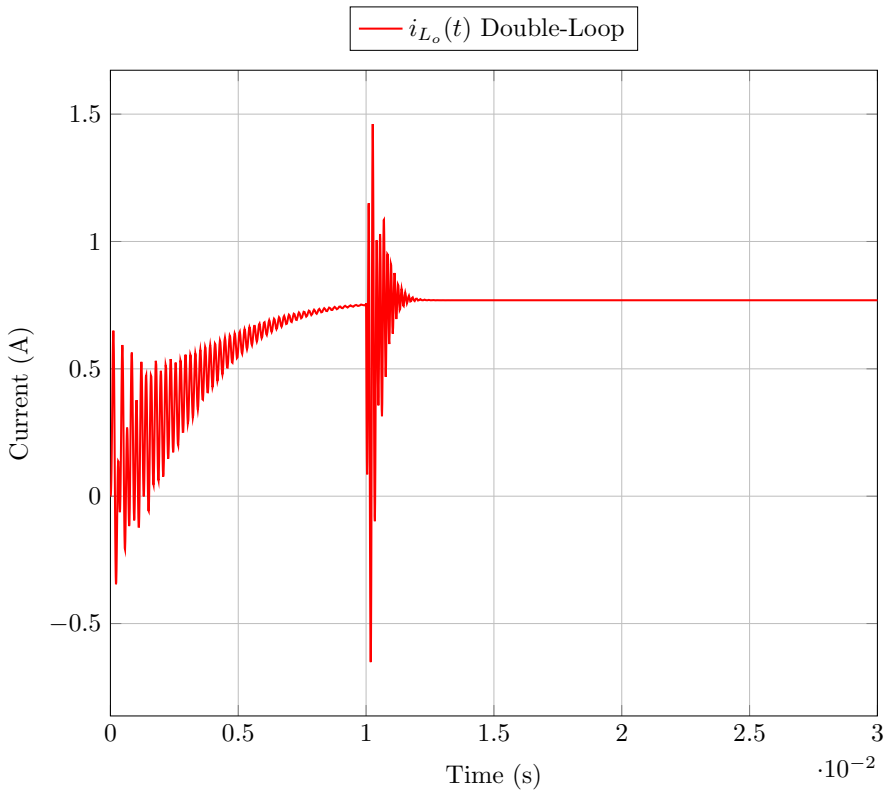

Figure 5.12: Current $i_{L_o}(t)$ in double-loop at nominal operation.

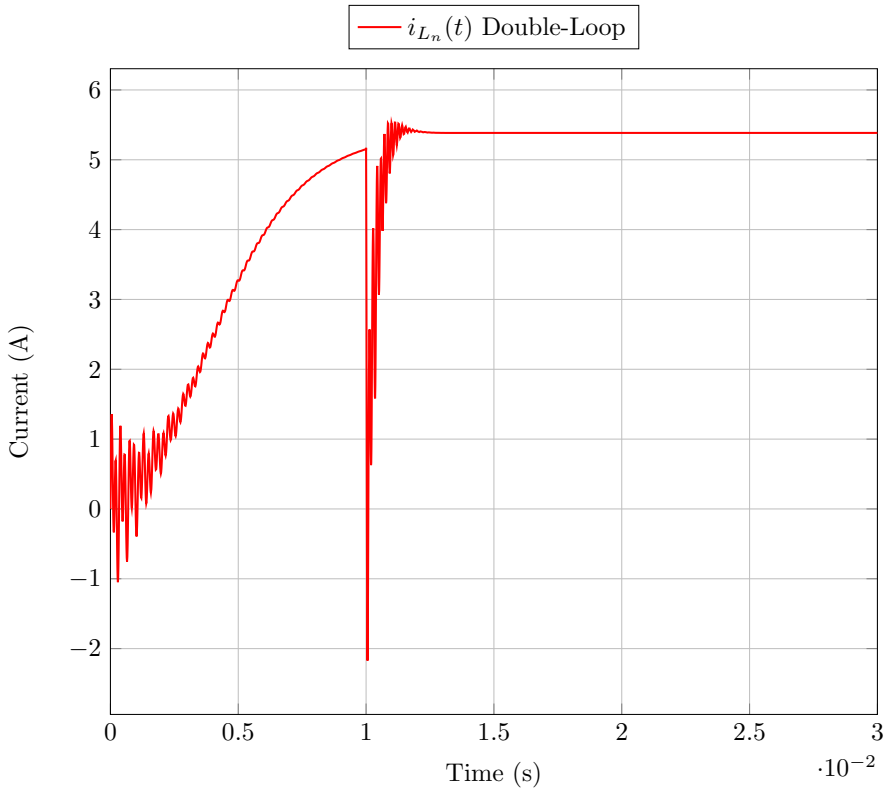

Figure 5.13: Current $i_{L_n}(t)$ in double-loop at nominal operation.

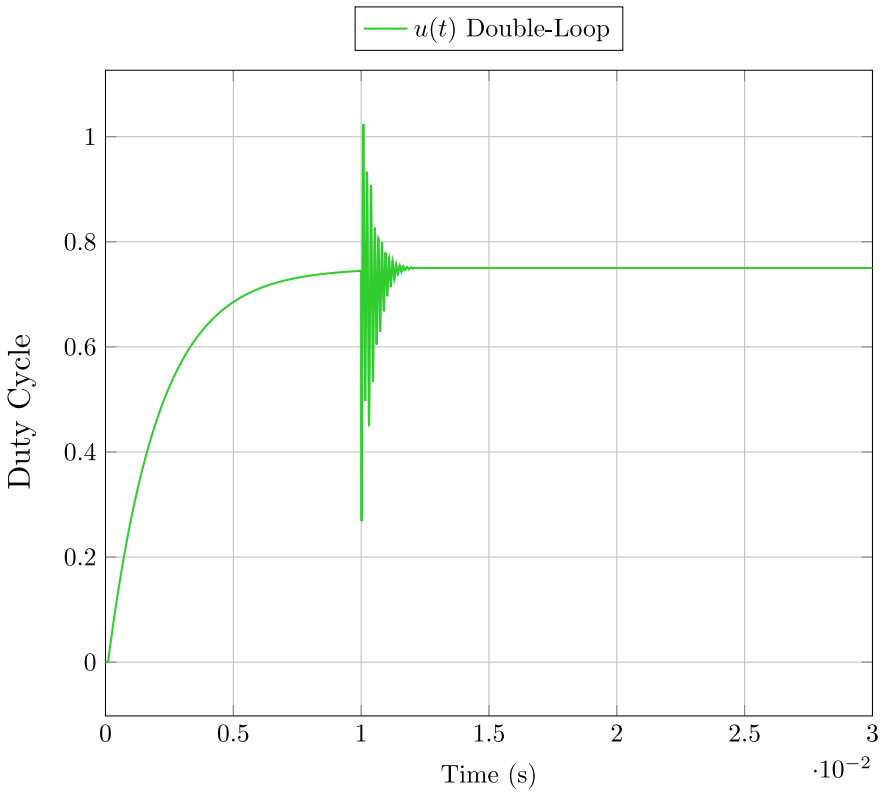

Figure 5.14: Control law $u(t)$ in double-loop at nominal operation.

From the simulations, an interesting observation in the control schemes are the behaviors when the control action is delivered to them; for a single-loop, voltages v_{C_n} and v_{C_o} has a slight overshoot as in currents i_{L_n} and i_{L_o} even though the design is only intended to regulate the voltage output. On the other hand, it does not occur in the double-loop where there is a voltage drop in the voltages producing brief overshoots and undershoots in currents; this is because we need to bring the system around the operating point and having only a single equilibrium point the control action could start before. However, it is an assumption that is made numerically speaking.
Furthermore, we present another case for the single-loop controller that highlights the importance of selecting the pair of gains in the parameter-space described in Figure 3.3. At nominal operation depicted in Figs. 5.15–5.16 presents an oscillating behavior for both voltage v_{C_o} and current i_{L_n} during steady-state by selecting $(k_p^{PI}, k_i^{PI}) = (0.038 \times 10^{-3}, 0.52)$, which is stable in the region $\sigma \geqslant -500$ but the proportional action is deficient, causing the oscillations associated to the integral action. This transient response illustrates a bad design for $\sigma-$stability that might occur because one feature of this method is that we can handle the speed convergence by its stability regions, but in some cases, the convergence is dependent regardless of pure proportional or integral action affecting steady-state response. Therefore,

as a good design practice, it is advisable to use other tuning criteria as a support (see, for instance, [66]).

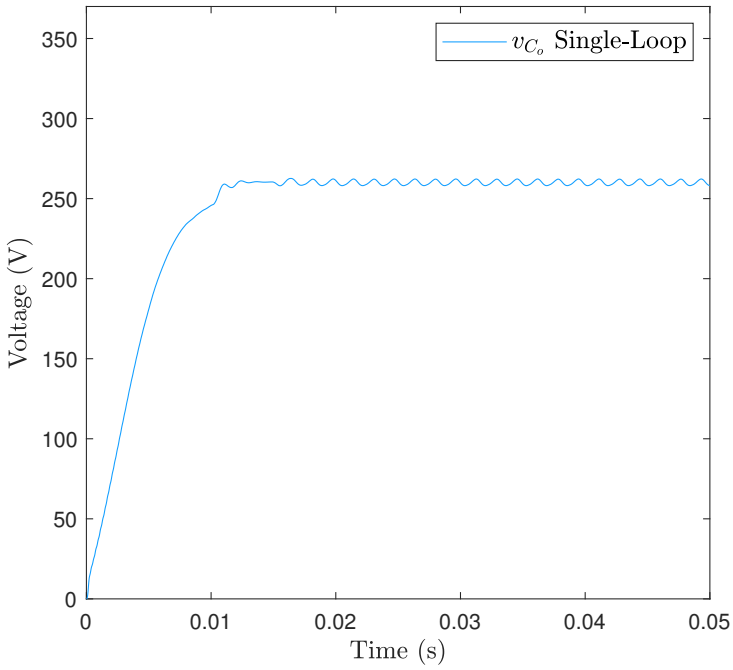

Figure 5.15: Voltage v_{C_o} with oscillating behavior.

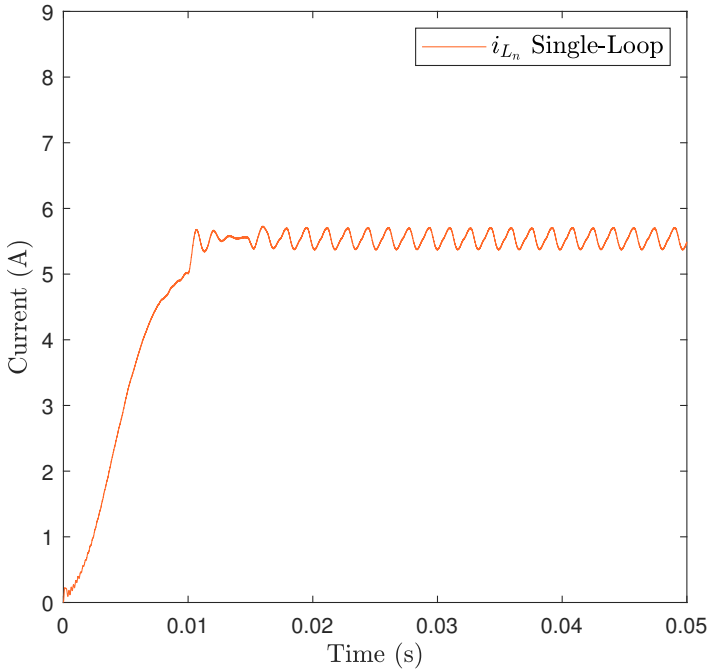

Figure 5.16: Voltage i_{L_n} with oscillating behavior.

5.3 NONLINEAR CONTROL

In the case of the nonlinear approach, we get the simulations depicted in Figs. 5.17–5.20 employing the parameters shown in Table 4.1, by selecting Sample 8 $K_p = 6 \times 10^{-4}$ and $K_i = 1$ as the pair of gains. The results for each state of ASL-SU2C are presented by the assumption of a known load without changes and initial conditions equal to zero, showing regulation in detail through capacitor voltages and inductors currents.

In this type of control, it is remarkable the kind of start-up we have from $t = 0$ until the system reaches the convergence of the desired value with any gain K_p, K_i (proof of detectability). In the simulation samples presented in Chapter 4, it is observed that all of them are asymptotically stable; however, we chose to take Sample 8 because we consider that it was the best trajectory for the states of interest.

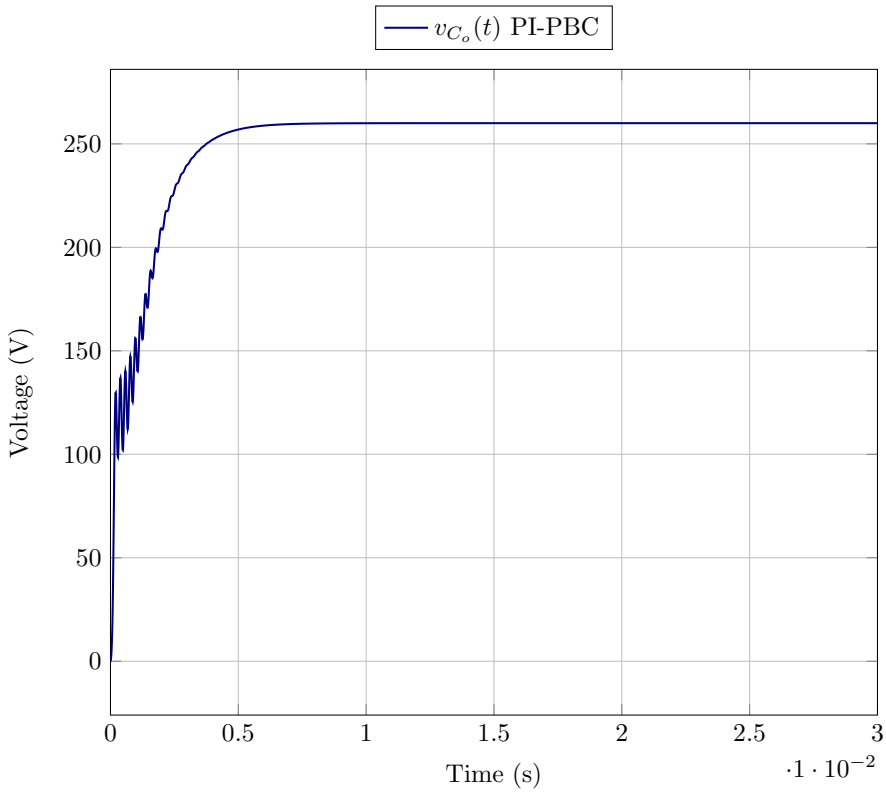

Figure 5.17: Voltage $v_{C_o}(t)$ PI-PBC at nominal operation.

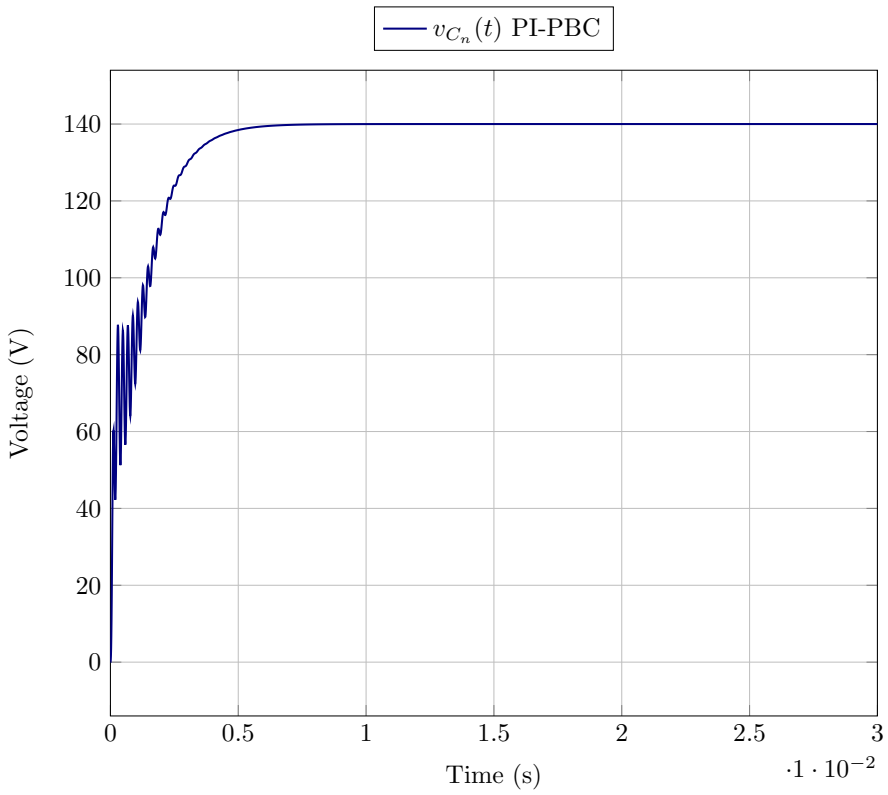

Figure 5.18: Voltage $v_{C_n}(t)$ PI-PBC at nominal operation.

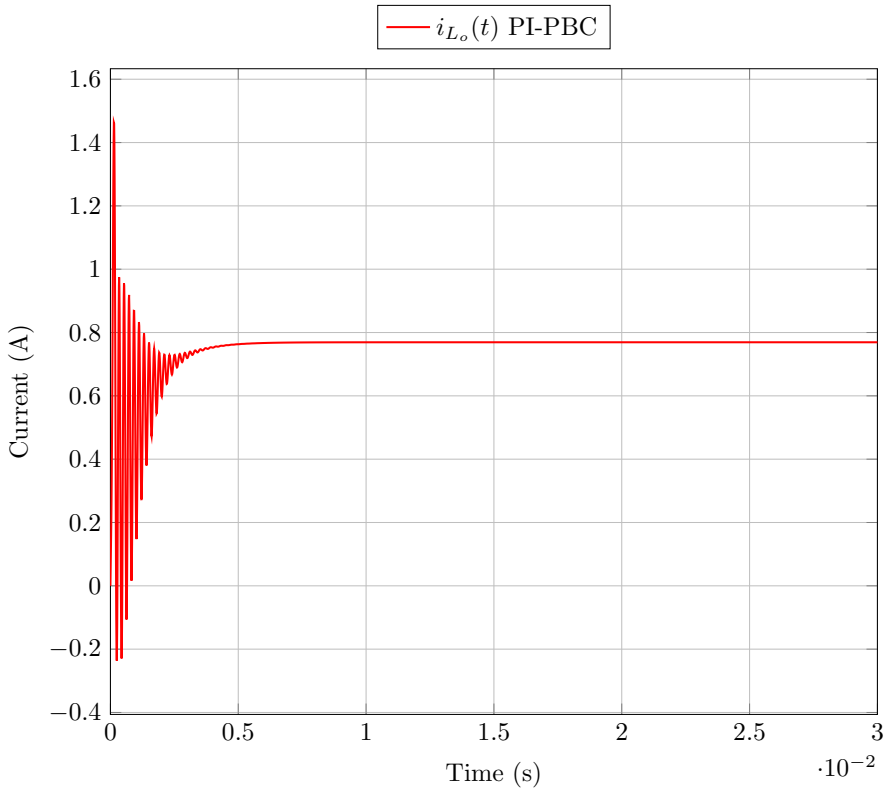

Figure 5.19: Current $i_{L_o}(t)$ PI-PBC at nominal operation.

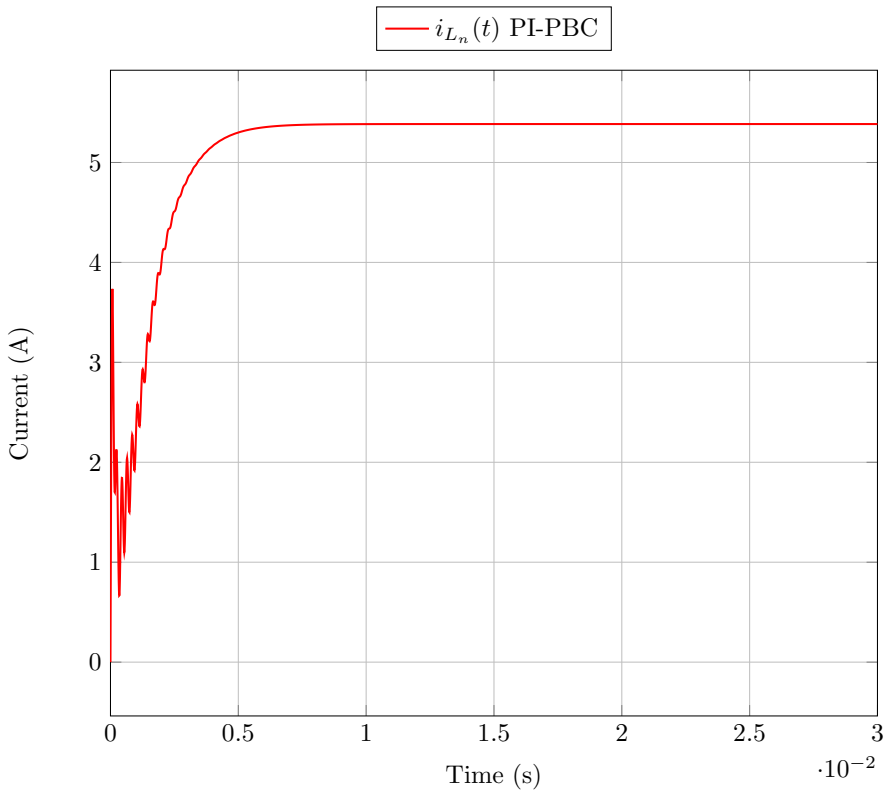

Figure 5.20: Current $i_{L_n}(t)$ PI-PBC at nominal operation.

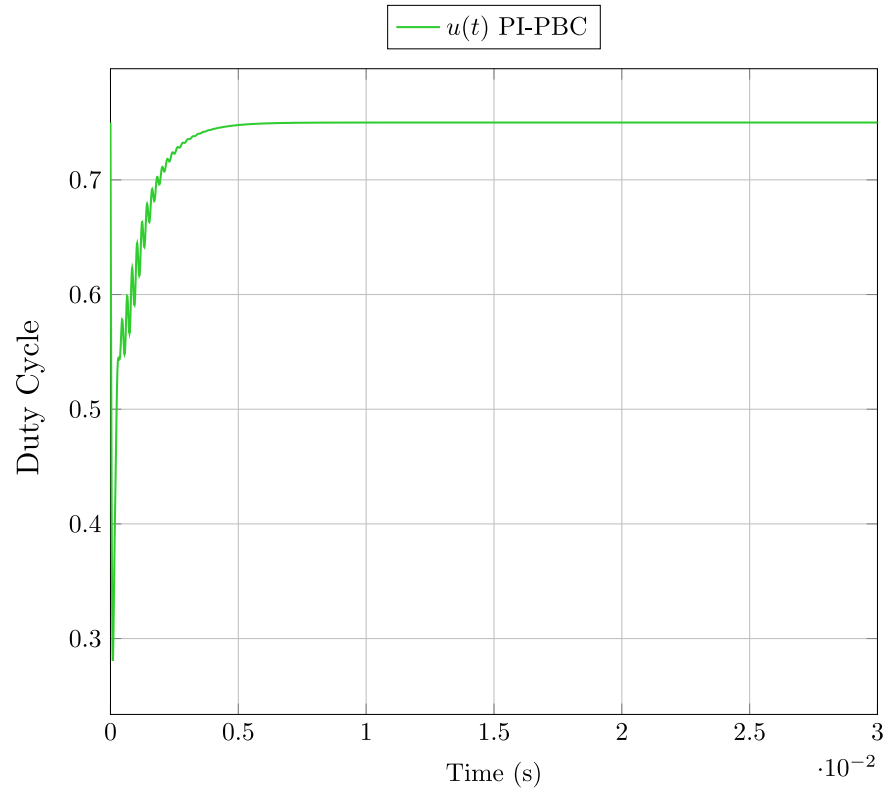

Figure 5.21: Control law $u(t)$ in PI-PBC at nominal operation.

5.4 TRANSIENT-RESPONSE COMPARISON

In this evaluation, three types of tests were performed where the load values were changed to emulate cases that could occur during specific time intervals. The load changes, in particular, were made in brief periods due to we want to highlight the properties of the σ-stability methodology since it is a result that performs the maximum speed of convergence. The simulation cases shown do not start from zero since when observing the previous results the nonlinear control would exceed widely in the start to the other controllers. At the end of this section, we depicted the specification tables of the transient response for tests 1 and 3 and some small observations and remarks for test 2, since, in test 2, the load value changes suddenly and in a staggered manner; for making transient response specification an evaluation would have to be made for each time interval.
Therefore, the robustness tests are divided into a) the dynamic load and the response of the I&I observer, fixing in all tests the parameters $\gamma = 10, \zeta = 5 \times 10^{-5}$, b) the response of the control laws, c), d), e) and f) correspond to the responses of each state of the converter, respectively. Then, the load shifting cases were performed to

1. holding the load at twice its nominal value and returning .
2. rise to twice its nominal value and fall in a staggered manner.
3. change to R_{crit}.

Table 5.1 shows the robustness tests in detail.

Table 5.1: Performance of controllers in robustness tests.

Test	Resistance Load	A-PI-PBC	Double-Loop	Single-Loop
1	$676\Omega,\ t < 0.02s$ $338\Omega,\ 0.02s \leqslant t < 0.024s$	$K_p = 6 \times 10^{-4}, K_i = 1$ $\gamma = 10, \zeta = 5 \times 10^{-5}$	$k_p^c = 0.056, k_i^c = 5.4 \times 10^3$ $k_p^v = 0.081, k_i^v = 95.5$	$k_p^{PI} = 0.1 \times 10^{-3}$ $k_i^{PI} = 0.5$
2	$338\Omega,\ t < 0.02s$ $576\Omega,\ 0.02s \leqslant t < 0.024s$ $676\Omega,\ 0.024s \leqslant t < 0.036s$ $338\Omega,\ 0.036s \leqslant t < 0.04s$ $238\Omega,\ 0.04s \leqslant t < 0.044s$	$K_p = 6 \times 10^{-4}, K_i = 1$ $\gamma = 10, \zeta = 5 \times 10^{-5}$	$k_p^c = 0.056, k_i^c = 5.4 \times 10^3$ $k_p^v = 0.081, k_i^v = 95.5$	$k_p^{PI} = 0.1 \times 10^{-3}$ $k_i^{PI} = 0.5$
3	$338\Omega,\ t < 0.03s$ $2597\Omega,\ 0.03s \leqslant t < 0.11s$ $338\Omega,\ 0.11s \leqslant t < 0.13s$	$K_p = 6 \times 10^{-4}, K_i = 1$ $\gamma = 10, \zeta = 5 \times 10^{-5}$	$k_p^c = 0.056, k_i^c = 5.4 \times 10^3$ $k_p^v = 0.081, k_i^v = 95.5$	$k_p^{PI} = 0.1 \times 10^{-3}$ $k_i^{PI} = 0.5$

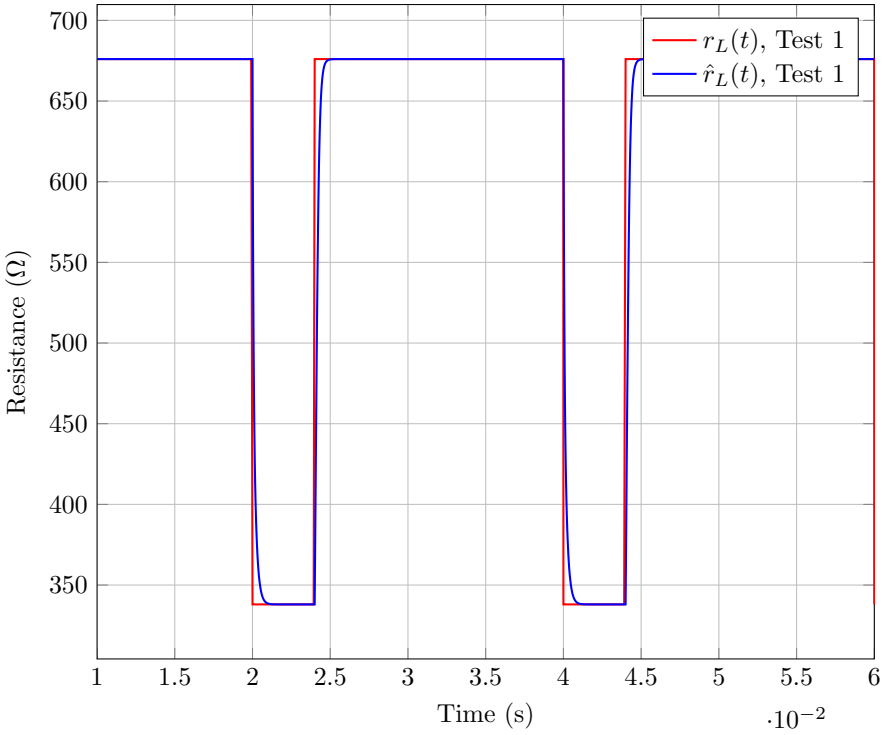

Figure 5.22: Robustness test 1.

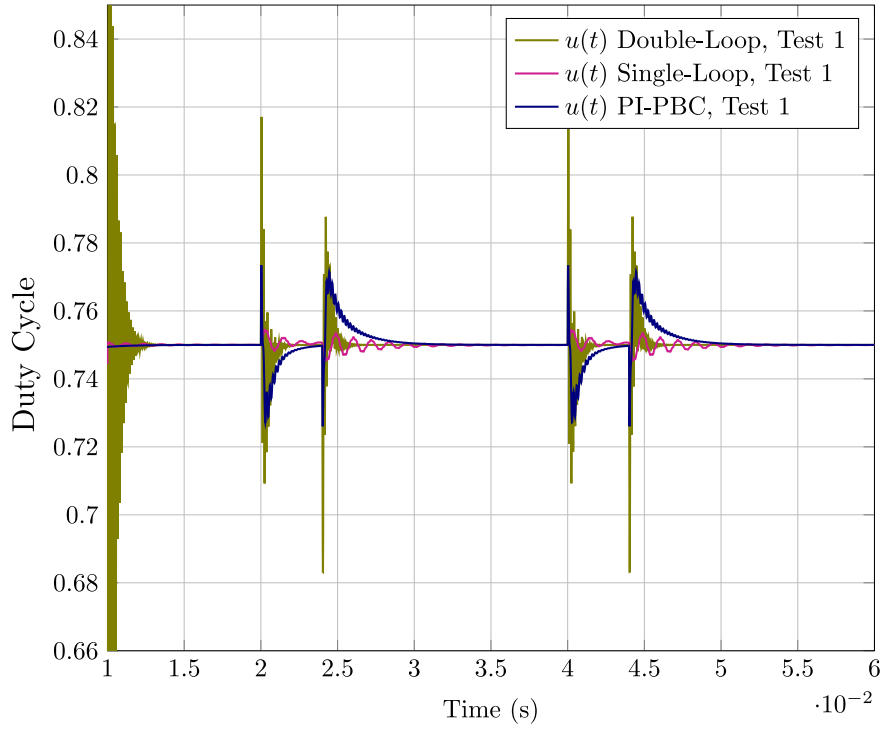

Figure 5.23: Control law under test 1.

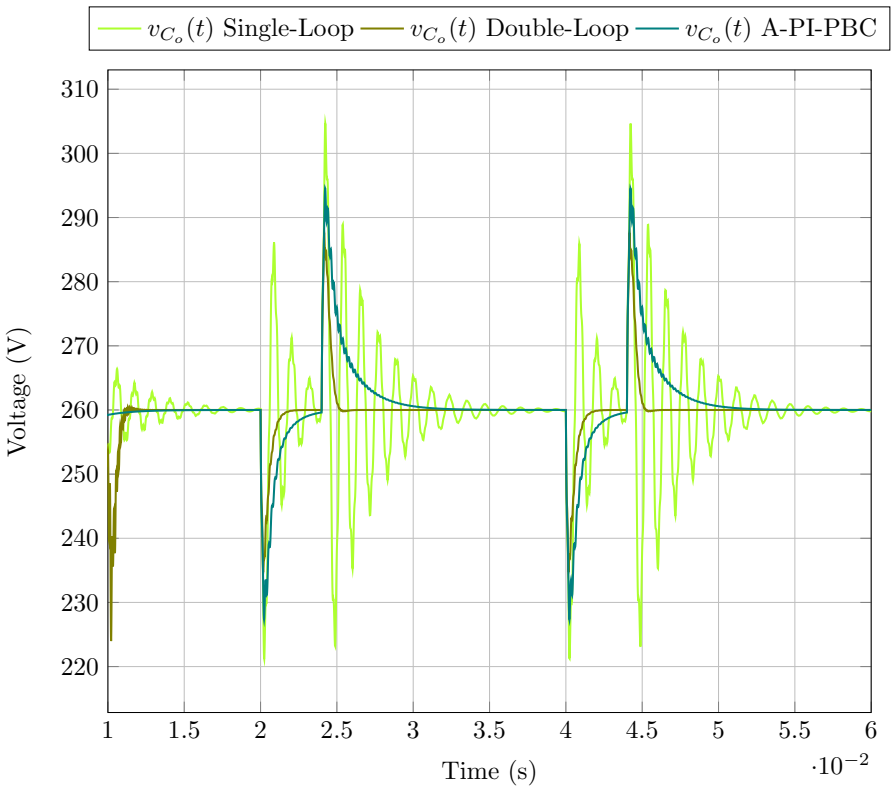

Figure 5.24: Voltage $v_{C_o}(t)$ of the proposed control tools under test 1.

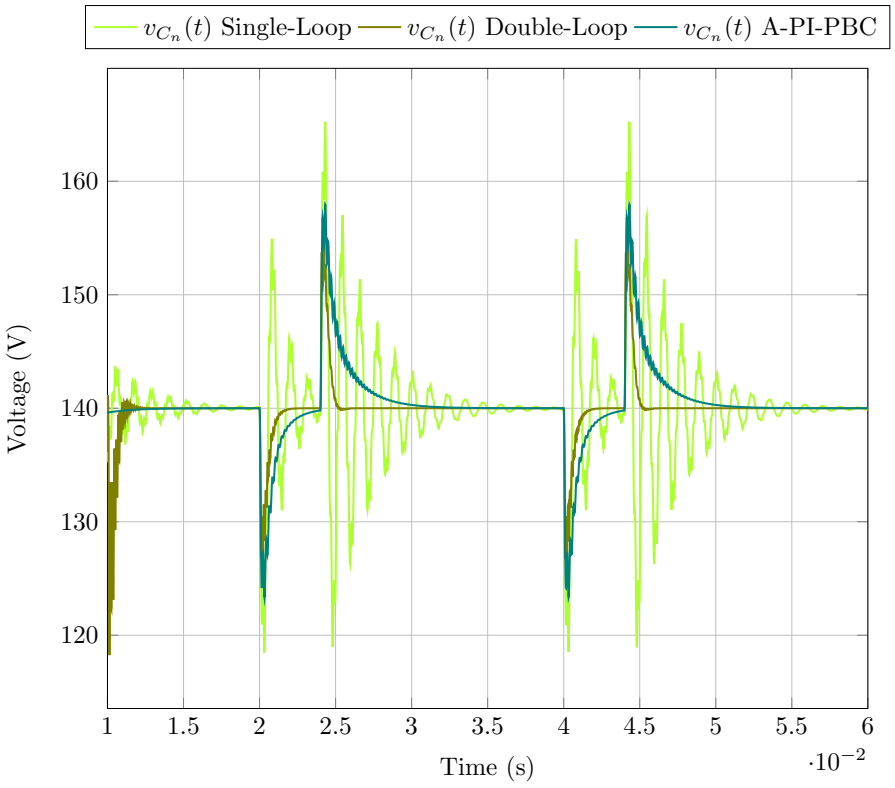

Figure 5.25: Voltage $v_{C_n}(t)$ of the proposed control tools under test 1.

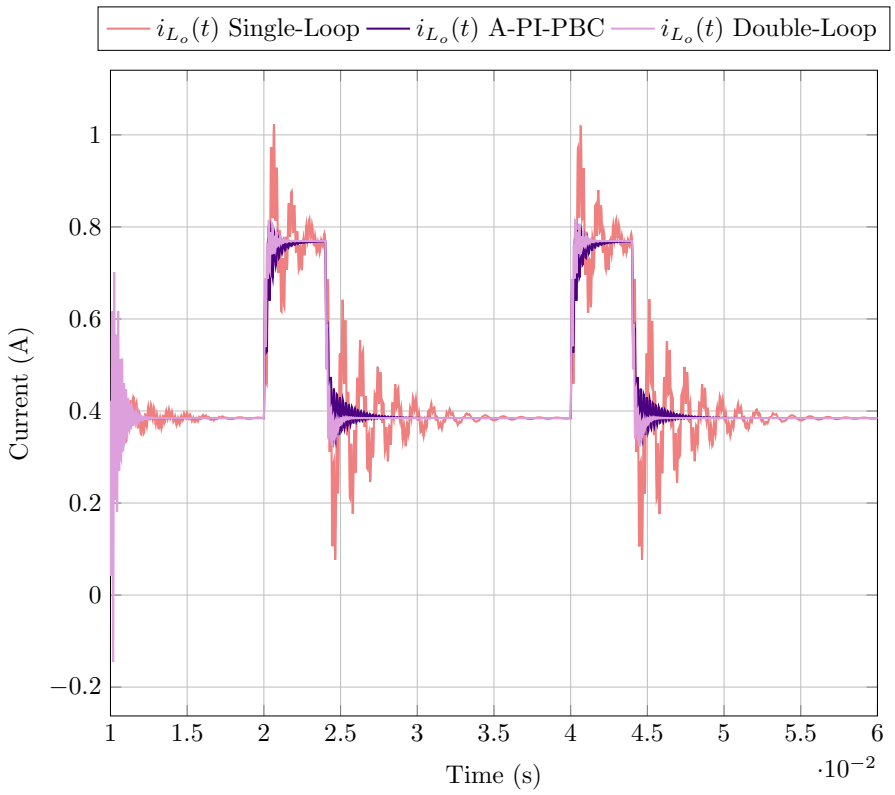

Figure 5.26: Current $i_{L_o}(t)$ of the proposed control tools under test 1.

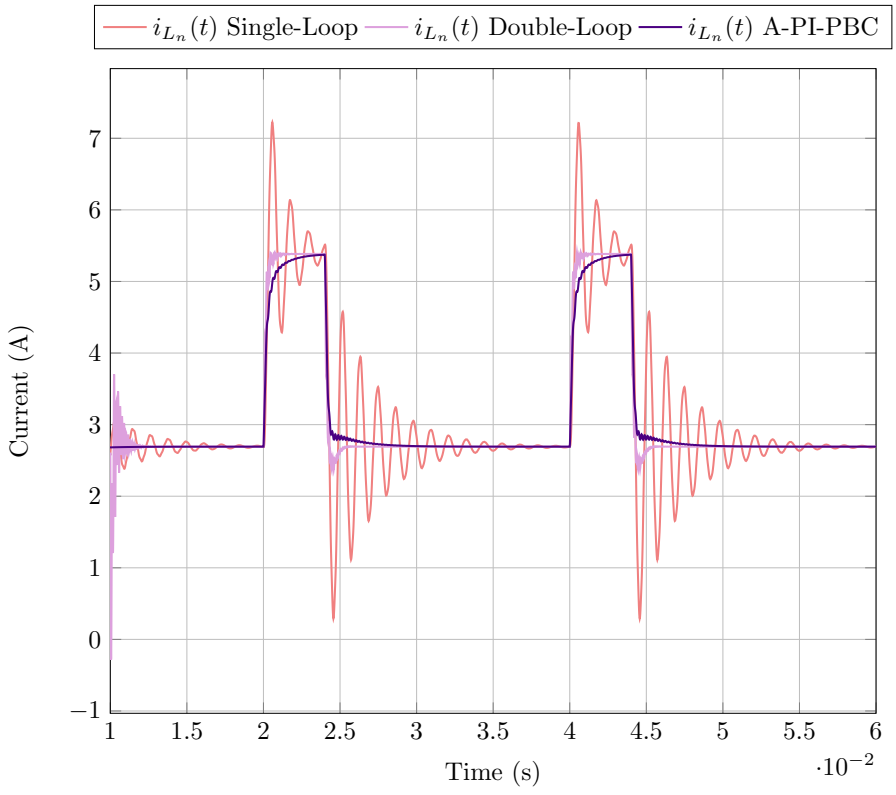

Figure 5.27: Current $i_{L_n}(t)$ of the proposed control tools under test 1.

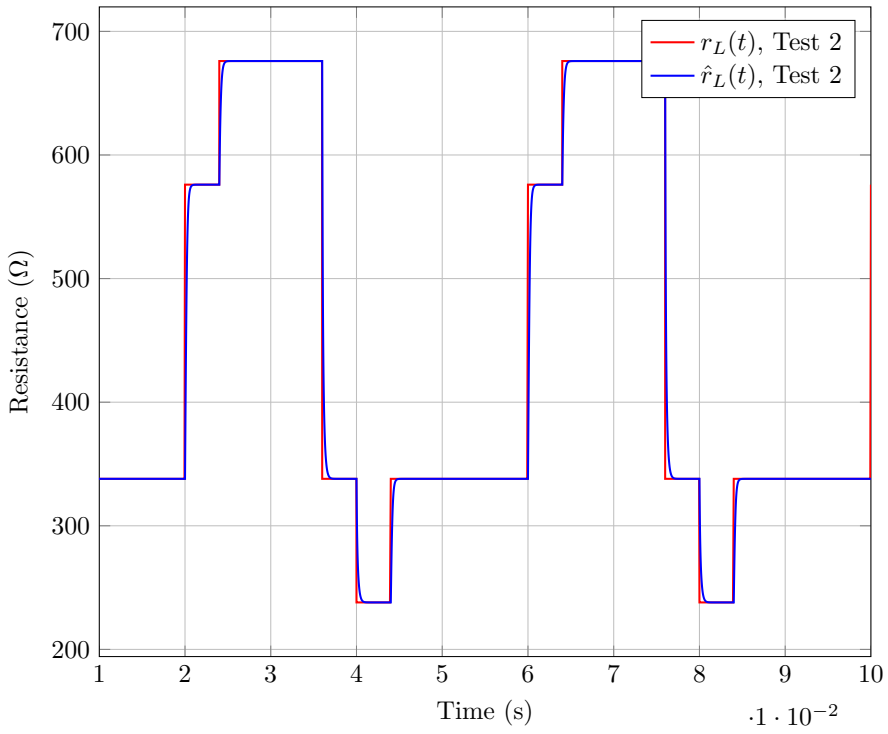

Figure 5.28: Robustness test 2.

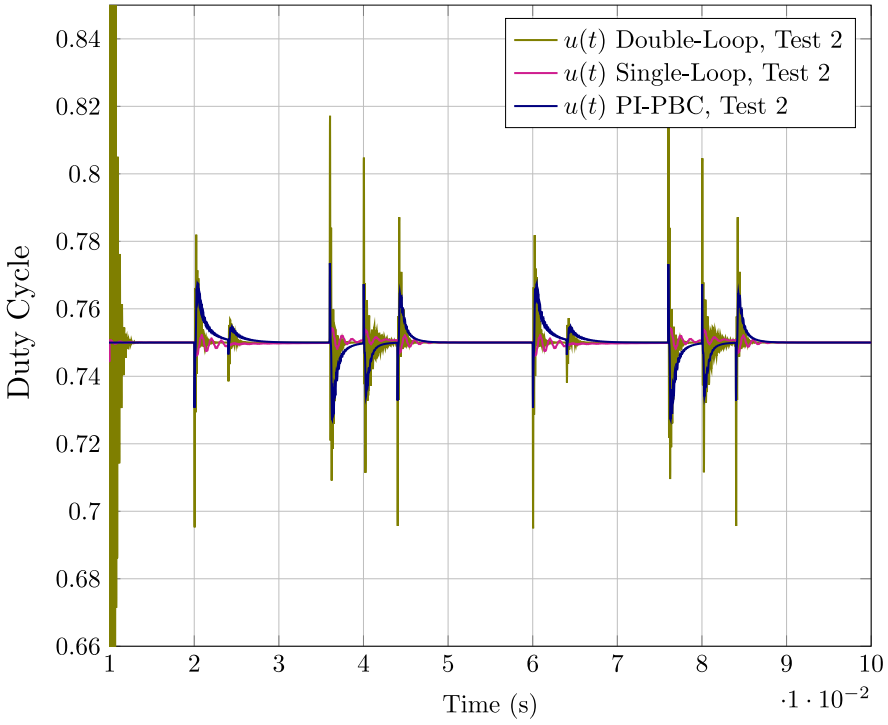

Figure 5.29: Control law under test 2.

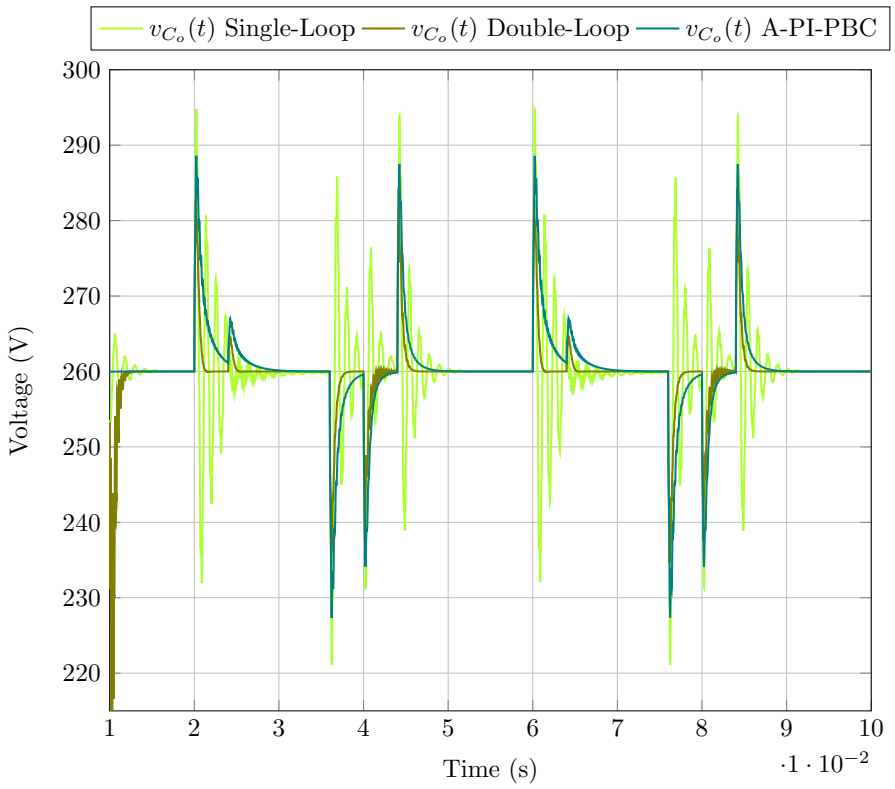

Figure 5.30: Voltage $v_{C_o}(t)$ of the proposed control tools under test 2.

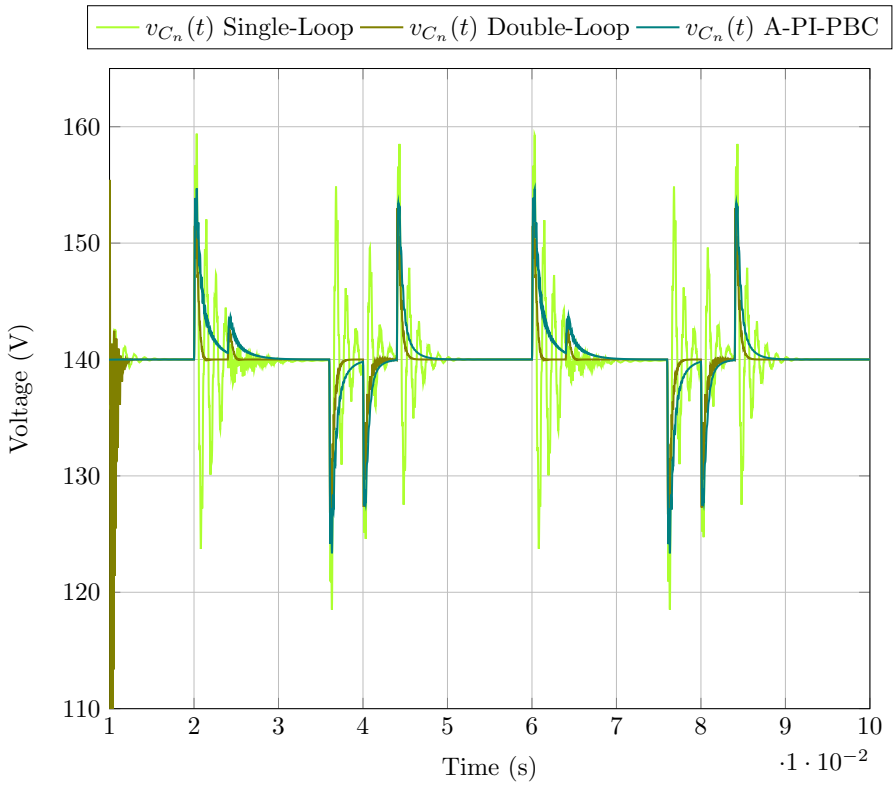

Figure 5.31: Voltage $v_{C_n}(t)$ of the proposed control tools under test 2.

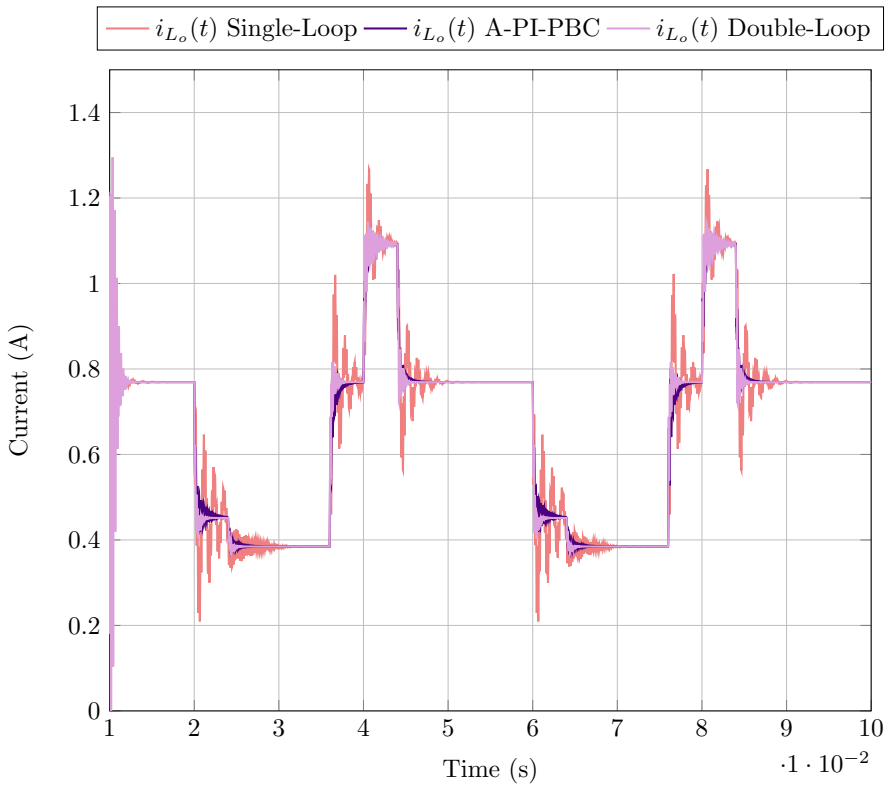

Figure 5.32: Current $i_{L_o}(t)$ of the proposed control tools under test 2.

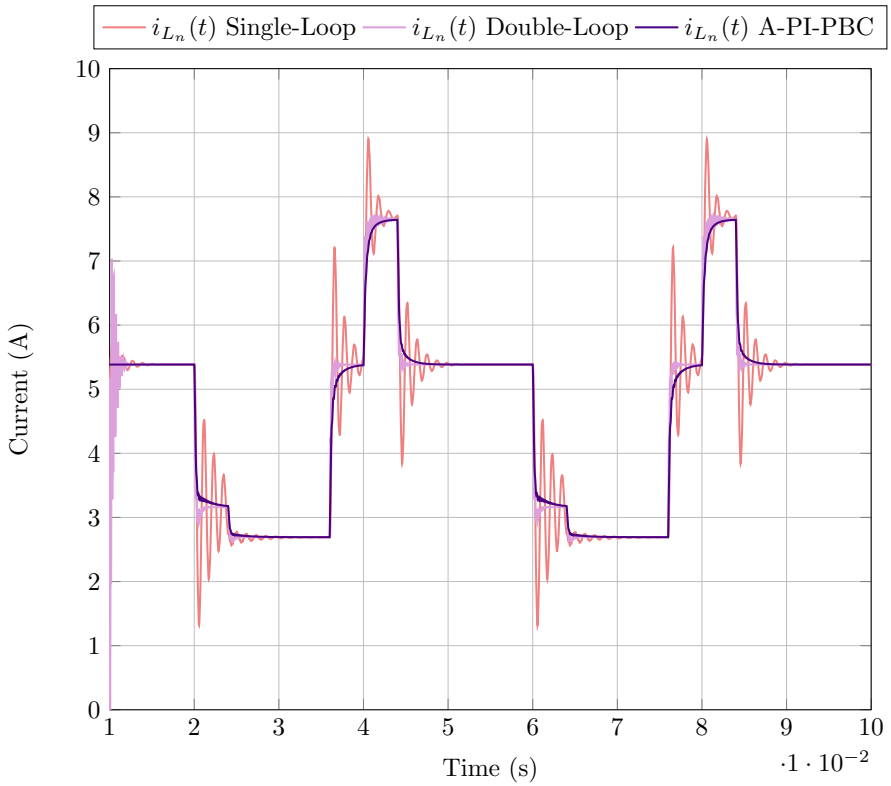

Figure 5.33: Current $i_{L_n}(t)$ of the proposed control tools under test 2.

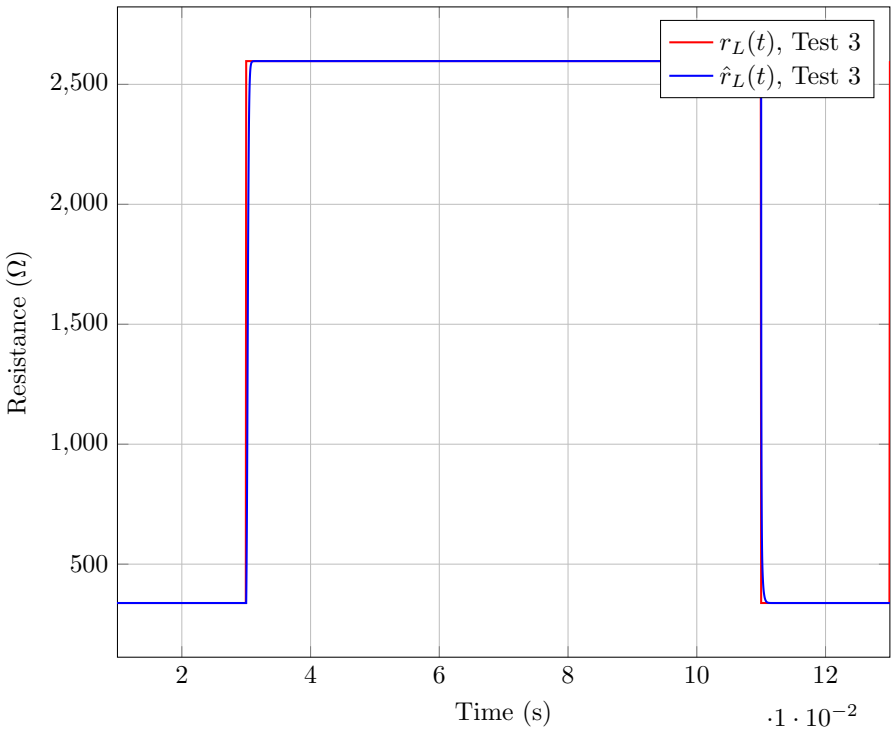

Figure 5.34: Robustness test 3.

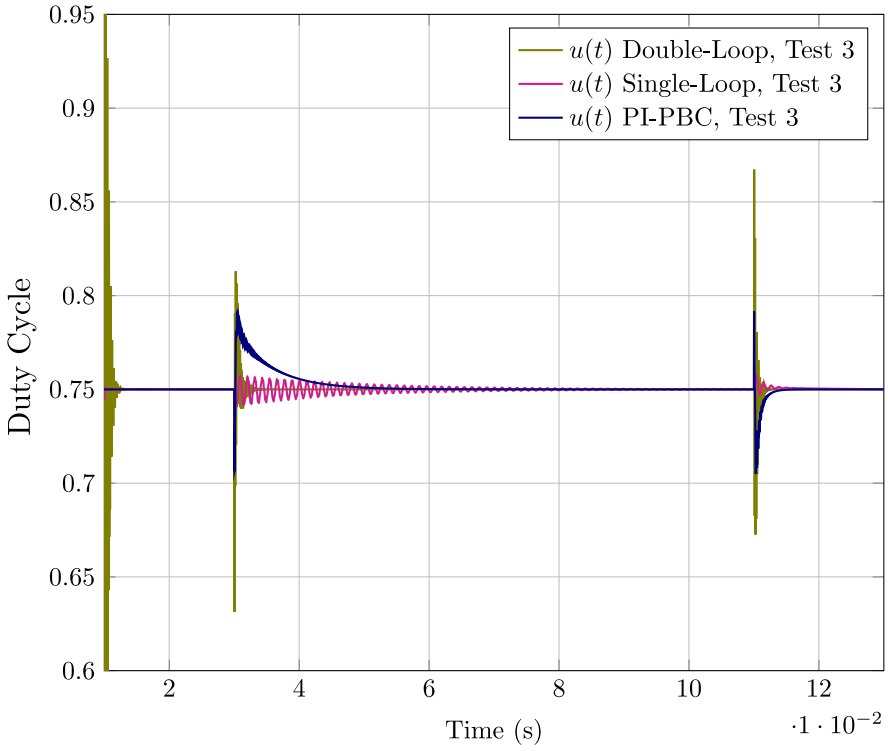

Figure 5.35: Control law under test 3.

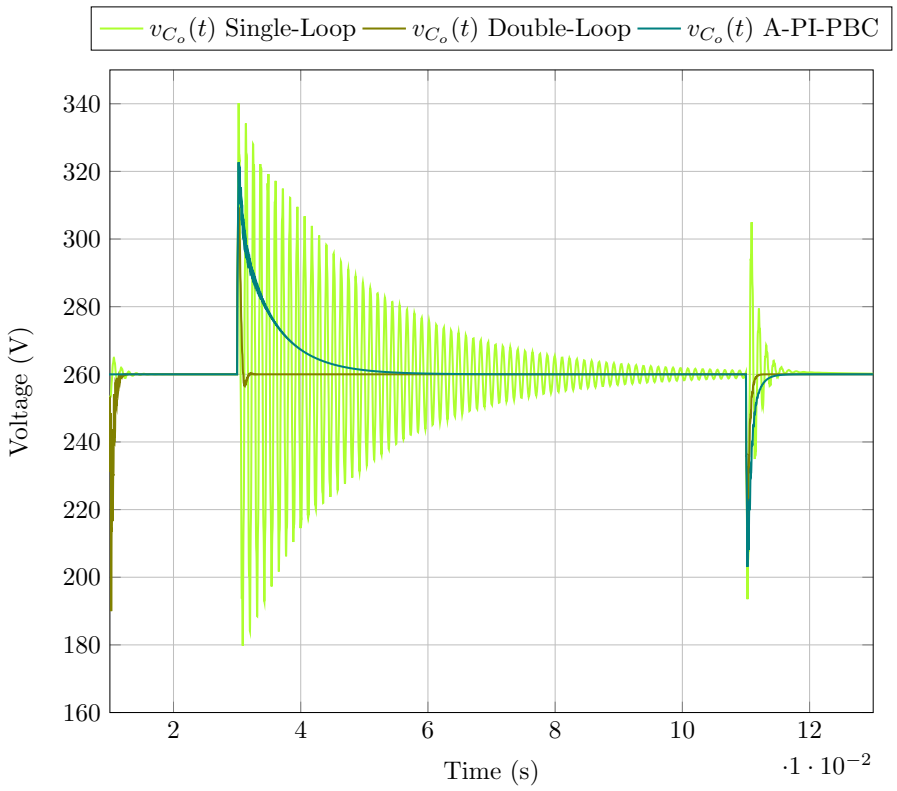

Figure 5.36: Voltage $v_{C_o}(t)$ of the proposed control tools under test 3.

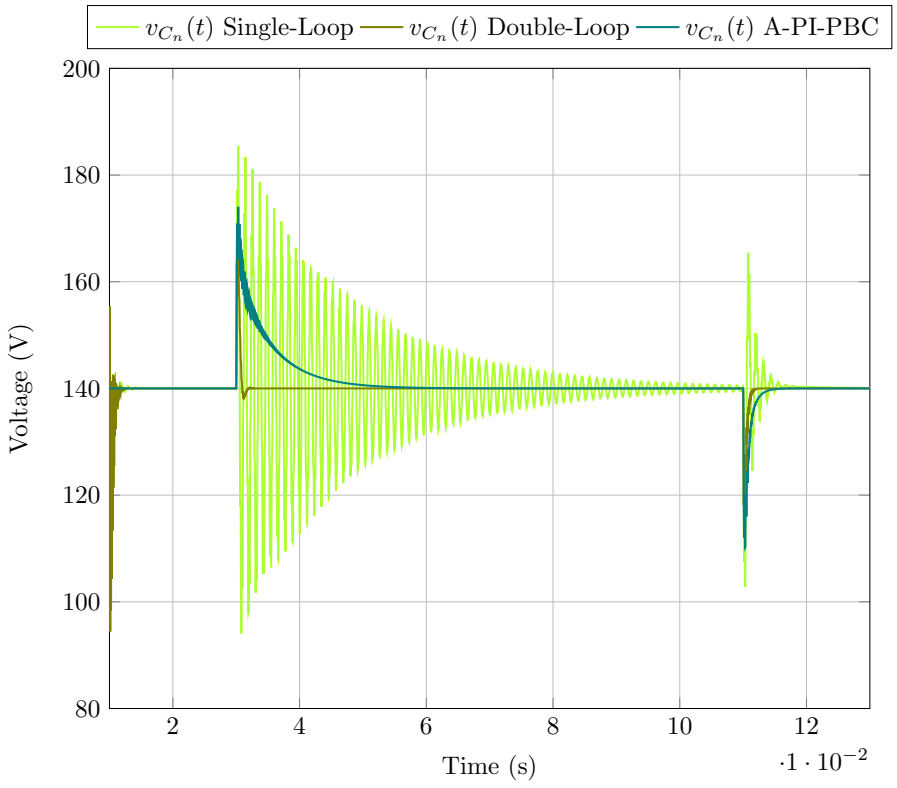

Figure 5.37: Voltage $v_{C_n}(t)$ of the proposed control tools under test 3.

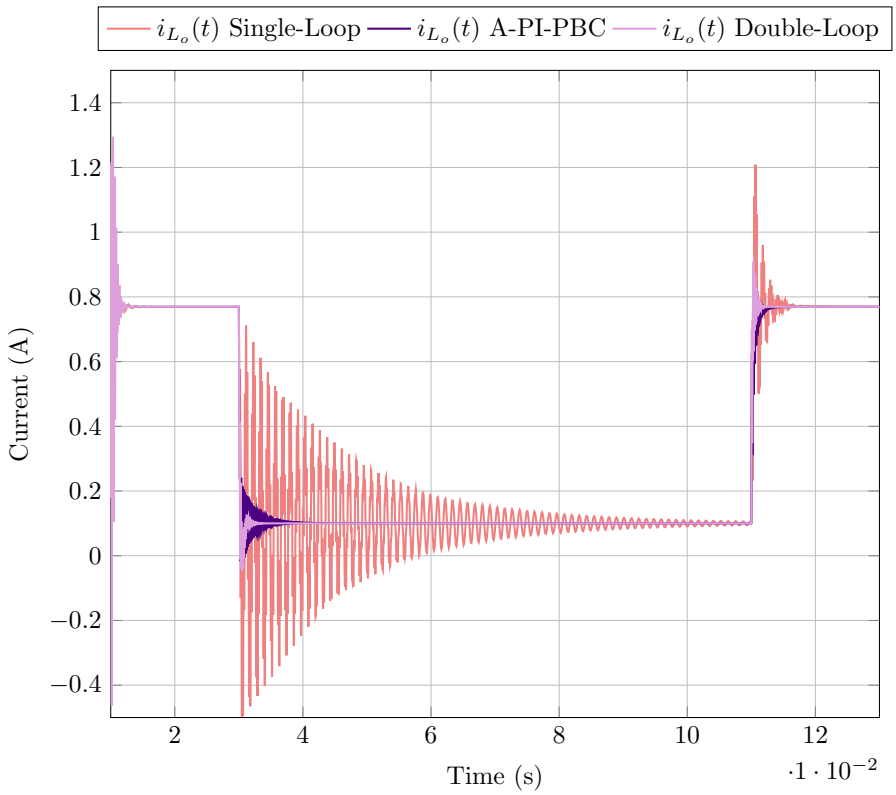

Figure 5.38: Current $i_{L_o}(t)$ of the proposed control tools under test 3.

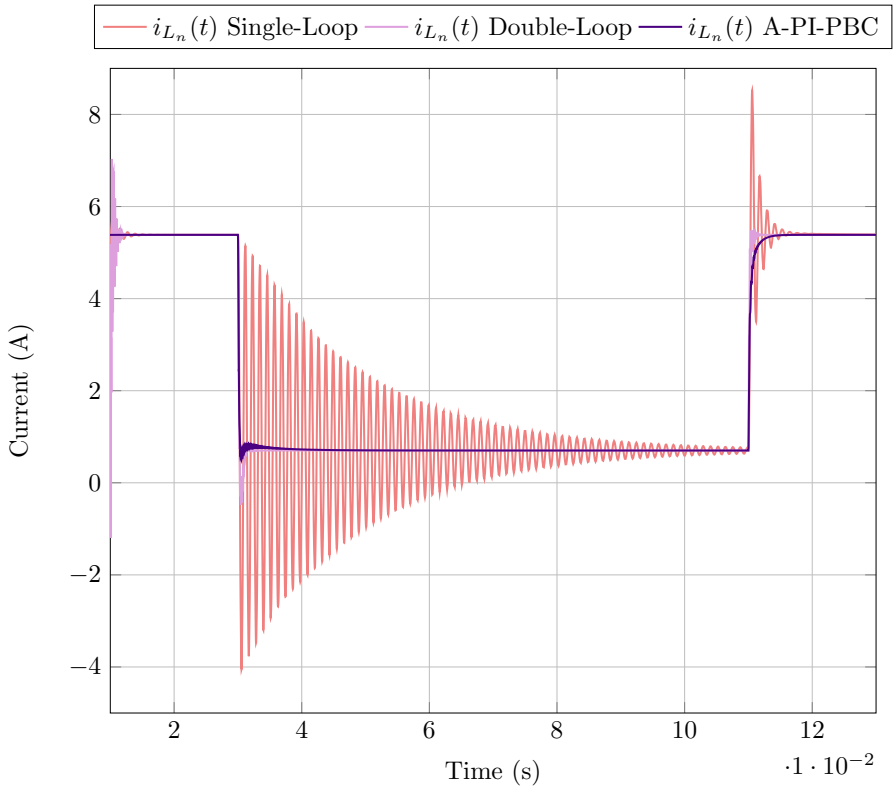

Figure 5.39: Current $i_{L_n}(t)$ of the proposed control tools under test 3.

The results shown in Figs. 5.22–5.39 summarize the three robustness tests of the system by changing the converter load values. For the evaluation of its transient-response, we took into account specific characteristics that occur when the state trajectory values are above and below its nominal response only for voltage v_{C_o} and current i_{L_n}, since the control schemes were designed for the best performance of these two states. Figure 5.40 shows an example of how we measured the characteristics for the specification tables in each robustness test. Therefore, bottom time, maximum undershoot, and under settling time refer to transients below their nominal values whereas peak time, maximum overshoot, and upper settling time to transients above their nominal operation.

Test 1

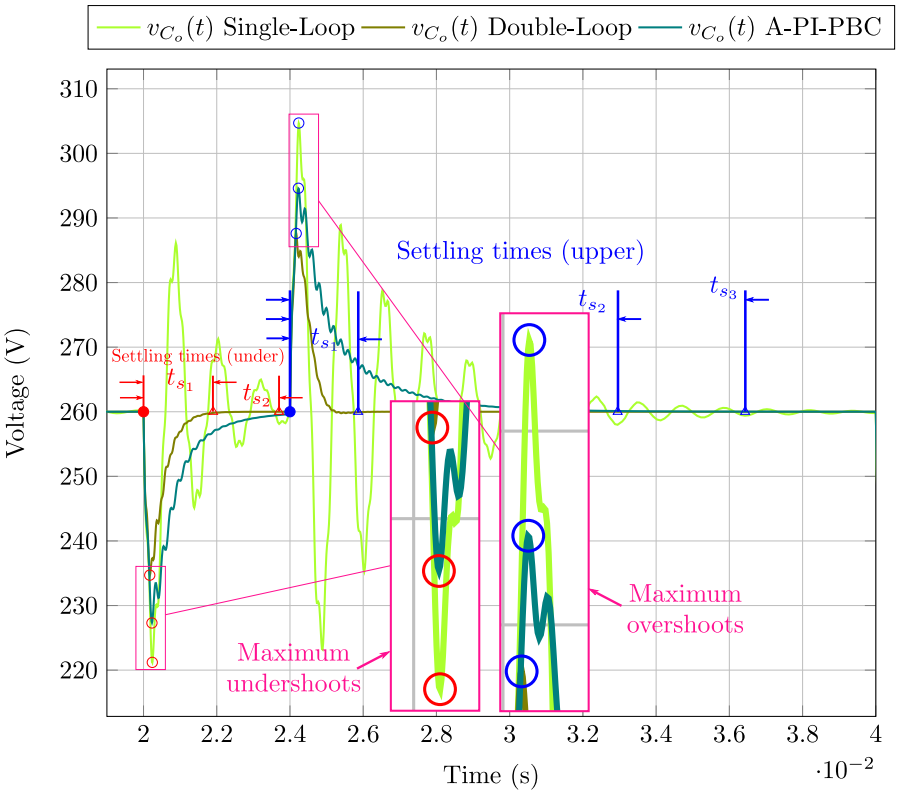

Figure 5.40: Example of transient-response for each specification.

Table 5.2: Transient-response specifications for voltage v_{C_o}, Test 1.

Specification	A-PI-PBC	Double-Loop	Single-Loop
Bottom Time, t_b (ms)	0.23	0.17	0.24
Peak Time, t_p (ms)	0.23	0.17	0.24
Maximum Overshoot (%)	13.3	10.61	17.2
Maximum Undershoot (%)	12.57	9.73	14.92
Settling time, under (ms)	3.7	1.9	N.A.
Settling time, upper (ms)	8.95	1.86	12.43

Not applicable (N.A.)

Table 5.3: Transient-response specifications for current i_{L_n}, Test 1.

Specification	A-PI-PBC	Double-Loop	Single-Loop
Bottom Time, t_b (ms)	N.A.	4.59	4.57
Peak Time, t_p (ms)	N.A	N.A.	0.58
Maximum Overshoot (%)	N.A.	N.A.	34.18
Maximum Undershoot (%)	N.A.	11.9	89.17
Settling time, under (ms)	12.1	7.08	N.A.
Settling time, upper (ms)	3.38	1.92	18.83

Not applicable (N.A.)

Test 2

REMARK 5.4.1

For the robustness Test 2, different types of changes were made, which we limited to making a comparison of their transients because it would have to be done for each time interval, something that would not be worth it since the test was carried out with powerful changes of its nominal load value and in a very short period. We can see in Figs. 5.29–5.33 that the double-loop control is hugely superior to the other tools, and this is clear to understand since the use of σ-stability gives the designer in a graphic way the speed limit, i. e., the

maximum exponential decay, due to this not only asymptotic stability is ensured; also exponential stability is guaranteed.

Test 3

Table 5.4: Transient-response specifications for voltage v_{C_o}, Test 3.

Specification	A-PI-PBC	Double-Loop	Single-Loop
Bottom Time, t_b (ms)	0.21	0.19	0.23
Peak Time, t_p (ms)	0.23	0.17	0.24
Maximum Overshoot (%)	24.11	19.03	130.84
Maximum Undershoot (%)	21.88	16.65	30.7
Settling time, under (ms)	6.6	2.6	11.1
Settling time, upper (ms)	36.03	4.14	N.A

Not applicable (N.A.)

Table 5.5: Transient-response specifications for current i_{L_n}, Test 3.

Specification	A-PI-PBC	Double-Loop	Single-Loop
Bottom Time, t_b (ms)	0.57	0.46	0.56
Peak Time, t_p (ms)	N.A	N.A.	0.6
Maximum Overshoot (%)	N.A.	N.A.	58.27
Maximum Undershoot (%)	27.5	167.14	679.14
Settling time, under (ms)	16.19	4.09	N.A.
Settling time, upper (ms)	4.8	2.3	14.9

Not applicable (N.A.)

5.5 CHAPTER CONCLUSION

In this chapter, the control proposals were performed numerically for both linear and nonlinear control. In addition to them, some transient-response specifications are attached for three robustness tests. All the control results are shown for each state; however, it must be taken into account that in the linear approach, only takes as a reference the

output voltage v_{C_o} and the inductors current i_{L_n}.
In nominal tests, a disadvantage of double-loop can be observed when starting the control action. There is a drop in output voltage and the current of the ASL inductors; this could happen for some numerical errors that the reset of the integrators can cause in the soft-start period, which on the other hand does not happen with the control of a single loop and even more so in the nonlinear control has an ideal start, with certain restraints of the output current i_{L_o}.
We observe the fast action of the I&I estimator in all load changes, which has fast convergence and does not present overshoots in load changes. The control laws of the three robustness tests do not present values far from their nominal values, so there are no efforts on the part of the controller.
The load changes were made in a short period and with a high load scale; since one of the advantages of the considered converter has a critical resistance value at a high nominal rate (approximately 769%). In the three robust tests, the convergence times are significantly faster in the double-loop than in the other controllers; however, in the test that we drive the converter to DCM, unlike A-PI-PBC, it reaches negative values, this without considering the inductor ripples but at the implementation, it could represent a high risk not only in the inductors but also could affect the power supply.
As a final comment, we conclude that these controllers would have to be carried out to experimentation to make a better comparison or make figures of merit. Since it is a numerical evaluation, some aspects that may occur in the instrumentation are not considered; in general, the controllers perform their work guaranteeing asymptotic stability, and even more, the double loop provides exponential stability; in Table 5.6, we write some comments on general performance.

Table 5.6: Performance of controllers in robustness tests.

Controller	Control action at $t = 0$	Convergence time Test 1	Convergence time Test 2	Convergence time Test 3
A-PI-PBC	Excellent	Good	Good	Excellent
Double-Loop	Fair	Excellent	Excellent	Good
Single-Loop	Good	Poor	Poor	Poor

Part V

OUTLOOKS AND CONCLUSIONS

6

CONCLUDING REMARKS AND FUTURE WORK

6.1 CONCLUDING REMARKS

The tools developed in this work left lessons learned that are mainly listed in two points for the linear and nonlinear controllers:

- We propose a new non-heuristic geometric design for tuning parameters in PI control. During the high nonlinear nature of the circuit, a linear model based on the well-known small-signal approach is presented to establish a control law. This work extends the results for designing single-loop and double-loop control schemes for a suitable power electronic converter. We characterize the stability boundaries of the controllers' parameters and exponential decay using the crossing roots stability theory. The cascade control increases the σ-stability analysis complexity due to the polynomial order and the parameter-space of the outer voltage-loop, which is dependent to selecting a pair of gains in the inner current-loop, resulting in at every choice, a new parameter-space. In addition, a comparison among the control schemes shows a faster convergence and exhibits an advantage of the double-loop during transient states for a full regulation for some level of disturbance granting asymptotic stability. Furthermore, we present a case with another pair of gains exclusively for the single-loop which values present pure integral action causing an oscillating behavior; hence, a good practice for selecting gains in the parameter-space is a combination of conventional methods following the σ-stability criteria.

- The nonlinear approach is mainly divided into three parts: the importance of representing a physical system by means of port-Hamiltonian, which in turn is a natural representation of power electronic converters. The identification of the problem, whose objective is to model a converter that explores the Hamiltonian formulation for a particular class of systems, in which we could see that the ASL-SU2C topology fits perfectly into this structure because of the scaling states for the inductor and capacitor networks, and the solution of the problem, given the guidelines for the control design via PI-PBC, a control law is generated, ensuring the detectability condition and guaranteeing the global asymptotic stability in the sense of Lyapunov as well as the design of an I&I estimator when the system faces load changes. As a final comment, this design methodology can be taken to

any converter; however, if a specification analysis is required, it is necessary to emphasize the transient response to generate figures of merit and comply with the required regulations.

6.2 FUTURE WORK

Rioverde is a municipality that has 289 communities, examples such as El Resumidero mentioned in the motivation of the thesis, is just an example of the deprivation of human needs such as electricity in Mexico. The proposal of these control tools can support and assist in monitoring small-scale systems such as microgrids in an individual approach. However, even with the tools developed in this thesis, there is still much work to be done to create a microgrid.
Energy independence will still be a topic of conversation in the future since we have to put in place actions that involve the sectors less benefited by the centralization of cities. Therefore the future work is listed as follows:

- Carry out the instrumentation of the device in open-loop to observe the viability of the modeling; if it does not satisfy the needs raised, the dynamic equations have to take into account the parasitic elements of the passive components.
- To mature σ-stability theory as a new approach for low-order controllers.
- Development and optimization of the converter prototype, using design values for a specific application using standardized dimensions for low voltage direct current systems (Standard IEC 60038).
- Perform robustness analysis, comparison tables and figures of merit for prototypes of the ASL-SU2C topology.
- Consider in the implementation of the prototype variations of the energy source to guarantee its reliability in the interconnection with systems that are intermittent in the generation and production of energy (solar panels, fuel cell), and ensure excellent performance.
- Interconnect off-grid different prototypes in a controlled system as an DC-microgrid for evaluation with different power supplies in island mode.
- Evaluate multiwinding transformer-based DC-DC converters as an approach for injecting multiple levels of power supplies.

Part VI

APPENDIX

A

APPENDIX

In this Appendix, the codes that were used for the creation of the stability regions for both types of controls, as well as the simulation schemes that were developed using MATLAB, are attached.

Listing 1: Inner Current Loop Analysis

```
%% INNER CURRENT LOOP REGIONS PLOT
clc

figure(1)
clf

% STEADY-STATE VALUES
IL=70/13;
VC=140;
ILO=10/13;
VCO=260;

% CIRCUIT PARAMETERS
L=223e-6;
Lo=2.34e-3;
C=1e-6;
Co=1e-6;
R=338;
E=20;
D=0.75;
Di=1-D;
Dii=1+D;

%% PLANT INFORMATION

% NUMERATOR
nc1 = (1/(2*L))*(E+VC);
nc2 = (1/(2*L))*(((1/(Co*R))*(E+VC))+((Di/(2*C))*(IL+ILO)));
nc3 = (1/(2*L))*(((Di/(2*C*Co*R))*(IL+ILO))+(((2*C+Co*(Dii
    ^2+Di*Dii))/(2*C*Co*Lo))*(E+VC)));
nc4 = (1/(2*L))*((((Dii*(Di+Dii))/(2*C*Co*Lo*R))*(E+VC))+(((
    Di)/(2*C*Co*Lo))*(IL+ILO)));

CurrentNum = [nc1 nc2 nc3 nc4];

% DENOMINATOR
```

```
d1=1/(Co*R);
d2=(Co*Lo*Di^2 + 2*Co*L*Dii^2 + 4*C*L)/(4*C*Co*L*Lo);
d3=((Lo*Di^2)+(2*L*Dii^2))/(4*C*Co*L*Lo*R);
d4=(Di^2)/(4*C*Co*L*Lo);

GenericDen=[1 d1 d2 d3 d4];

%% STABILITY BOUNDARY

sigma_inicial = 0;
sigma_final = 4000;
inc = 500;
sgma = sigma_inicial:inc:sigma_final;
vcolor = [0, 0.6, .4];

%% PLOTS OF SIGMA
for iter = 1:1:length(sgma)
    sigma = sgma(iter);
    vcolor(1)=iter/length(sgma);
    w=linspace(0,1e5,10000);

    %% DEFINE s AS s(sigma;omega)
    s = -sigma+1i.*w;

    N0 = nc1*sigma^3 + nc2*sigma^2 + nc3*sigma + nc4;
    D0 = sigma^4 + d1*sigma^3 + d2*sigma^2 + d3*sigma + d4;

    N = nc1*s.^3 + nc2*s.^2+nc3*s+nc4;
    D = s.^4 + d1*s.^3 + d2*s.^2 + d3*s + d4;

    %% LINES IN w=0
    Kp_rect = linspace(-0.04,2,10000);
    Ki_rect = sigma*Kp_rect+sigma*(D0/N0);
    hold on

    %% SWEEP OF OMEGA
    vKp=-real(D./N)+((sigma./w).*imag(D./N));
    vKi=(w+((sigma^2)./w)).*imag(D./N);
    hold on

    cruce  = InterX([vKp; vKi], [Kp_rect; Ki_rect]);

     if sigma==0
        vKp0=vKp;
        vKi0=vKi;
        hold on
```

```
        mask=Ki_rect<vKi;
        fx=[vKp(mask),fliplr(Kp_rect(mask))];
        fy=[vKi(mask),fliplr(Ki_rect(mask))];
        str = '#f29e4c';
        color = sscanf(str(2:end),'%2x%2x%2x',[1 3])/255;
        hinicial=fill(fx,fy,color, 'EdgeColor', [0 0 0])
        set(gcf,'units','points','position',[10,10,500,470])
        axis([0 .32 0 10000])
        box on
            xlabel('$$k_p$$','FontSize', 24 , 'interpreter',
                'latex');
            ylabel('$$k_i$$','FontSize', 24 ,  'interpreter'
                , 'latex');
            legend('Stability Boundary',  'interpreter', '
                latex')
     else
%% STABILITY REGIONS

    if sigma==4000
        str = '#2c699a';
        color = sscanf(str(2:end),'%2x%2x%2x',[1 3])/255;
        hfinal=fill(vKp(3492:4555),vKi(3492:4555),color, '
            EdgeColor', [0 0 0])
        set(hfinal,'EdgeColor','k')
    end

    if sigma==3500
        str = '#048ba8';
        color = sscanf(str(2:end),'%2x%2x%2x',[1 3])/255;
        hfinal=fill(vKp(3464:4935),vKi(3464:4935),color, '
            EdgeColor', [0 0 0])
        set(hfinal,'EdgeColor','k')
    end

    if sigma==3000
        str = '#0db39e';
        color = sscanf(str(2:end),'%2x%2x%2x',[1 3])/255;
        hfinal=fill(vKp(3445:5610),vKi(3445:5610),color, '
            EdgeColor', [0 0 0])
        set(hfinal,'EdgeColor','k')
    end

    if sigma==2500
        str = '#16db93';
        color = sscanf(str(2:end),'%2x%2x%2x',[1 3])/255;
```

```
        hfinal=fill(vKp(3432:7390),vKi(3432:7390),color, '
            EdgeColor', [0 0 0])
        set(hfinal,'EdgeColor','k')
    end

    if sigma==2000
        lim=[0 .32 0 16000];
        str = '#83e377';
        color = sscanf(str(2:end),'%2x%2x%2x',[1 3])/255;
        hfinal=fill(vKp(3440:10000),vKi(3440:10000),color, '
            EdgeColor', [0 0 0])
    end

    if sigma==1500
        lim=[0.02 .32 0 16000];
        str = '#b9e769';
        color = sscanf(str(2:end),'%2x%2x%2x',[1 3])/255;
        hfinal=fillout(vKp(3000:10000),vKi(3000:10000),lim,
            color, 'EdgeColor', [0 0 0])
        set(hfinal,'EdgeColor','k')
    end

    if sigma==1000
        lim=[0.02 .32 0 16000];
        str = '#efea5a';
        color = sscanf(str(2:end),'%2x%2x%2x',[1 3])/255;
        hfinal=fillout(vKp(3000:10000),vKi(3000:10000),lim,
            color, 'EdgeColor', [0 0 0])
        set(hfinal,'EdgeColor','k')
    end

    if sigma==500
        lim=[0.02 .32 0 16000];
        str = '#f1c453';
        color = sscanf(str(2:end),'%2x%2x%2x',[1 3])/255;
        hfinal=fillout(vKp(3000:10000),vKi(3000:10000),lim,
            color, 'EdgeColor', [0 0 0])
        set(hfinal,'EdgeColor','k')
    end
            axis([0 .32 0 10000])
            hold on

    end
end
```

Listing 2: Outer Voltage Loop Analysis.

```
%% OUTER VOLTAGE LOOP REGIONS PLOT
clc

figure(1)
clf

nv1=(E+VC)/(Co*Lo);
nv2=-(Dii*(IL+ILO))/(2*C*Co*Lo);
nv3=((Di^2+Di*Dii)*(E+VC))/(4*C*Co*L*Lo);

nc1 = (1/(2*L))*(E+VC);
nc2 = (1/(2*L))*(((1/(Co*R))*(E+VC))+((Di/(2*C))*(IL+ILO)));
nc3 = (1/(2*L))*(((Di/(2*C*Co*R))*(IL+ILO))+(((2*C+Co*(Dii
    ^2+Di*Dii))/(2*C*Co*Lo))*(E+VC)));
nc4 = (1/(2*L))*((((Dii*(Di+Dii))/(2*C*Co*Lo*R))*(E+VC))+(((
    Di)/(2*C*Co*Lo))*(IL+ILO)));

d1=1/(Co*R);
d2=(Co*Lo*Di^2 + 2*Co*L*Dii^2 + 4*C*L)/(4*C*Co*L*Lo);
d3=((Lo*Di^2)+(2*L*Dii^2))/(4*C*Co*L*Lo*R);
d4=(Di^2)/(4*C*Co*L*Lo);

%% INNER CURRENT LOOP GAINS
kp1=0.056;
ki1=5.4e3;



n1=nv1*kp1;
n2=nv1*ki1+nv2*kp1;
n3=nv2*ki1+nv3*kp1;
n4=nv3*ki1;

VoltageNum = [n1 n2 n3 n4];

cpc1 = d1 + (kp1*nc1);
cpc2 = d2 + (kp1*nc2) + (ki1*nc1);
cpc3 = d3 + (kp1*nc3) + (ki1*nc2);
cpc4 = d4 + (kp1*nc4) + (ki1*nc3);
cpc5 = ki1*nc4;

VoltageDen = [1 cpc1 cpc2 cpc3 cpc4 cpc5];

sigma_inicial = 0;
sigma_final = 360;
inc = 120;
sgma = sigma_inicial:inc:sigma_final;
```

```
vcolor = [0, 0.6, .4];


for iter = 1:1:length(sgma)
    w=linspace(-0.001,1e5,10000);
    sigma = sgma(iter);
    vcolor(1)=iter/length(sgma);

    % Definicion de s
s = -sigma+1i.*w;

N0 = n1*sigma^3 + n2*sigma^2 + n3*sigma + n4;
D0 = sigma^5 + cpc1*sigma^4 + cpc2*sigma^3 + cpc3*sigma^2 +
    cpc4*sigma + cpc5;


N = n1*s.^3 + n2*s.^2 + n3*s + n4;
D = s.^5 + cpc1*s.^4 + cpc2*s.^3 + cpc3*s.^2 + cpc4*s + cpc5
    ;

% Recta en w=0
Kp_rect = linspace(-.2,.09,2063);
Ki_rect=sigma*Kp_rect+sigma*(D0/N0);
hold on

% Barrido en frecuencia
vKp=-real(D./N)+((sigma./w).*imag(D./N));
vKi=(w+((sigma^2)./w)).*imag(D./N);
hold on


cruce = InterX([vKp; vKi], [Kp_rect; Ki_rect])


 if sigma==0
        hinicial=fill(vKp(500:4000),vKi(500:4000),[1 0.5 1])
            ;
        axis([0 .12 0 1400])
        xlabel('$$K_p$$','FontSize', 24 , 'interpreter', '
            latex');
        ylabel('$$K_i$$','FontSize', 24 ,  'interpreter', '
            latex');
        legend('Stability Boundary','Location','best','
            interpreter', 'latex')
        hold on
        box on
```

```
else
if sigma==120
       x=vKp(276:2278);
       y=vKi(276:2278);

       x1=Kp_rect(1:2003);
       y1=Ki_rect(1:2003);

       mask=y>y1
       fx = [x1(mask), fliplr(x(mask))];
       fy = [y1(mask), fliplr(y(mask))];
       fill_color = [1 1 0];
       fh = fill(fx,fy,fill_color);

end

if sigma==240
       x2=vKp(286:2279);
       y2=vKi(286:2279);
       x3=Kp_rect(1:1994);
       y3=Ki_rect(1:1994);

       mask=y2>y3
       fx = [x2(mask), fliplr(x3(mask))];
       fy = [y2(mask), fliplr(y3(mask))];
       fill_color = [1 0.6 0];
       fh = fill(fx,fy,fill_color);

end

if sigma==360
       x4=vKp(296:2281);
       y4=vKi(296:2281);
       x5=Kp_rect(1:1986);
       y5=Ki_rect(1:1986);

       mask=y4>y5
       fx = [x4(mask), fliplr(x5(mask))];
       fy = [y4(mask), fliplr(y5(mask))];
       fill_color = [1 0.4 0.4];
       fh = fill(fx,fy,fill_color);



end
end
```

```
end
```

Listing 3: PI-PBC Main Program.

```
%% PARAMETERS

E  = 20;     % Voltage input   (V)
L1 = 223e-6; % Inductance      (H)
L2 = 2.34e-3; % Inductance      (H)
C1 = 1e-6; % Capacitance     (F)
C2 = 1e-6; % Capacitance     (F)
rL = 338;     % Load Resistance (Ohms)

D = 0.75;     % Duty Cycle      *for OL test*

Ki = 0.05;
Kp = 1e-4;


%% EQUILIBRIUM CRITERIA

vd       = 260;

u_star   = (vd-E)/(vd+3*E);
u_p      = 1 + u_star;
u_n      = 1 - u_star;

phi_ee_1 = (L1/rL)*(u_p/u_n)*vd;
phi_ee_2 = (1/rL)*L2*vd;
q_ee_1   = ((vd-(E*u_star))/(vd*u_p))*C1*vd;
q_ee_2   = C2*vd;

p1 = ((q_ee_1 +(E*C1))/(2*C1*L1))*phi_ee_1;
p2 = (((L2*phi_ee_1)+(L1*phi_ee_2))/(2*C1*L1*L2))*q_ee_1;
p3 = ((q_ee_1 +(E*C1))/(C1*L1))*phi_ee_2;
y0 = p1-p2+p3;

%% PLOTS

figure(1)
plt1=plot(out.tout,out.simout(:,1),'k');
title('Control Law','FontSize', 12, 'interpreter', 'latex')
xlabel('Time (s)','FontSize', 12, 'interpreter', 'latex')
ylabel('$\tilde{u}$','FontSize', 12, 'interpreter', 'latex')
legend({'$\tilde{u}$ Error','$V_{out}$ PI-PBC'},'Location','
    best','FontSize', 12, 'interpreter', 'latex')
plt1(1).LineWidth = 2;
```

```
figure(2)
plt2=plot(out.tout,out.simout(:,2),'b',out.tout,out.simout
    (:,3),'r--');
title('Voltage Output','FontSize', 12, 'interpreter', 'latex
    ')
xlabel('Time (s)','FontSize', 12, 'interpreter', 'latex')
ylabel('Voltage (V)','FontSize', 12, 'interpreter', 'latex')
legend({'$V_{out}$ PI-PBC','$V_{out}$ Open Loop'},'Location'
    ,'best','FontSize', 12, 'interpreter', 'latex')
plt2(1).LineWidth = 2;
plt2(2).LineWidth = 1;

figure(3)
plot(out.simout(:,2),out.simout(:,4),'b',out.simout(:,3),out
    .simout(:,5),'r');
title('Phase Portrait','FontSize', 12, 'interpreter', 'latex
    ')
xlabel('Voltage $v_{C_o}$ (V)','FontSize', 12, 'interpreter'
    , 'latex')
ylabel('Current $i_{L}$ (A)','FontSize', 12, 'interpreter',
    'latex')



%% Save .txt file

 Table1=[out.tout,out.simout(:,1)];
 Table2=[out.tout,out.simout(:,2)];
 Table3=[out.tout,out.simout(:,3)];
 Table4=[out.simout(:,2),out.simout(:,4)];
 Table5=[out.simout(:,3),out.simout(:,5)];
 Table6=[out.simout(:,2),out.simout(:,4)];

 Table7=[out.tout,out.simout(:,2),out.simout(:,4)]; %
     Control
 Table8=[out.tout,out.simout(:,3),out.simout(:,5)]; % Sin
     Control
 Table9=[out.simout(:,2),out.simout(:,4),out.simout(:,6)]; %
      Control
 Table10=[out.simout(:,3),out.simout(:,5),out.simout(:,6)];
     % Sin Control
%
%
 save('yTilde.txt','Table1', '-ASCII','-append');
```

```
save('PIPBC.txt','Table2', '-ASCII','-append');
save('OL.txt','Table3', '-ASCII','-append');
save('PhasePort.txt','Table5', '-ASCII','-append');
save('PPControl.txt','Table6', '-ASCII','-append');
save('x1x2tC4.txt','Table7', '-ASCII','-append');
save('x1x2tNC.txt','Table8', '-ASCII','-append');
save('x1x2HdC4.txt','Table9', '-ASCII','-append');
save('x1x2HdNC.txt','Table10', '-ASCII','-append');

%% II parameters

Lambda = 5e-5;
Gamma = 10;
```

A.1 SIMULINK MODELS

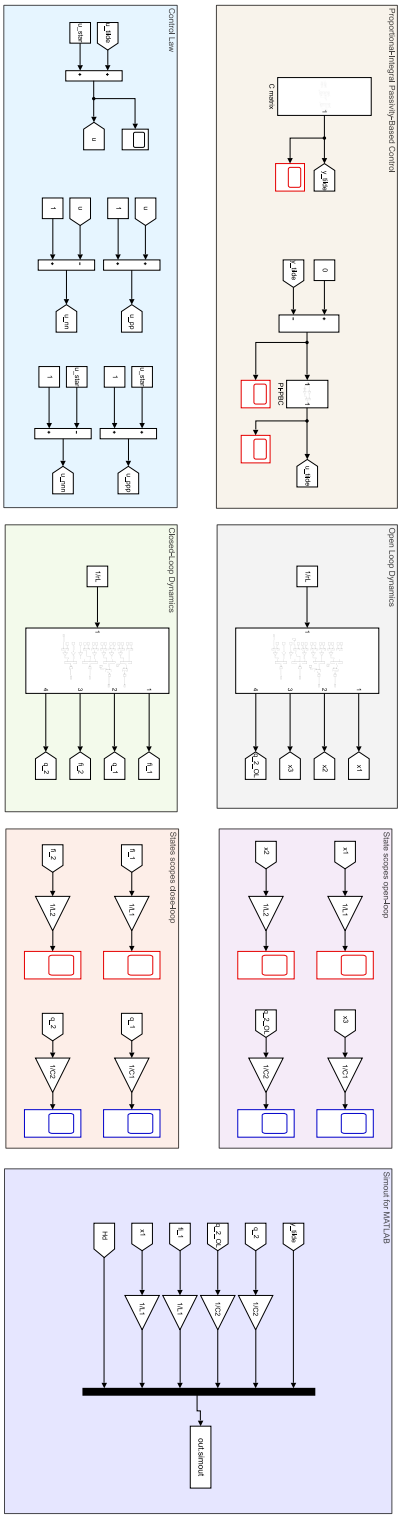

Figure A.1: Schematic of Simulation PI-PBC.

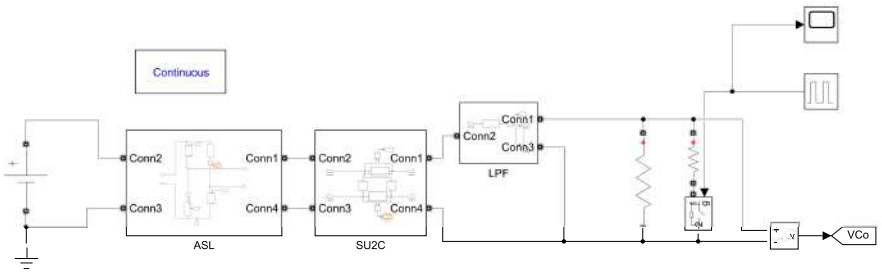

Figure A.2: Simscape Power Systems Model for ASL-SU2C.

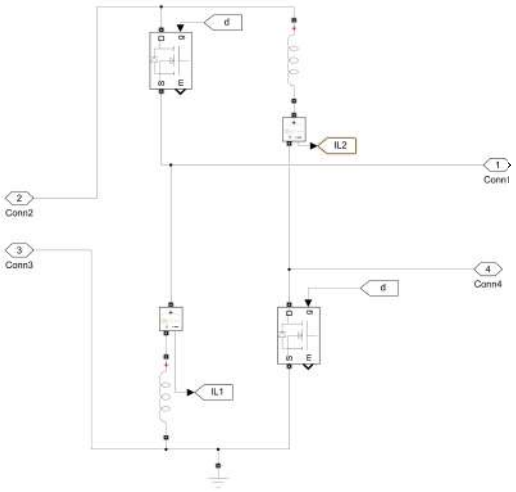

Figure A.3: Simscape Active Switching Inductors.

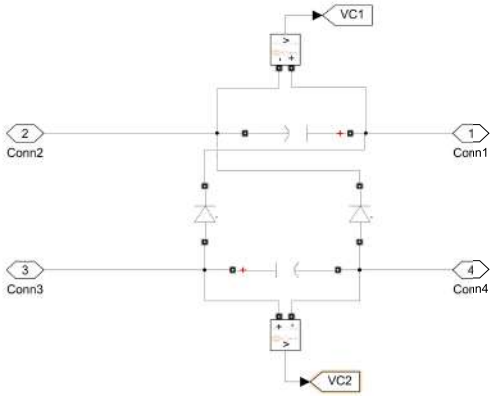

Figure A.4: Simscape Passive Switching Capacitors.

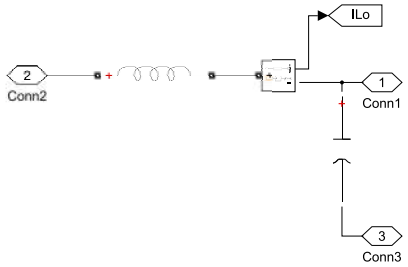

Figure A.5: Simscape Low-Pass Filter.

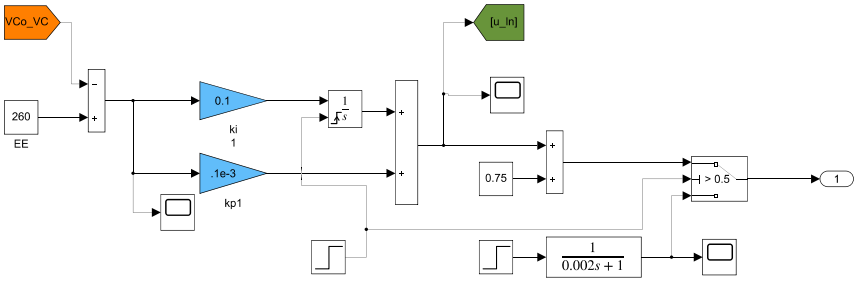

Figure A.6: Single-loop controller.

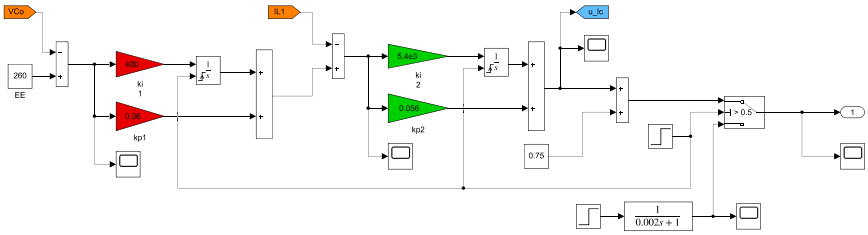

Figure A.7: Double-loop controller.

REFERENCES

[1] Secretaría de Energía. *Programa de Desarrollo del Sistema Eléctrico Nacional 2018-2032*. https://www.gob.mx/cms/uploads/attachment/file/331770/PRODESEN-2018-2032-definitiva.pdf. 2018.

[2] Luis Fabián Fuentes Cortés and José María Ponce Ortega. "Perspectivas del desarrollo de sistemas de generación distribuida en México." In: *Serie de Ponencias, Perspectivas de Sustentabilidad en México* (2017), p. 5.

[3] Luz Ireri León-Trigo, Enrique Reyes-Archundia, José Antonio Gutiérrez-Gnecchi, Arturo Méndez-Patiño, and Gerardo Marx Chávez-Campos. "Smart Grids en México: Situación actual, retos y propuesta de implementación." In: *Ingeniería, investigación y tecnología* 20.2 (2019), pp. 0–0.

[4] Comisión Reguladora de Energía. *Oportunidades de negocio para el nuevo Mercado Eléctrico, Generación Distribuida y Abasto Aislado, Unidad de Electricidad*. https://www.gob.mx/cms/uploads/attachment/file/368023/03_Merida_CRE.pdf. 2018.

[5] Derilinx. *ENERGYDATA.INFO An Innovation of World Bank Group*. https://energydata.info/. 2020.

[6] Magdi S Mahmoud and M Fouad. *Control and optimization of distributed generation systems*. Springer, 2015.

[7] "IEEE Standard for Interconnection and Interoperability of Distributed Energy Resources with Associated Electric Power Systems Interfaces." In: *IEEE Std 1547-2018 (Revision of IEEE Std 1547-2003)* (2018), pp. 1–138. DOI: 10.1109/IEEESTD.2018.8332112.

[8] Comisión Reguladora de Energía. *Resolución SEN: Código de Red, Diario Oficial de la Federación*. https://acortar.link/FExEDd. 2016.

[9] Jan CJ Bart, Natale Palmeri, and Stefano Cavallaro. *Biodiesel science and technology: from soil to oil*. Elsevier, 2010.

[10] Nancy Lizet Hernández. *Parque eólico de SLP abastece el 80% de energías de Bosch México*. https://sanluis.eluniversal.com.mx/cartera/05-07-2019/parque-eolico-de-slp-abastece-el-80-de-energias-de-bosch-mexico. 2019.

[11] Forbes Staff. *Parque en Sonora inicia operaciones con 68,000 paneles solares*. https://www.forbes.com.mx/parque-en-sonora-inicia-operaciones-con-68000-paneles-solares/. 2018.

[12] Tesla. *Massive Energy Storage, Megapack*. https://www.tesla.com/megapack. 2019.

[13] Huang Jiayi, Jiang Chuanwen, and Xu Rong. "A review on distributed energy resources and MicroGrid." In: *Renewable and Sustainable Energy Reviews* 12.9 (2008), pp. 2472–2483.

[14] R.H. Lasseter. "MicroGrids." In: *2002 IEEE Power Engineering Society Winter Meeting. Conference Proceedings (Cat. No.02CH37309)*. Vol. 1. 2002, 305–308 vol.1. DOI: 10.1109/PESW.2002.985003.

[15] Bilal M. Eid, Nasrudin Abd Rahim, Jeyraj Selvaraj, and Ahmad H. El Khateb. "Control Methods and Objectives for Electronically Coupled Distributed Energy Resources in Microgrids: A Review." In: *IEEE Systems Journal* 10.2 (2016), pp. 446–458. DOI: 10.1109/JSYST.2013.2296075.

[16] Phatiphat Thounthong, Pongsiri Mungporn, Serge Pierfederici, Damien Guilbert, and Nicu Bizon. "Adaptive Control of Fuel Cell Converter Based on a New Hamiltonian Energy Function for Stabilizing the DC Bus in DC Microgrid Applications." In: *Mathematics* 8.11 (2020), p. 2035.

[17] Phillip A Laplante. *Electrical engineering dictionary*. CRC Press LLC, 2000.

[18] Rajiv J. Shah & Natarajan Chandrasekaran. *Why microgrids are the key to solving energy poverty worldwide*. https://fortune.com/2020/01/21/microgrids-energy-poverty-africa-asia/. 2020.

[19] Robert Hebner. *Nanogrids, Microgrids and Big Data: The Future of The Power Grid*. https://spectrum.ieee.org/nanogrids-microgrids-and-big-data-the-future-of-the-power-grid. 2017.

[20] M. Forouzesh, Y. P. Siwakoti, S. A. Gorji, F. Blaabjerg, and B. Lehman. "Step-Up DC–DC Converters: A Comprehensive Review of Voltage-Boosting Techniques, Topologies, and Applications." In: *IEEE Transactions on Power Electronics* 32.12 (2017), pp. 9143–9178. DOI: 10.1109/TPEL.2017.2652318.

[21] Rafael Cisneros, Matteo Pirro, Gilbert Bergna, Romeo Ortega, Gianluca Ippoliti, and Marta Molinas. "Global tracking passivity-based PI control of bilinear systems: Application to the interleaved boost and modular multilevel converters." In: *Control Engineering Practice* 43 (2015), pp. 109–119.

[22] N. Elsayad, H. Moradisizkoohi, and O. Mohammed. "Analysis and Design of a High Step-Up Transformerless DC-DC Converter with an Integrated L2C3D2 Network." In: *2019 IEEE Applied Power Electronics Conference and Exposition (APEC)*. 2019, pp. 1301–1306.

[23] N. Elsayad, H. Moradisizkoohi, and O. Mohammed. "A New SEPIC-Based Step-Up DC-DC Converter with Wide Conversion Ratio for Fuel Cell Vehicles: Analysis and Design." In: *IEEE Transactions on Industrial Electronics* (2020), pp. 1–1.

[24] L. Yang, T. Liang, and J. Chen. "Transformerless DC–DC Converters With High Step-Up Voltage Gain." In: *IEEE Transactions on Industrial Electronics* 56.8 (2009), pp. 3144–3152.

[25] Press Releases Analog Devices. *500mA, 1.5MHz, 65V Boost DC/DC Converter*. https://www.analog.com/en/about-adi/news-room/press-releases/2015/500ma-1-5mhz-65v-boost-dc-dc-converter.html. 2015.

[26] B. Axelrod, Y. Berkovich, and A. Ioinovici. "Switched - Capacitor / Switched - Inductor Structures for Getting Transformerless Hybrid DC–DC PWM Converters." In: *IEEE Transactions on Circuits and Systems I: Regular Papers* 55.2 (2008), pp. 687–696. DOI: 10.1109/TCSI.2008.916403.

[27] L. Yang, T. Liang, and J. Chen. "Transformerless DC–DC Converters With High Step-Up Voltage Gain." In: *IEEE Transactions on Industrial Electronics* 56.8 (2009), pp. 3144–3152. DOI: 10.1109/TIE.2009.2022512.

[28] Y. Tang, D. Fu, T. Wang, and Z. Xu. "Hybrid Switched-Inductor Converters for High Step-Up Conversion." In: *IEEE Transactions on Industrial Electronics* 62.3 (2015), pp. 1480–1490. DOI: 10.1109/TIE.2014.2364797.

[29] A. R. Solangi, Q. Huang, G. Raza, M. Abbas, and S. H. Solangi. "DC Bus Voltage Regulation for Distributed Energy Sources through Buck-Boost Converter in a Direct Current Micro Grid." In: *2019 IEEE Innovative Smart Grid Technologies - Asia (ISGT Asia)*. 2019, pp. 1822–1827. DOI: 10.1109/ISGT-Asia.2019.8881193.

[30] Marcos Antonio Salvador, Telles Brunelli Lazzarin, and Roberto Francisco Coelho. "High step-up DC–DC converter with active switched-inductor and passive switched-capacitor networks." In: *IEEE Transactions on Industrial Electronics* 65.7 (2017), pp. 5644–5654.

[31] Farzin Asadi. "Robust Control of DC-DC Converters: The Kharitonov's Theorem Approach with MATLAB® Codes." In: *Synthesis Lectures on Power Electronics* 6.2 (2018), pp. 1–135.

[32] Robert W Erickson and Dragan Maksimovic. *Fundamentals of power electronics*. Springer Science & Business Media, 2007.

[33] Simon Ang, Alejandro Oliva, Gary Griffiths, and Richard Harrison. *Power-switching converters*. CRC press, 2010.

[34] H Chappellat, M Mansour, and SP Bhattacharyya. "Elementary proofs of some classical stability criteria." In: *IEEE Transactions on Education* 33.3 (1990), pp. 232–239.

[35] Shankar P Bhattacharyya and Lee H Keel. "Robust control: the parametric approach." In: *Advances in control education 1994*. Elsevier, 1995, pp. 49–52.

[36] Oleg Viro. "From the sixteenth Hilbert problem to tropical geometry." In: *Japanese Journal of Mathematics* 3.2 (2008), pp. 185–214.

[37] Elena N Gryazina. "The D-decomposition theory." In: *Automation and Remote Control* 65.12 (2004), pp. 1872–1884.

[38] EN Gryazina and BT Polyak. "On the root invariant regions structure for linear systems." In: *IFAC Proceedings Volumes* 38.1 (2005), pp. 90–95.

[39] JC Maxwell, IA Vyshnegradskii, and A Stodola. "Teoriya avtomaticheskogo regulirovaniya (Automatic Regulation Theory), Moscow: Akad." In: *Nauk SSSR* (1949).

[40] Yu I Neimark. "On the problem of the distribution of the roots of polynomials." In: *Dokl. Akad. Nauk SSSR*. Vol. 58. 1947, pp. 357–360.

[41] Jürgen Ackermann. *Robust control: the parameter space approach*. Springer Science & Business Media, 2002.

[42] Dragoslav D Siljak. "Nonlinear systems: the parameter analysis and design." In: (1969).

[43] Iván D Díaz-Rodríguez, Sangjin Han, and Shankar P Bhattacharyya. *Analytical design of PID controllers*. Springer, 2019.

[44] E. Polak. "A note on D-decomposition theory." In: *IEEE Transactions on Automatic Control* 9.1 (1964), pp. 107–109. DOI: 10.1109/TAC.1964.1105618.

[45] J-E Hernández-Díez, C-F Méndez-Barrios, Sabine Mondié, S-I Niculescu, and Emilio J González-Galván. "Proportional-delayed controllers design for LTI-systems: a geometric approach." In: *International Journal of Control* 91.4 (2018), pp. 907–925.

[46] Mark W Spong. "Energy based control of a class of underactuated mechanical systems." In: *IFAC Proceedings Volumes* 29.1 (1996), pp. 2828–2832.

[47] Romeo Ortega, Julio Antonio Loría Perez, Per Johan Nicklasson, and Hebertt J Sira-Ramirez. *Passivity-based control of Euler-Lagrange systems: mechanical, electrical and electromechanical applications*. Springer Science & Business Media, 2013.

[48] Anders Rantzer. "On the Kalman-Yakubovich-Popov lemma for positive systems." In: *IEEE Transactions on Automatic Control* 61.5 (2015), pp. 1346–1349.

[49] Wassim M Haddad and VijaySekhar Chellaboina. *Nonlinear dynamical systems and control*. Princeton university press, 2011.

[50] JL Wyatt, LO Chua, JW Gannett, IC Göknar, and DN Green. "Foundations of nonlinear network theory, Part I: Passivity." In: *Electronics Research Laboratory, CoUege of Engineering, University of California, Berkeley, CA* 94720 (1978).

[51] Arjan Van Der Schaft and Dimitri Jeltsema. "Port-Hamiltonian systems theory: An introductory overview." In: *Foundations and Trends in Systems and Control* 1.2-3 (2014), pp. 173–378.

[52] Peter E Wellstead. *Introduction to physical system modelling*. Vol. 4. Academic Press London, 1979.

[53] Michael Hernandez-Gomez, Romeo Ortega, Françoise Lamnabhi-Lagarrigue, and Gerardo Escobar. "Adaptive PI stabilization of switched power converters." In: *IEEE Transactions on Control Systems Technology* 18.3 (2009), pp. 688–698.

[54] R. Ortega, A. van der Schaft, F. Castanos, and A. Astolfi. "Control by Interconnection and Standard Passivity-Based Control of Port-Hamiltonian Systems." In: *IEEE Transactions on Automatic Control* 53.11 (2008), pp. 2527–2542. DOI: 10.1109/TAC.2008.2006930.

[55] Daizhan Cheng, Alessandro Astolfi, and Romeo Ortega. "On feedback equivalence to port controlled Hamiltonian systems." In: *Systems & control letters* 54.9 (2005), pp. 911–917.

[56] Michael Hernandez-Gomez, Romeo Ortega, Françoise Lamnabhi-Lagarrigue, and Gerardo Escobar. "Adaptive PI Stabilisation of Switched Power Converters Described by Port-Hamiltonian Models." In: *Dynamics and Control of Switched Electronic Systems*. Springer, 2012, pp. 355–388.

[57] Alessandro Astolfi, Dimitrios Karagiannis, and Romeo Ortega. *Nonlinear and adaptive control with applications*. Springer Science & Business Media, 2007.

[58] Karl Johan Åström and Tore Hägglund. *PID controllers: theory, design, and tuning*. Vol. 2. Instrument society of America Research Triangle Park, NC, 1995.

[59] Chih-Fan Chen, Zhifan Chen, and Ignatius John Haas. *Elements of control systems analysis: classical and modern approaches*. Prentice-Hall, 1968.

[60] Liuping Wang. *PID control system design and automatic tuning using MATLAB/Simulink*. John Wiley & Sons, 2020.

[61] Jorge-Antonio Lopez-Renteria, Baltazar Aguirre-Hernandez, and Fernando Verduzco. "The boundary crossing theorem and the maximal stability interval." In: *Mathematical Problems in Engineering* 2011 (2011).

[62] Bayu Jayawardhana, Romeo Ortega, Eloisa Garcia-Canseco, and Fernando Castanos. "Passivity of nonlinear incremental systems: Application to PI stabilization of nonlinear RLC circuits." In: *Systems & control letters* 56.9-10 (2007), pp. 618–622.

[63] Hassan K Khalil. *Nonlinear systems; 3rd ed.* Upper Saddle River, NJ: Prentice-Hall, 2002.

[64] B. Brogliato, O. Egeland, R. Lozano, and B. Maschke. *Dissipative systems analysis and control: theory and applications*. Springer, 2007.

[65] Alessandro Astolfi and Romeo Ortega. "Immersion and invariance: A new tool for stabilization and adaptive control of nonlinear systems." In: *IEEE Transactions on Automatic control* 48.4 (2003), pp. 590–606.

[66] Jeffrey W Umland and Mohammed Safiuddin. "Magnitude and symmetric optimum criterion for the design of linear control systems: what is it and how does it compare with the others?" In: *IEEE Transactions on Industry Applications* 26.3 (1990), pp. 489–497.